Crustal- to Nano- Scale Influences on Orogenic Gold Deposits: Insights from the Central Victorian Goldfields

by

Christopher R. Voisey
Bsc (Hons), G.I.T

A thesis submitted for the degree of

Doctor of Philosophy

Main supervisor: Dr. Andrew G. Tomkins
Associate supervisors: Dr. Steven Micklethwaite

School of Earth, Atmosphere & Environment
Monash University, Clayton, Victoria, Australia

MONASH University

Copyright notice

© Christopher Voisey (2019).

I certify that I have made all reasonable efforts to secure copyright permissions for third-party content included in this thesis and have not knowingly added copyright content to my work without the owner's permission.

"I dunno dude. It's like a heavy magnetic basalt... or something?"

Abstract

Orogenic type Au deposits are responsible for contributing over 30% of the Au recovered globally throughout history and Victoria contains one of the most prosperous orogenic Au regions ever discovered, producing approximately 2,500 tonnes of Au since the mid 1800's. However, the mechanisms behind Au mineralisation itself and the generation of bonanza-grade ores remain enigmatic. Geochemical studies tend to focus on phenomena related to local changes in fluid chemistry to explain the deposition of Au, whereas structural geologists independently focus on physical mechanisms that affect fluids with little consideration of geochemistry. In reality, neither approach alone is capable of explaining the complexity behind Au localisation. The innovation of this study will be to unite these subdisciplines to obtain a better understanding of the mechanism(s) responsible for the formation of these world-class Au deposits. To bridge this disconnect, a range of Au deposits in Victoria exposed at different crustal levels will be examined in terms of their mineralogical and structural controls on metal deposition and how the scale of fluid migration influences the destabilisation of auriferous fluids. This investigation will combine principles from stable isotope geochemistry, petrography, micro-tectonics, thermodynamics, electrochemistry, and material science in ways not previously considered by the economic geology community. Ag stable isotope signatures of Au grains are employed as a geochemical tracer of ore-forming processes. Detailed petrography on diverse Au samples is used to identify fundamental controls on mineralisation from different depths of different deposits. These data are used as the backbone for geochemical modelling of Au-bearing fluids in the context of Victoria's geological framework, providing pressure, temperature and composition constraints on Au-rich areas. Integrating these different disciplines provides a holistic view on deposit formation that can fill in gaps of knowledge that are critical to both academia and industry. Results from this study will allow mineral explorationists to prioritise their targeting programs on both the regional and deposit-scale, as well as further the understanding of the key processes involved in the genesis of orogenic Au-type deposits and bonanza-grade Au zones.

Declaration

I hereby declare that this thesis contains no material which has been accepted for the award of any other degree or diploma at any university or equivalent institution and that, to the best of my knowledge and belief, this thesis contains no material previously published or written by another person, except where due reference is made in the text of the thesis.

This thesis includes two original papers published in peer reviewed journals and two unpublished publications. The core theme of the thesis is the formation of orogenic-type gold deposits. The ideas, development and writing up of all the papers in the thesis were the principal responsibility of myself, the student, working within the School of Earth, Atmosphere and Environment under the supervision of Andrew G. Tomkins.

(The inclusion of co-authors reflects the fact that the work came from active collaboration between researchers and acknowledges input into team-based research.)

In the case of chapters 2-5 my contribution to the work involved the following:

Thesis Chapter	**Publication Title**	**Status** *(published, in press, accepted or returned for revision)*	**Nature and % of student contribution**	**Co-author name(s) Nature and % of Co-author's contribution***	**Co-author(s), Monash student Y/N***
2	Extreme Silver Isotope Variation if Orogenic Gold Systems Implies Multi-staged Metal Remobilisation During Ore Genesis	Published	80 % - Majority of data interpretation and manuscript preparation	1)Roland Maas – data collection & manuscript preparation 7.5% 2) Andrew G. Tomkins – supervisory role 7.5% 3) Michael Brauns – data collection 2.5% 4) Gerhard Brügmann – data collection 2.5%	N Y N N
3	Aseismic Refinement of Orogenic Gold Systems	Accepted	75 % - Idea generation, majority of data interpretation and manuscript preparation	1) David Willis – Idea generation and field work 10% 2) Andrew G. Tomkins – supervisory role 5% 3) Christopher J. L.Wilson – data collection & idea generation 2% 4) Steven Micklethwaite – supervisory role 2% 5) Filomena Salvemini - data collection 2% 6) Jeremy Bougoure - data collection 2% 7) William D. A. Rickard - data collection 2%	Y Y Y Y N N N

4	The first analysis of a telescoped orogenic gold system: Insights from the Fosterville deposit	Not Submitted	85 % - Idea generation, majority of data interpretation and manuscript preparation	1) Andrew G. Tomkins – supervisory role 7.5% 2) Yanlu Xing – assistance with thermodynamic modelling 7.5%	Y Y
5	Gold Accumulations in Quartz Driven by Earthquake-Induced Piezoelectricity	Not Submitted	80 % - Idea generation, majority of data interpretation and manuscript preparation	1) Andrew G. Tomkins – supervisory role 10% 2) Nicholas J. R. Hunter – theory generation, manuscript preparation & data collection 10%	Y Y

I have / have not renumbered sections of submitted or published papers in order to generate a consistent presentation within the thesis.

Student signature: **Date: 3/10/2019**

The undersigned hereby certify that the above declaration correctly reflects the nature and extent of the student's and co-authors' contributions to this work. In instances where I am not the responsible author I have consulted with the responsible author to agree on the respective contributions of the authors.

Main Supervisor signature: **Date: 3/10/2019**

Contents

Abstract *5*

Declaration *7*

Acknowledgements *16*

Chapter: 1 Introduction

1.1 Orogenic Gold Systems *21*

1.2 Geology of Central Victoria *27*

1.2.1 Western Lachlan Orogen *28*

1.2.2 The Stawell Zone *28*

1.2.3 The Bendigo Zone *29*

1.2.4 The Melbourne Zone *30*

1.3 Gold Mineralisation of Central Victoria *32*

1.3.1 Ore Assemblages and Mineralogical Domains *33*

1.3.2 Timing of Gold Mineralisation *35*

1.3.3 Genetics & Source of Gold-Bearing Fluids *36*

1.4 Thesis Structure *41*

Chapter 2: Extreme Ag isotope variation in orogenic gold systems implies multi-staged metal remobilisation during ore genesis

Abstract *51*

1. Introduction *52*

2. Geological Setting *53*

3. Methodology *55*

4. Results *60*

5. Discussion *60*

5.2 The Nuclear Volume Effect *60*

5.3 Physio-chemical Fractionation in Ore Deposit Environments *64*

5.4 Ag isotope constraints on orogenic Au deposition in the Victorian Goldfields *65*

6. Conclusions *67*

Chapter 3: Aseismic Refinement of Orogenic Gold Systems

Abstract *77*

1. Orogenic Gold Systems *78*

1.1 Geological Setting & Sampling *80*

2. Methodology *82*

3. Gold Textures *84*

4. Discussion *90*

4.1. Generation of Vein-Hosted Au Nanoparticles *92*

4.2. Au Nanoparticle Transport and Aggregation *92*

4.3. Dissolution of Vein Material *93*

4.4 Nanoparticles to Nuggets *95*

4.5 Sulphide-hosted Au Nanoparticles *97*

4.6 Secondary Au in Sulphide-Hosted Ores *97*

4.6.1 Au Nanoparticle Exsolution during cooling *98*

4.6.2 Hydrothermal Alteration & Chemical Remobilisation of Sulphide-Hosted Au *98*

4.6.3 Coupled Dissolution-Reprecipitation of Sulphide-Hosted Au Ore *99*

4.7 Electrochemical Potential & Au Nanoparticle Formation *100*

5. The Aseismic Refinement Model *103*

6. Conclusion *106*

Chapter 4: The first analysis of a telescoped orogenic gold system: Insights from the Fosterville deposit.

Abstract *115*

1. Introduction *116*

2. Regional Geology *114*

2.1 The Western Lachlan Orogen *118*

2.2 The Bendigo Zone *119*

2.3 Timing of Mineralisation *120*

3. Deposit Geology and Mineralisation *121*

3.1 Ore Deposit Features *121*

3.2 Mineralisation Styles *123*

4. Methods *135*

5. Results *128*

5.1 Vein and Ore Textures *123*

5.2 Thermodynamic Modelling of the Fosterville System *132*

6. Discussion *136*

6.1 Relative Timing and Styles of Mineralisation *136*

6.2 Mechanisms for Au-Sb Precipitation *138*

6.3 Genesis of Ore Telescoping at Fosterville *141*

7. Conclusion *145*

Chapter 5: Gold Accumulations in Quartz Driven by Earthquake-Induced Piezoelectricity

Abstract *152*

1. Introduction *153*

2. Piezoelectricity and Quartz *155*

2.1 Previous Studies of Piezoelectricity in Geological Materials *157*

3. Textures in Quartz Veins *157*

3.1 Piezoelectric Tensors in Au-Quartz Veins *159*

4. Piezoelectricity & Electrochemical Processes *161*

4.2 The Piezocatalyst *163*

4.3 Electrochemistry for Metal Deposition *164*

5. Piezopotential of Orogenic Gold Systems *166*

6. Implications for Gold Exploration *168*

7. Conclusions *170*

Chapter 6: Conclusions

1.1 Key Outcomes *177*

1.2 Summary of Findings *178*

1.2.1 Extreme Ag Isotope Variation in Orogenic Gold Systems Implies Multi-Staged Metal Remobilization During Ore Genesis *178*

1.2.2 Aseismic Refinement of Orogenic Gold Systems *179*

1.2.3 The First Analysis of a Telescoped Orogenic Gold System: Insights from the Fosterville Deposit. *180*

1.2.3 Piezoelectricity in Earth's Crust and the Potential to Form Gold Deposits *181*

2.0 Holistic Implications of the Research Results *182*

3.0 Recommendations for Future Work *184*

Acknowledgements

"Dude, sick!" is just about the only statement that can appropriately sum up my entire experience throughout this journey of scholastic pursuit and worldly travels. This sitcom life that I have led has had many characters, both permanent and reoccurring, that deserve much more credit than I am about to give them, however, let's give it a go.

Dr. Andy Tomkins (Dr. Buddy) is first up to bat as he is the protagonist in my PhD episode. Upon graduating from an undergraduate degree in Newfoundland, I very maturely – with nothing but my most fortuitous intentions in mind - googled "funnest cities to live in" and Melbourne hit the top of the list. I got in contact with this Tomkins fellow, who was located in Fun Town, and had similar research interests to mine; after a ~7-minute-long skype conversation it was decided I'd have a crack and apply to travel across the planet to be a professional nerd. Best decision I've ever made. Dr. Buddy was not only a supervisor and mentor, he was genuinely a friend of mine throughout all the good and bad that accompanies abandoning your life in the pursuit of high-calibre rock licking. He challenged my thinking and nurtured my ideas in a way that I'm not sure any other supervisor could have provided – especially considering what a distractible, high-energy, foul-mouthed Newfie he quickly learned that I was (am?). Andy taught me what it takes to bring an idea from good enough to great, and how to push a hypothesis to the next level in order to fearlessly, and shamelessly, promote genuinely awesome science. Andy had more confidence in me than I had in myself, he is an irreplaceable asset to developing me into the science bloke I am today (so blame him for all my future blunders).

Dr. Steven Micklethwaite – whose name I can finally spell without looking at my gmail history – cannot go without mention. This fella is the embodiment of enthusiasm. Any idea, any thought, any anything, this guy always had my back. Like a cheerleader squad entering at half-time to bolster the troops, Steve made sure I was always in good spirits. Although he by now has left us at Monash to pursue industry avenues (boo!), his support throughout my journey cannot go unmentioned. Thank you, Steve.

Office 109. Oh my… office 109. The "Jerry's apartment" of my PhD episode. I honestly don't know how we got through an entire 3.5 years without getting separated to different parts of the EAE building like naughty boys in a high school classroom. I cannot thank the denizens of this office enough for countless laughs, pranks, loud music, trash-talk, and rounds of in-office-basketball. Similarly, I cannot thank the surrounding offices enough for not filing noise complaints against us…sincerest apologies. It has been expressed by many people, at many times, that they don't understand how any work could have ever gotten done inside the dwellings of 109.Yanlu Xing and Nikk Hunter provide the fun-fueled steam engine that operates inside those walls. With a constant "good mindset leads to good work" attitude, we managed to fill the bulletin board in the hallway with proof that work can indeed get done inside the so-called "bachelors' pad". Thank you both for being exactly who you are.

The misfit group of desert-roaming, space rock enthusiasts known as the "Piney Slices" cannot go unmentioned for their integral role as being not only my first field crew in Australia, but perhaps the first group of friends I acquired during this season. Consisting of actual adults (Andy, Andrew, Marion & Nat), honours students (Sarah & Soph), and other grad-students (Mitch & Pru) you lot provided not only a monumental field season I will never forget, but genuine acceptance into my new life.

There are countless others at Monash University who deserve a shout out who I will surely forget. Helen McFarlane at the very least deserves credit for being the first Monash person to take a chance hanging out with the skinny, tattooed, funny-sounding foreigner. Dave Willis needs to be credited for drinking countless amounts of pints with me over countless discussions regarding structural geology and genuine nonsense. It is because of him that my thesis panned out the way that it did! Our mutual love for good beer and local dive-bar gigs provided a foundation for friendship that I'm sure will last a lifetime.

The opportunity to teach field mapping in Broken Hill year after year is one of the best experiences of this entire ordeal. Referred to as "Australian Christmas" by yours

truly, this time of year provides material for the special seasonal episodes in my sitcom. Spending 3 weeks at a time with the likes of Robin Armit, Laurent Ailleres, Pete Betts and Casey Blundell is something that is irreplaceable – I even learned a thing or two about structural geology! Honorable mentions go out to Matt Sisson, Lachlan Grosse, Khumo Leseane, Andrea Rielli, and the Schmidts themselves.

The geology crew at Fosterville Gold Mine are without a doubt the most enthusiastic and genuinely interested group of people I have had the pleasure to work with. Regardless of my countless wild ideas, blunders, and inquisitions they were always interested and grateful (or at least feigned it). You're all rad and I wish nothing but the best for all of you.

Speaking of enthusiasm, Chris Wilson must be thanked for both his unwavering excitment regarding every step of my PhD research, and willingness to help on any aspect, even when I comandeered his ANSTO research grant... Sorry Chris.

Emily, Silvana, and Christine have been irreplaceable in helping me do adult tasks in a office situation (although I'm still miserable at it...). These ladies have been nothing but a cheerful and helpful asset throughout my adventure, and are always good for a laugh when I needed it! Special shout outs to Christine for getting coffee stains out of my new white shirt when I missed my mouth and didn't know how to be a grown man.

Yuzhou and Rob have both been intgral in helping me adjust to my new Monash, and Australian, life. Both were there for me when I arrived to help me settle in and get accustomed to the maze of red tape that is Monash University paper work. Rob also provided me with a near infinite amount of Aussie music and comedy to help me swiftly adjust to my new (bogan) lifestyle. Hey Yuzhou, if you're reading this, have you done your research integrity form? OI COME BACK.

My partner Casey Blundell must be put on a pedestal for being the most supportive, caring, and encouraging person throughout this entire PhD struggle. Without her constant reminders of who I am, what I have done, and generally keeping me in check, I

would have crumbled long before finishing this silly book. Thank you so much.

My family back home need to be thanked for their personal sacrifice of giving up their son so he may run across the world pursuing his dreams of being a rock doctor. Their constant support and belief in my potential is second to none. Brenda, Rick and Jen, you're all the best people this world has ever made.

Speaking of back home, all the b'ys back in Newf are the most best kind b'ys that anyone could have ever asked to have in their life. Thanks for being you b'ys!

This acknowledgements section is quickly turning into a full-blown chapter that is growing tedious to anyone who is foolish enough to read it. Therefore, I would just like to thank anyone who has taken time from their life to be apart of mine. We are all just Frankenstein-style collages of people we have had the opportunity to interact with, and as such, I thank each and everyone of you personally for sculpting me into the person I am today. You're all bestkind.

Mitchell O'Mara is a living acquaintance and nothing more.

Chapter 1

Introduction

“It’ll just be like doing honours 3 times.”
-Words of an ignorant man

1.1 Orogenic Gold Systems

Orogenic Au deposits, also known as “mesothermal” or “lode-Au” deposits, are a distinct family of mineral deposits that are responsible for ~30% of the Au recovered globally through history - if their derived placer deposits are considered (Groves et al., 1998; Goldfarb and Groves, 2001; Phillips and Powell, 2015). This family of Au deposits formed in distinct periods across much of the Earth’s geological history, with peaks of formation in the Late Archean cratons, Paleoproterozoic mobile belts, and Phanerozoic orogenic fold and thrust belts (Goldfarb et al., 2001; Tomkins, 2013). Forming during convergent tectonics, these wide-spread hydrothermal systems are hosted in rocks of variable metamorphic grade involving mid- to upper-crustal temperatures and pressures between 200-650 °C and 1-5 kbar (Groves, 1993; Tomkins and Grundy, 2009). Under these conditions, the abundant episodic quartz-carbonate veining found in these deposits indicates formation from fluids that attained supra-lithostic pressures numerous times during deposit formation (Sibson, 1975; Cox, 1995). These seismic pumping or fault-valving events are widely considered a vital component of their formation. Considering the formation depth of these deposits (i.e., > 3 km from surface), there is no way to directly monitor their formation, or analogous systems, as can be done with other Au-mineralizing systems (e.g., black smokers for VMS-style deposits, Hannington et al., 2016; or geothermal hot springs for epithermal-style deposits, Pope et al., 2005). Therefore, the study of orogenic-type Au deposits provides vast and exciting grounds for academic inquiry. Here, the key characteristics that are widely accepted about the formation of orogenic deposits will be briefly discussed. For further information the reader is advised to consult comprehensive reviews such as Groves et al., (1998), Goldfarb et al., (2005), Goldfarb & Groves (2015), and Wyman et al., (2016).

Orogenic Au deposits dominantly form within metamorphic rocks in mid to shallow crustal levels (5–15 km depth), at or above the brittle-ductile transition, and in compressional tectonic settings that allow the transfer of Au-bearing fluids from relatively deeper levels (Goldfarb et al. 2005). The term “orogenic” refers to the

understanding that these deposits are associated with accretionary tectonic regimes (Kerrich & Wyman , 1990; Groves et al. 1998). This is in accordance with most deposits being hosted within greenschist facies rocks and that the accepted source for generating auriferous fluids in orogenic systems is by metamorphic devolatilization of hydrated rocks at the greenschist-amphibolite boundary (Phillips & Powell, 2010). A key aspect of this setting is that earthquakes and aftershocks control the transfer of slightly reduced, low-salinity auriferous fluids from the source to the sites of ore accumulation (e.g. Sibson et al. 1988; Robert et al., 1995; Cox 1995, 2005; Micklethwaite et al. 2010). Therefore, the formation of orogenic Au deposits is dependent on structural discontinuities, effective permeability of the system, and changes in physico-chemical conditions of the ore-forming fluid.

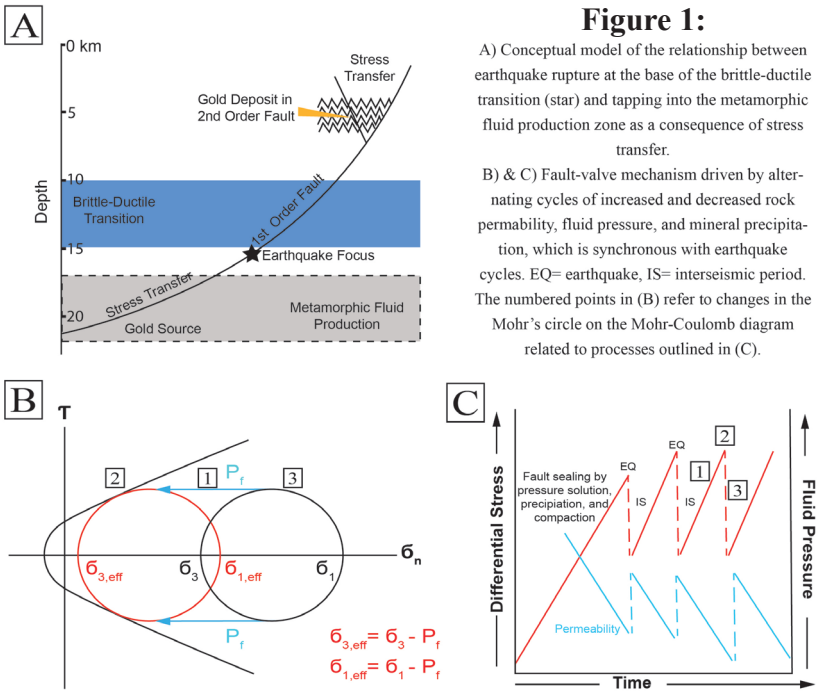

Figure 1:
A) Conceptual model of the relationship between earthquake rupture at the base of the brittle-ductile transition (star) and tapping into the metamorphic fluid production zone as a consequence of stress transfer.
B) & C) Fault-valve mechanism driven by alternating cycles of increased and decreased rock permability, fluid pressure, and mineral precipitation, which is synchronous with earthquake cycles. EQ= earthquake, IS= interseismic period. The numbered points in (B) refer to changes in the Mohr's circle on the Mohr-Coulomb diagram related to processes outlined in (C).

Structural discontinuities (e.g., brittle faults, shear zones, fold noses, competency contrasts, etc.) provide conduits for fluid flow from the source region into discrete sites of precipitation in the upper crust. The fault systems that host orogenic deposits behave episodically, alternating between cycles of increased and decreased fluid pressures and permeability, which is attributed to the earthquake cycle (Fig. 1) (Sibson et al., 1988). Differential stress changes combined with metamorphic fluid release act together to trigger periodic brittle failure in the gold source region (Fig. 1),

allowing rapid fluid extraction along fracture networks into traps for mineralisation. This is due to increases in fluid pressures reducing the amount of differential stress needed to cause failure along a fault plane, potentially triggering an earthquake (Fig. 1) (Sibson et al., 1988). Then ensues a period of seismicity whereby instantaneous increase in rock permeability allows for pervasive fluid flow into many small faults in the periphery of the system, which rupture as aftershocks, creating numerous localised drops in effective fluid pressure. Post-rupture, during the inter-seismic period, mechanisms such as mineral precipitation, compaction, and pressure-solution promote sealing of fault surfaces leading to a new period of fluid-pressure increase until the next failure event. This fault-valving mechanism allows for large volumes of ore-forming fluids to be flushed along narrow, interconnected faults and fractures and become concentrated in depositional sites thereby forming orogenic Au deposits.

The most productive Au fields in metamorphic terranes are linked to major crustal structures, however the Au deposits themselves are not directly hosted within them (Goldfarb, 2005). Although fluid migration is structurally controlled, fluid evolution which destabilizes Au and other metals, must be influenced by the chemistry of the system. For example, pressure and temperature changes experienced by hydrothermal fluids that rapidly ascend from deep crustal levels into shallow depths should significantly change the solubility of Au and other elements. However, if this were the case then Au deposits would form on large crustal-scale faults where the greatest changes in pressure and temperature occur. Instead, orogenic deposits are mostly found on 2nd and 3rd order faults where there is a greater capacity for long-lasting fluid-rock interaction (e.g., Micklethwaite et al. 2010), and Au precipitates in particular mineralogical and geochemical domains. Therefore, reactions during fluid-rock interaction must be critical for deposit formation and many mechanisms have been proposed for the precipitation of orogenic Au ores.

Hydrogen sulphide complexes are the dominant ligands for Au transportation in hydrothermal fluids that form orogenic deposits (William-Jones et al., 2009; Phillips and Powell, 2011). Two fundamental conditions that govern maximum Au solu-

bility in these fluids are near-neutral fluid pH and an oxygen fugacity at and just below the sulphate-sulphide boundary (Fig. 2). Therefore, changes in the redox state and acidity of auriferous fluids is important for Au-forming reactions, as well as processes that consume sulphur, thereby stripping the Au-stabilising ligand from the fluid phase causing Au to precipitate. Gold mineralisation in orogenic deposits commonly occurs as either native Au particles or within sulphide minerals. Consider the reactions:

$$Au + (HS)^- + H^+ + O_2 \rightarrow Au(HS)^0 + \tfrac{1}{2}H_2O \quad (1)$$

$$Au + 2(H_2S) + \tfrac{1}{4}O_2 \rightarrow Au(HS)_2^- + H^+ + \tfrac{1}{2}H_2O \quad (2)$$

$$Au(HS)_2^- + Fe^{2+} \rightarrow FeS_2 + Au + 2H^+ \quad (3)$$

$$Au(HS)_2^- + FeO \rightarrow FeS_2 + Au + H_2O \quad (4)$$

In reactions (1) and (2), if the activity of HS^- or H_2S decreases then Au will precipitate from the fluid phase. Reactions (3) and (4) show that Au is destabilised from the fluid as S is consumed during the formation of pyrite, leading to the precipitation of Au within the sulphide mineral, as well as changes in fS_2 and fO_2. The significance of sulfidation to Au precipitation depends on the reactivity of Fe in the host rock to HS^- in the fluid phase. Therefore, rock types of a specific chemical composition are more favourable for hosting orogenic Au deposits via this mechanism. In general, lithologies with high Fe/Fe + Mg ratios are ideal for forming Au from sulfidation reactions (Böhlke, 1988), such as iron formations (e.g., Phillips et al., 1984), tholeiites (e.g., Phillips & Groves, 2007) and ferruginous shales (e.g, Hofstra et al., 1991).

Contrary to the above, there may be several mechanisms whereby native Au is deposited without consumption of S^- being directly linked to the mineralisation of sulphide minerals. Phase separation, evidenced by observations of co-existing liquid- and vapour-rich inclusions in orogenic quartz veins, has been suggested to partition HS^- from auriferous fluids into the vapour phase (Naden & Shepherd, 1989). In carbonaceous rocks, the generation of CH_4 and CO_2 by the interaction of hydrothermal fluids with graphite can occur by:

$$2C + 2H_2O \rightarrow CH_4 + CO_2 \quad (5)$$

This is significant because in the graphite-saturated C-O-H-S (GCOHS) system, addition of small amounts of CH_4 (≥ 5 mol %) expands the immiscibly field dramatically over a wide range of pressure and temperatures, and H_2S will partition into the vapour phase (Naden & Shepherd, 1989). This would result in Au precipitation by the reverse of reactions (1) and (2). Phase separation is further enhanced by the cyclic fluid pressure decreases associated with the earthquake cycle (Sibson et al., 1988; Wilkinson & Johnston, 1996). Indeed, numerous models have attributed Au deposition in orogenic systems to fluid pressure fluctuations that can change fluid chemistry (Sibson, 1987; Sibson et al., 1988; Wilkinson & Johnston, 1996; Gaboury & Daigneault, 2000; Weatherley & Henley, 2013), although not all are widely accepted (Craw, 2013).

Precipitation of native Au is not solely dependent on sulphur fugacity, reactions involving pH changes are also widely considered to be critical for the formation of orogenic Au deposits (Fig. 2). The CO_2 that is ubiquitous in neutral pH orogenic fluids should coexist with small proportions of carbonic acids (H_2CO_3, HCO^-, CO^-), which act as pH buffers for Au transport (Phillips & Evans, 2004). Phase separation (i.e., separation of H_2O and CO_2) can also cause significant fluctuations in pH leading to the deposition of free Au (Fig. 2) (e.g., Fougerouse et al., 2016; Kaszuba et al., 2006). Phanerozoic orogenic Au deposits are most commonly hosted in turbidite packages that are rich in phyllosilicate minerals, which have the capacity to buffer ore-forming fluids to a relatively low pH (Williams-Jones and Normand 1997). Additionally, hydrolysis of carbonaceous material found in these shale packages can lower pH by reaction (5) (Williams-Jones and Normand 1997). Finally, precipitation of sulphide minerals, such as pyrite and arsenopyrite, can cause fluid acidification by the release of H^+ ions during formation, e.g. equation (3), shifting Au solubility in the fluid phase (Fig. 2).

Reactions involving changes in fO_2 have also been suggested to induce Au precipitation in orogenic systems (Fig. 2) (e.g., Phillips & Gibb, 1993). Hematite

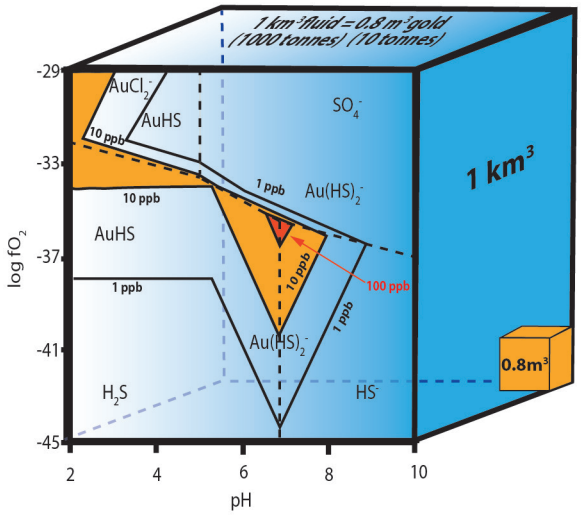

Figure 2: Gold solubility (in parts per billion; solid lines) and speciation at 500 bar and 250°C as a function of log fO_2 and pH in a solution containing 1 m NaCl with ΣS = 0.01 m. The dashed lines separate regions of predominance of H_2S, HS^-, SO_4^{2-} and HSO_4^-. Modified from William-Jones et al., (2009). Large blue box represents 1 km3 volume of fluid (1000 tonnes) required to form 0.8m3 of gold (10 tonnes), which is represented by the small yellow box.

is an alteration product in some goldfields (e.g., Kalgoorlie). Under hematite-stable conditions sulphur in solution is present in the oxidized form as SO_4^{2-}, rather than the reduced sulphur needed to transport Au (Phillips & Powell, 2010). Evolution of an auriferous fluid into the field of hematite stability would drive equations (1) and (2) to the left by decreasing the amount of reduced sulphur in the fluid needed to carry Au in solution. Fluid oxidation driven by phase separation has been proposed for the formation of orogenic Au deposits in the Yilgarn belt of Western Australia (Hodkiewicz et al., 2009). Similar to the discussion above, during phase separations reduced gas species such as H_2S, H_2 and CH_4 preferentially partition into the vapour phase (Naden & Shepherd, 1989). When this occurs, the residual Au-bearing fluid undergoes a relative increase in the SO_4/H_2S ratio, leading towards more oxidizing fluid conditions and thus destabilizing Au. If the auriferous fluid evolved close to the sulphate-sulphide boundary during generation or transport to begin with, then even small increases in fO_2 could lead to Au precipitation (Fig. 2). Fluid reduction is particularly important in fluid-rock reactions involving rocks that contain reduced carbon (Connolly & Cesare, 1993), such as black slates in Phanerozoic deposits (e.g., central Victorian goldfields) or localised carbonaceous shales in Archean deposits (e.g, Kalgoorlie). As little as a few percent of graphite can chemically reduce large volumes of Au-sulphide complexes in infiltrating fluids without exhausting the carbon content of the host rock (Phillips & Powell, 2010).

In conclusion, during the evolution of a mineralised orogenic fault system, large earthquake events rapidly introduce deeply sourced fluids into the shallower crust (Fig. 1). These fluids may be in an Au-saturated or supersaturated state, or they may saturate at the sites of deposition where the processes discussed above occur. However, Au then precipitates wherever there is the greatest local chemical potential; e.g., within or on the surfaces of sulphides, or in fracture networks permitting interaction of the fluid with graphite. In general, understanding orogenic Au systems requires integration of many sub-disciplines of geology, and, as I will show in this thesis, other fields of science, in order to obtain a holistic view on their formation and advance exploration models for their discovery.

1.2 Geology of Central Victoria

Eastern Australia is composed of a series of geologic terranes, known as the Tasmanides, that were accreted to the Paleo-Pacific margin of Gondwana during the Paleozoic (VandenBerg et al., 2000; Willman et al., 2010; Phillips et al., 2012). The terranes that make up the Tasman Fold Belt System include the Delamerian, Lachlan, and New England Orogens (Fig. 3). The Lachlan Orogen forms the remnant of a Paleozoic subduction-accretionary system consisting of various oceanic tholeiites, turbiditic sandstone and mudstone sequences, as well as arc-related volcanics (VandenBerg et al., 2000; Cayley et al., 2002; Gray & Foster, 2004). It is also believed that this orogenic belt contains fragments of Neoproterozoic continental crust that have been underthrust into the system from the Selwyn Block during late-stage collisional tectonics (Willman et al., 2010; and references therein). Pilia et al. (2015) used Bayesian transdimensional tomography to highlight these exotic continental fragments and their effect on the development of the accretionary orogen. The Lachlan Orogen itself has been divided into western, central, and eastern sub-provinces, where the western sub-province is host to almost all of the orogenic gold-style mineralisation in Victoria (Phillips et al., 2012).

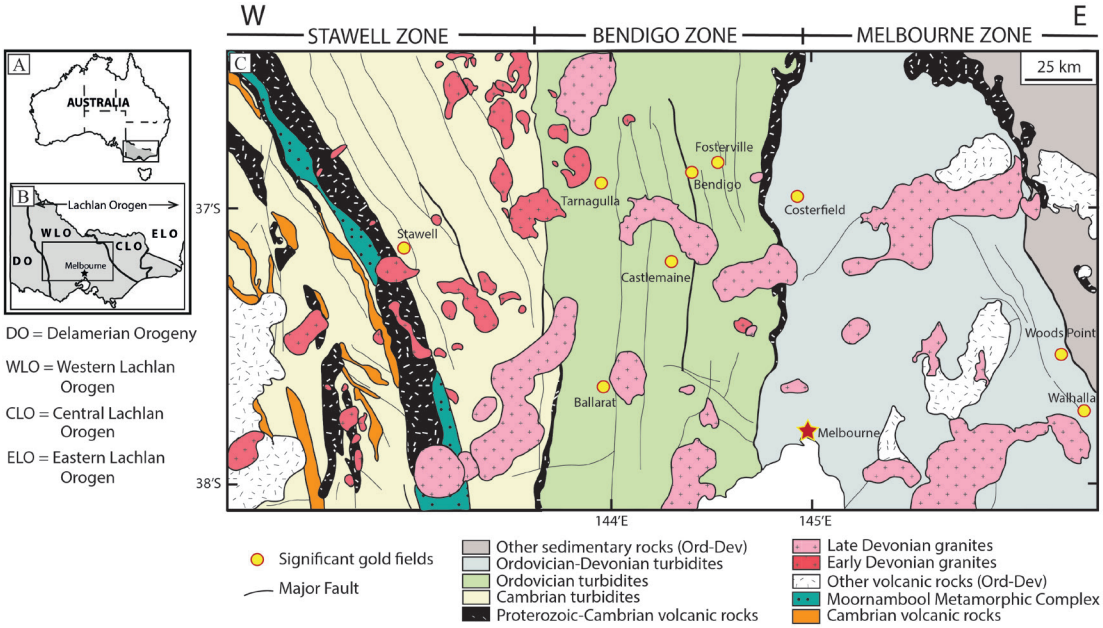

Figure 3:A) Schematic of map Australia with the state of Victoria highlighted in grey, and the position of B indicated. B) The locations of the Lachlan and Delamerian Orogens in a map of Victoria (modified from Willman et al., 2010), and the position of C is indicated. C) Simplified geological map of central Victoria modified from Phillips et al. (2012). Yellow circles indicate the major goldfields.

1.2.1 Western Lachlan Orogen

The Western Lachlan Orogen is defined by ~12km thick, Cambrian to Silurian turbidite sequences, that overlie a ~25km thick Cambrian basement of oceanic mafic volcanics (VandenBerg et al., 2000; Gray & Foster, 2004). This sub-province is also host to post-tectonic granitic plutons and their associated lithologies that intruded throughout the Devonian (Paterson et al., 1990; Tobisch & Paterson, 1990). The sedimentary and volcanic rocks have undergone sub-greenschist to amphibolite facies metamorphism and were strongly deformed into dominantly north-south trending chevron folds that are cut by thick-skinned thrust systems (VandenBerg et al., 2000). The Western Lachlan Fold Belt is further sub-divided into three major lithological/structural zones, the Stawell, Bendigo, and Melbourne Zones, which are separated by north-south striking, high angle reverse faults (Fig. 4) (VandenBerg et al., 2000). Cayley et al., 2011).

1.2.2 The Stawell Zone

The Stawell Zone is the westernmost sub-division of the Western Lachlan

Orogen. It is bounded in the west by a major crustal-scale fault known as the Moyston Fault, which is thought to extend down as far as the mohorovicic discontinuity, and to the east by a listric reverse fault known as the Avoca fault (Figs. 3 & 4). The Avoca fault has been interpreted to extend to a depth of 22km where it intersects the Moyston Fault, forming a V-shaped geometry (Fig 4) (Willman et al., 2010; Cayley et al., 2011). The Stawell Zone is consists of Cambrian mafic volcanics, with secondary interbedded sedimentary rocks, that are conformably overlain by Cambrian and Ordovician, quartz-rich, deep-marine turbidites that belong to the St. Arnaud Group (Squire et al., 2006; Cayley et al., 2011). Early Silurian granitic plutons can be found in the western Stawell Zone and Late Devonian granites are located in the southeast (Cayley et al., 2011). The dominant rock exposures in this area are of the St. Arnaud Group, which are now sub-greenschist grade meta-turbidites that have been folded into upright, NNW-SSE striking, chevron folds (Squire et al., 2006). The largest exposure of mafic rocks in this area exist along the hanging wall of the Moyston Fault within the Moornambool Metamorphic Complex. This complex hosts interlayered mafic volcanics and turbidites that have been highly deformed and metamorphosed under greenschist to amphibolite facies conditions (Phillips et al., 2002; Squire et al., 2006). The Stawell Zone is host to numerous gold districts, including the Stawell, Magdala, Wonga, Fiddlers Reef, and Linton Reef deposits, among others (Fig. 3) (Sandiford & Keays, 1986; Wilson et al., 1999; Miller & Wilson, 2002 ; Phillips et al., 2012).

1.2.3 The Bendigo Zone

Although the Stawell and Bendigo Zones are considered separate entities, they share similar stratigraphic and structural features. The Bendigo Zone is bound by two steeply dipping reverse faults, the Avoca Fault to the west and the Mt William Fault, belonging to the Heathcote Fault Zone, to the east (Figs. 3 & 4) (Willman et al., 2010; Cayley et al., 2011). This zone also contains a basement composed of Cambrian mafic volcanics/volcaniclastic rocks, similar to the Stawell Zone, but is overlain by a thick sequence of Ordovician turbiditic sandstones and mudstone belonging to the Castle-

maine Group (VandenBerg et al., 2000). The relationship between the mafic basement rocks and the turbidites can best be seen in the Heathcote Fault Zone, where the Castlemaine Group conformably overlies interbedded Cambrian boninites and tholeiites (Cayley et al., 2011). Late Silurian to Early Devonian granitic intrusions are located in the northwest of the Bendigo Zone, and Middle to Late Devonian granites can be found throughout (Chappell & White, 1992). The volcanic and sedimentary sequences have been deformed into chevron folds, which have north-south axial trends, and were metamorphosed at greenschist facies conditions (Phillips et al., 2012). It is believed that the Stawell and Bendigo Zones originated as ocean backarc successions, and although there are differences in timing and orientation of deformation, they both appear to belong to a single, east-vergent, fold and thrust belt system (Gray et al., 1998; Gray et al., 2004; Cayley et al., 2011). Phillips et al. (2003) estimated that ~80% of historic gold production from Victoria was derived from the Bendigo Zone. This zone is host to major goldfields such as the Bendigo, Ballarat, Castlemaine and Fosterville goldfields, among others (Fig. 3) (Phillips et al., 2012).

1.2.4 The Melbourne Zone

The Melbourne Zone is the eastern most sub-division of the Western Lachlan Orogen and is uniquely distinguishable from the rest of Victorian geology. This zone is bound between the Mt William Fault to the west and the Wellington Fault to the east (Figs. 3 & 4) (VandenBerg et al., 2000; Gray et al., 2003). Host to a conformable succession of marine sediments, which remain unbroken from the Ordovician to the Early Devonian, the Melbourne Zone is primarily composed of the Murrindindi Supergroup, which overlies Ordovician black shales and localised Cambrian calc-alkaline volcanics (VandenBerg et al., 2000; Willman et al., 2010; Cayley et al., 2011; Phillips et al., 2012). Beneath the Melbourne Zone the Proterozoic crust of the Selwyn Block is located below a major décollement (Moresi et al., 2014). The Melbourne Zone sedimentary successions have been metamorphosed to sub-greenschist facies and deformed into north-south trending, shallowly plunging chevron folds. It

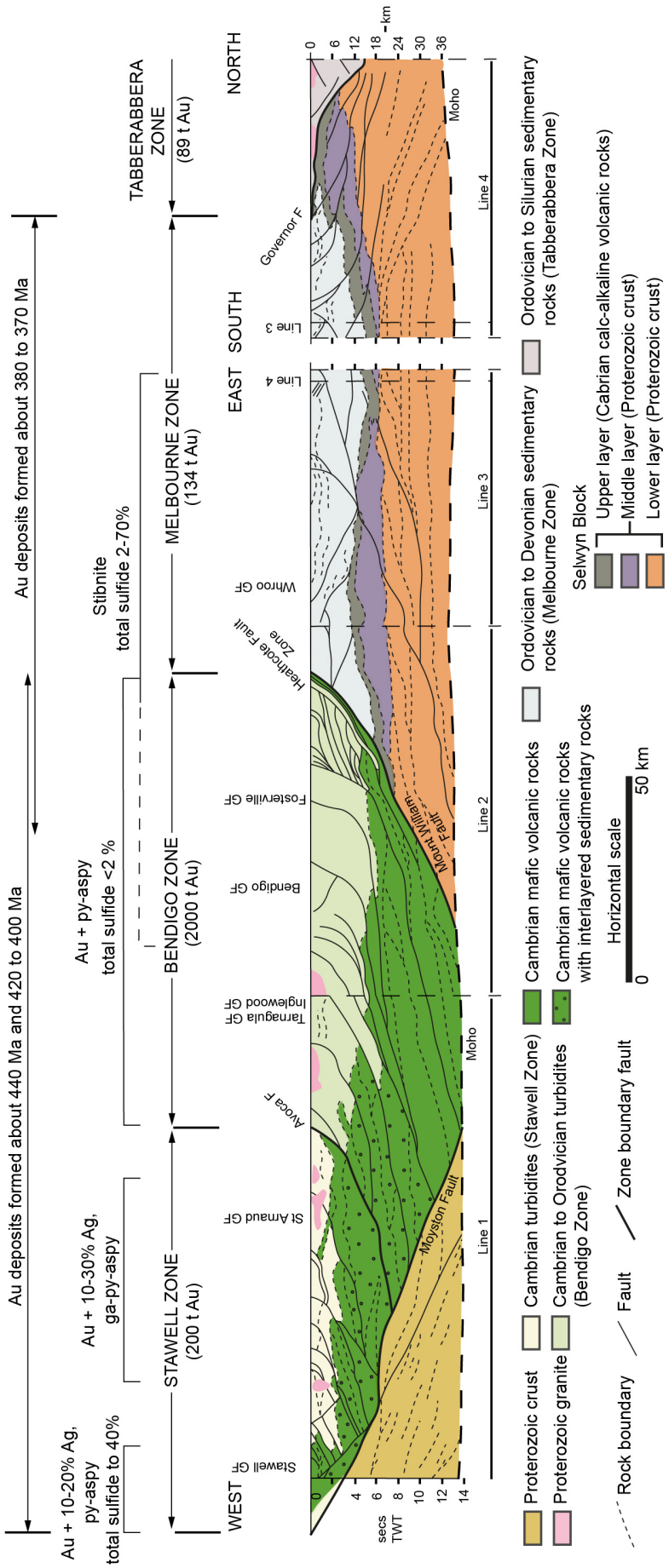

Figure 4: Interpreted cross section of the Western Lachlan Fold Belt via seismic lines. From Willman et al. (2010).

is thought that the lower metamorphic grade of this zone may be due to the stability provided by the existence of underlying Selwyn Block fragments beneath this area (Cayley et al., 2002, 2011). The Melbourne Zone contains Late Devonian granitic plutons, as well as Middle Devonian dyke swarms that vary in composition from felsic to mafic, such as the Woods Point dyke swarm (Richards & Singleton, 1981). Based on stratigraphic, structural, and sedimentary features, it is thought that the Melbourne zone may have formed as a foreland basin to the uplifted Bendigo Zone (Cayley et al., 2002, 2011). Historic gold production was largely from the Woods Point and Walhalla goldfields, but minor deposits also include Nagambie, Costerfield and Mount Piper (Fig. 3) (Phillips et al., 2012).

1.3 Gold Mineralisation of Central Victoria

Victoria has been one of the world's leading gold producers and is responsible for contributing 2% of all the gold ever mined globally (Phillips et al., 2003). The Victorian gold province is a principal example of the "slate belt" gold deposit type, which is a grouping referring to any slate-, turbidite-, shale-, and/or greywacke-hosted, orogeny-related gold mineralisation. Extensive work has been done to describe the structure, mineralogy, timing, and origin of gold deposits located in Central Victoria, and although much of the data have been accepted, other attributes are still debated (e.g. source reservoir of gold-bearing fluids and deposit genesis). Nevertheless, such characteristics described in previous work will be discussed below.

Goldfields in Victoria are clustered along regional north-south trending structures within Paleozoic, dominantly sedimentary rocks (Phillips & Hughes, 1996; Phillips et al. 2003). It is believed that gold field clusters around major fault zones depict shallow expressions of lower crustal fluids that were channelised along these deep seated faults (Hughes & Phillips, 1997). On a deposit scale, ore bodies seem to be associated with local structures (i.e., upright chevron folds and reverse fault zones on the scale of kilometers to tens of kilometers), which act as traps for mineralising fluids. Although the early Paleozoic turbidites host almost all of the Victorian gold

deposits, metamorphosed mafic volcanics, high-grade schists and gneisses, felsics and mafic dykes, felsic volcanics, and red beds have also been observed to host gold mineralisation to a lesser extent (Hughes & Phillips, 2015). Gold occurs in two main styles, 1) free gold within quartz veins associated with brittle-ductile shear zones, saddle reefs, and faults (e.g. Bendigo), and 2) refractory gold locked into fine disseminated pyrite and arsenopyrite crystals throughout the wall rock proximal to veining (e.g. Fosterville) (Hughes & Phillips, 2015). In the former, coarse arsenopyrite (up to 2cm) and pyrite (up to 0.5cm) are also disseminated in the wallrock, but do not contain gold.

1.3.1 Ore Assemblages and Mineralogical Domains

Non-genetic classifications have been assigned to the various gold mineralisation styles of central Victoria by Hughes et al. (1997), Bierlein et al. (2001a), and Phillips et al. (2003). These classifications are based upon ore mineralogy, geochemistry, as well as alteration assemblages, and include 1) 'pyrite-arsenopyrite' type gold deposits; 2) 'pyrite-arsenopyrite-stibnite' gold deposits; and 3) 'polymetallic', intrusion-related gold deposits.

The 'pyrite-arsenopyrite' classification is the most common throughout Victoria and deposits with this character are prevalent in the Stawell and Bendigo Zones. Deposits that fall under this classification occur in the Stawell-Magdala, Ballarat, Bendigo, and Castlemaine goldfields, and there are many small more isolated deposits (Fig. 3) (Phillips et al., 2003). In this style of mineralisation, gold typically occurs as coarse particles hosted within laminated quartz veins related to chevron-style folding of turbidites or dilation structures; the world's largest gold nuggets come from these deposits. Mineralisation is often sulphide poor (<2%) and coarse gold grains in quartz are spatially associated with enrichment in pyrite, arsenopyrite, and trace amounts of galena, sphalerite, chalcopyrite +/- pyrrhotite (Phillips et al., 2003, Phillips et al., 2012).

The Melbourne Zone and eastern Bendigo Zone are host to the 'pyrite-arseno-

pyrite-stibnite' style of gold mineralisation, where elevated amounts of Sb occur along with Au and As (Fig. 3). The Costerfield and the Fosterville deposits are examples of mineralisation of this fashion. Here, gold is present as finely disseminated particles and as refractory Au within pyrite, arsenopyrite, and aurostibite grains that are hosted by, or associated with, stibnite-bearing, quartz-carbonate stockwork veins (Phillips et al., 2003, Phillips et al., 2013). Stibnite is commonly present as fine veins or disseminations throughout quartz-carbonate veins, but has occurred in some areas as massive veins up to tens of centimeters thick (e.g. Costerfield) (Phillips et al., 2003). Trace amounts of galena, sphalerite, chalcopyrite, berthierite and pyrrhotite are commonly found associated with this style of mineralisation. Foster et al. (1998) and Bierlein et al. (2001a) suggested that gold in this association may be temporally associated Late Devonian felsic magmatism.

Bierlein et al. (2001a, 2001b, 2001d) described the 'polymetallic' gold mineralisation in Victoria, where elevated levels of Sb, W, Mo, Cu, Te +/- Bi are diagnostic of a distinct period of gold precipitation. These enrichments were attributed to Early and Late Devonian magmatism throughout the Western Lachlan Orogen that emplaced the dykes and plutons (Bierlein et al. 2001a; 2001b; 2001d). Deposits formed primarily by these processes are typically small (e.g., Wonga, Maldon, Leven Star, Myrtle Creek) and are less economic compared to their metamorphism-associated counterparts. However, it is thought that this intrusive activity may have been responsible for remobilising and concentrating metals into structures, as well as providing new pulses of mineralisation, which could have enriched previously existing gold deposits (Bierlein et al., 2001a). The 'polymetallic' mineralisation style is most prominent in the Melbourne Zone, but has also been considered for the Wonga deposit in the Stawell Zone, as well as the Fosterville and Maldon deposits in the Bendigo Zone (Fig. 3) (Bierlein et al., 2001b).

1.3.2 Timing of Gold Mineralisation

Attempts to constrain the timing of gold mineralisation in central Victoria using the $^{40}Ar/^{39}Ar$, U-Pb, and Re-Os isotopic methods, as well as traditional cross-cutting and field relationships. Gold is generally believed to have been introduced in three main events, at ca 450-435 Ma, 420-400 Ma, and 380-370 Ma (Fig. 3) (VandenBerg et al., 2000; Arne et al., 2001 ; Bierlein et al., 2001; Phillips et al., 2003; and others). These three mineralising episodes share temporal links with significant events in the orogenic history of the Western Lachlan Fold Belt.

The first gold mineralisation episode (450-435 Ma), with most notable activity at 440 Ma, occurred during the Benambran Orogeny (Fig. 4) (VandenBerg et al., 2000; Bierlein et al., 2001; Phillips et al., 2003). Widespread throughout the Stawell and Bendigo Zones, the most productive gold deposits in Victoria (e.g., Stawell, Fosterville and Bendigo) are associated with this mineralisation event. It is believed that during stages of crustal shortening and heating related to the Benambran Orogeny, regional scale metamorphism and deformation produced hydrothermal ore-bearing fluids from a large crustal reservoir and concentrated them within host structures (Vandenberg et al., 2000; Bierlein et al., 2001; Phillips 2012).

The second mineralisation event (420-400 Ma), is thought to be a minor episode, and gold deposits related to this event are constrained to the Stawell and western Bendigo Zones (Fig. 4) (Phillips, 2012). This episode is thought to be related to the onset of magmatism during the waning stages of the Benambram Orogeny, in which extensive melting of structurally thickened crust lead to widespread plutonism (Vandenberg et al., 2000, Bierlein et al., 2001). ‘Polymetallic’ deposits enriched in Sb, W, Mo, Cu, Te, Bi, and perhaps even the so-called ‘pyrite-arsenopyrite-stibnite’ type deposits, are believed by some to be genetically related to, or at least enriched by, this 420-400 Ma gold event (Bierlein et al., 2001).

The third and final gold episode (380-370 Ma) is related to the Tabberabberan Orogeny and post-tectonic plutonism (Fig. 4) (VandenBerg et al., 2000; Bierlein et al.,

2001). Mineralisation of this period is distinctively antimony-rich – the 'pyrite-arsenopyrite-stibnite' type mineralisation – and can be found throughout the Melbourne Zone and parts of the eastern Bendigo Zone. In this major gold mineralisation event, the heat generation associated with partial melting of the crust (to produce the granites) is thought to have been the driver for metamorphic fluid generation related to gold deposit formation (Phillips et al., 2003; Willman et al., 2010).

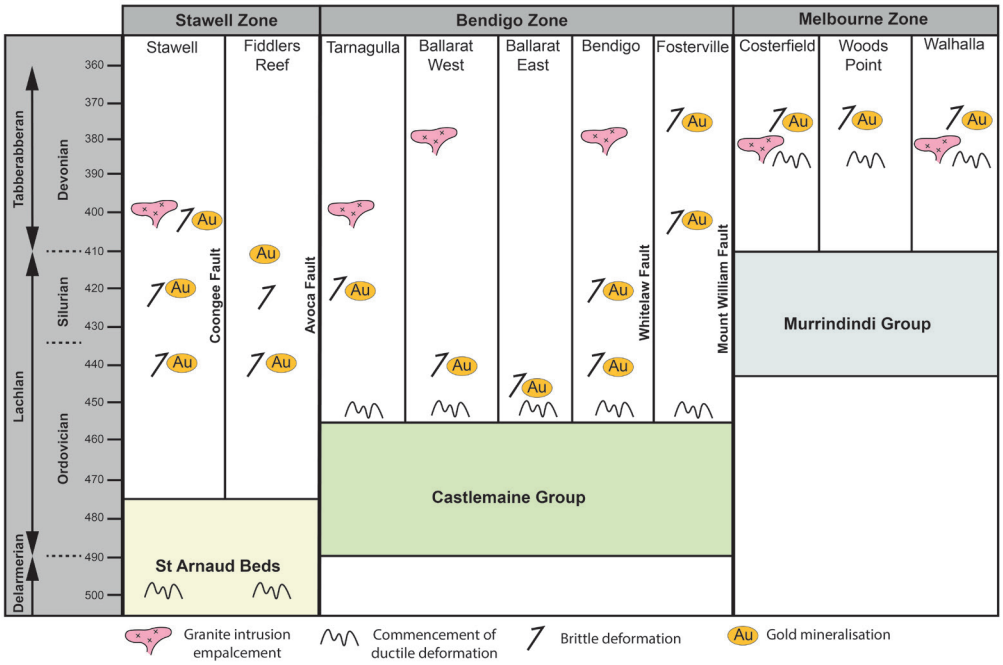

Figure 5: Schematic time-space summary of stratigraphy, deformation, magmatism, and mineralisation for significant Victorian Au deposits, south east Australia. The late stage (~380 Ma) mineralisation for Fosterville is interpreted in this manuscript.

1.3.3 Genesis & Source of Gold-Bearing Fluids

The ore genesis of Victorian gold deposits is a topic that is still debated in the literature. To date, there are two models for the source of gold-bearing fluids in metamorphic belts: 1) metamorphic rocks that liberate gold-bearing fluids as temperature increases across the greenschist-amphibolite facies transition; and 2) felsic-intermediate magmas that exsolve gold-bearing hydrothermal fluids during emplacement. Magmatic-hydrothermal gold deposits are commonly enriched in Cu, Mo, Sb, Bi, As, Te, W, Pb, Zn, and Ag (Goldfarb et al., 2005). This is because intrusion-related deposits form from high-temperature (>550°C), high-salinity magmatic waters that are

capable of mobilising suites of transition metals, in addition to gold, as chloride complexes (William-Jones et al., 2009). In comparison, most orogenic gold deposits are enriched in only As and Ag, and are formed from moderate-temperature (250-350°C), low-salinity, metamorphic fluids that contain enough S to mobilize Au as bisulphide complexes, but insufficient Cl to transport much base metals (Phillips & Groves, 1983 ; William-Jones et al., 2009). Most gold deposits in central Victoria fall into this "gold-only" group and are therefore believed to have formed from metamorphic fluids (Wilson et al., 2013). Here, most intrusive activity post-dates periods of significant gold mineralisation. Moreover, the "polymetallic" deposits that are thought to be associated with magmatism are minor in comparison to their gold-only counter-parts.

Geochemical studies on a number of deposits throughout Victoria suggest the same theory for their formation. An investigation of C, O, and S stable isotopes by Bierlein et al. (2004) on alteration haloes associated with gold deposits in the Stawell, Percydale, Ballarat, Bendigo and Fosterville goldfields implied extensive interaction between the sedimentary wall rock and an externally derived hydrothermal fluid which is indicative for a distal fluid source reservoir. Although the metamorphic source model is accepted for the majority of Victorian gold deposits, there is still debate about whether hydrated, pyrite-bearing mafic rocks of the deeper crust of Victoria, or pyritic carbonaceous sedimentary turbidites of the overlying sedimentary successions were the source of the fluids and gold (Pitcairn et al. 2006; Phillips & Powell 2010; Large et al. 2009; Tomkins 2010; Tomkins 2013; Wilson et al. 2013; Pitcairn et al. 2015). Cambrian basement mafic volcanic sequences were early considered to be the most likely source for Victoria's gold (e.g., Glasson & Keays, 1978; Phillips & Groves, 1983; Phillips & Powell, 2010). Elmer et al. (2006) show that mafic volcanic rocks are capable of producing large volumes of the metamorphic hydrothermal fluids that are needed to carry gold in solution. If a body of rock contains a sufficient amount of gold throughout its volume that it may be leached and mobilized, it is considered to be "fertile" with respect to gold. It has been suggested that the Cambrian volcanic successions beneath Victoria are indeed "fertile" and the likely source for auriferous

fluids (Glasson & Keays, 1978; Bierlein et al., 1998). This was shown in a study by Bierlein et al. (1998b) who found up to 5 ppb Au in the underlying tholeiitic basalts, and up to 67 ppb Au in the interbedded sediments that accompanied them as part of this volcano-sedimentary package. Based on mineral equilibria (Yu et al. 2012)modelling, Elmer et al. (2008) suggested that the Stawell deposit formed from mineralising fluids derived from these metamorphosed Cambrian successions.

However, noble gas and halogen analyses by Fairmaid et al. (2011) provided evidence for at least two fluid reservoirs: 1) a deeply sourced fluid which is compatible with metamorphic devolatilisation of altered basalts; and 2) a sedimentary component, which may have resulted from fluid-rock interaction or mixing with sedimentary formation waters. Fluid inclusion work by Yu et al. (2012) across eight deposits in central Victoria similarly concluded that there was evidence of sedimentary involvement during gold mineralisation, but fluids were likely derived from basement mafic volcano-sedimentary rocks. A fluid inclusion study done on quartz veins from the Bendigo deposit by Wilson et al. (2013) concluded that there was little evidence for an association between original metal content in the metasedimentary host rocks and the gold mineralisation. It was suggested that gold was externally derived from a deep source that utilised fault systems as a conduit to become focused in discrete depositional sites.

In more recent years, evidence that pyritic carbonaceous sedimentary rocks are suitable source rocks for producing auriferous hydrothermal fluids has grown. Thermodynamic calculations done by Tomkins (2010) demonstrated that metamorphism of pyritic carbonaceous sedimentary rocks can produce one to two orders of magnitude more H_2S than mafic rocks. Gaboury (2013) studied fluid inclusions from world-class Mesoarchean to Cretaceous orogenic gold deposits and found that C_2H_6 was sourced from degraded organic matter in arsenian pyrite-bearing sedimentary rocks, perhaps explaining why CO_2-rich are associated with economic gold districts. Laser ablation inductively coupled plasma mass spectrometry (LA-ICP-MS) on diagenetic and biogenic pyrite grains in sedimentary rocks near the Bendigo gold deposit revealed

that these contain elevated Au, Ag, As, as well as other elements, compared to mafic rocks (Large et al., 2009; 2011; Thomas et al., 2011). Pyrrhotite found nearby contains Ni and Co levels similar to that of the diagenetic pyrite, but depleted levels of Au and As (Thomas et al. 2011). These authors concluded that these biogenic/diogenetic pyrites likely became the source of Au, As, and S when converted to pyrrhotite during metamorphism, releasing these elements into a fluid phase. Whole rock analyses of the Otago and Alpine schists in New Zealand (a turbiditic sequence of greywackes and pelites) revealed that metamorphism led to depletion of Au, Ag, As, Sb, Hg, Mo, and W (Pitcairn et al., 2006). The same suite of elements was found to be enriched in the orogenic gold deposits in Otago. Further investigation revealed that the depletion was caused by the disappearance of pyrite, galena, sphalerite, and cobaltite across the greenschist-amphibolite boundary. Pitcairn et al. (2006) concluded that leaching of these metasediments by a metamorphic fluid, produced due to dehydration reactions at the greenschist-amphibolite boundary, is likely to have formed the Otago gold deposits. Pitcairn et al. (2015) duplicated this study on metabasaltic rocks associated with the Otago and Alpine schists, which are interpreted to be accreted fragments of subducted oceanic crust. Average gold concentrations of the metabasalts did decrease as metamorphic grade increased from greenschist to amphibolite facies, in similar amounts to those observed in the metasediments. However, arsenic concentrations increased as metamorphic grade increased, indicating that mafic rocks act as a sink for this element. Also, Sb and Hg concentrations remained similar to those in the unaltered basaltic protoliths. It was concluded that metasedimentary rocks are a more likely source rock for fluids and metals responsible in the formation of orogenic gold deposits, considering that they exhibit mobility of all elements enriched in this style of deposit during metamorphism.

In a model presented by Large et al. (2011), gold and arsenic are introduced into carbonaceous shales and turbidites in a reduced basin setting during diagenesis and are later concentrated into ore grades by hydrothermally and structurally controlled processes. Similarly, Tomkins (2013) suggested that bacterial sulfate reduction should

produce Au-bearing sedimentary pyrite in the oxygenated Phanerozoic oceans, potentially providing a partial explanation for the temporal variations in orogenic gold mineralisation.

Regardless of the preferred source rock, all models agree that reduced, low salinity, H_2O-CO_2-rich hydrothermal fluids were generated by metamorphic devolatilisation processes and carried the gold as hydrosulphide complexes [$Au(HS)_2^-$ and Au(HS)] (Phillips et al., 2012; Tomkins, 2013). Gold is then precipitated via physiochemical processes involving seismic pumping, fault valve action, and extensive interaction with iron-bearing or carbon-rich wall rocks, or changes in fluid pH and/or oxygen fugacity (Sibson et al., 1988; William-Jones et al., 2009). This mechanism is known to be active in mid to shallow crustal levels (5–15 km depth) in compressional settings, such as accretionary or collisional orogens, that facilitate the transfer of gold-bearing fluids from deeper levels of the crust to shallower levels where they may be deposited (Goldfarb et al., 2005; Phillips & Powell 2009; Tomkins, 2013).

However, the metamorphic devolatilisation model is not universally accepted for all of the gold deposits in central Victoria. As mentioned previously, it was suggested by Bierlein et al. (2001a) that deposits which existed in the contact aureoles of magmatic plutons may have been augmented by this intrusive activity. Moreover, it is proposed that other deposits which appear to be spatially and temporally associated with magmatism are genetically related to these events and owe their mineralisation to them (Bierlein et al., 2001b; Bierlein & McKnight, 2005). Such “intrusion-related” deposits include the Malmsbury, Myrtle Creek, Mount Piper, and the Wonga deposits. In contrast to typical Victorian style orogenic gold deposits, these are characterized by disseminated and/or stockwork-style mineralisation and enrichments in Au ± Mo-W-Bi-Te-Cu as well as various types of alteration such as, sericitization, sulfidation, silicification, carbonatization and tourmalinization. Furthermore, Hough et al. (2007) suggested that the Devonian Woods Point-Walhalla gold deposits are also magmatic in origin and are genetically related with mafic to intermediate dyke swarms in the area. Jowitt et al. (2012) investigated the Morning Star dike, a gabbro-diorite dike

that has produced ~28 tonnes of hydrothermal vein-hosted gold. It was suggested that the source of gold within the Morning Star dike, as well as the rest of the Woods Point dike swarm, was Cu-PGE-Au sulphides that remain at depth within the magma chamber. It was concluded that hydrothermal fluids that were mobilized along these dikes during post-magmatic metamorphism leached Au from magmatic sulphides and deposited them at higher levels in quartz-carbonate veins.

1.4 Thesis Structure

This thesis is composed of four individual, discrete manuscripts prepared for submission to peer-reviewed journals, bookended by this introductory chapter and a final synthesis chapter. This is in accordance with the Monash University regulations for thesis by publication. However, this also means that background and literature review information may be partially repetitive (and therefore partially tedious). Chapter 2 has been accepted and published in the journal *Economic Geology*. Chapter 3 has been accepted in *Economic Geology*; but likely won't be published until after the submission of this thesis. Chapter 4 has been prepared for submission to *Economic Geology* as well, but will be submitted after the thesis. Chapter 5 is presented in a longer format for the thesis and will be shortened for submission to *Nature* after completion of the thesis. A brief summary for each chapter is given below.

Chapter 2 – *Extreme Silver Isotope Variation if Orogenic Gold Systems Implies Multi-staged Metal Remobilisation During Ore Genesis*:

We report the first Ag isotope data for the orogenic Au deposits in the Victorian Goldfields, southeast Australia. The data show no correlation with mineralisation age or host-rock composition, and there is no obvious isotopic link to established "mantle" or "crustal" Ag isotope values, implying that source rock signatures are unlikely to be the main control on Ag isotope variations. Instead it is suggested that multiple physicochemical fractionation processes are dominant. Silver isotope fractionation via numerous deposition-dissolution cycles provides a different perspective

into large-scale ore genesis that has not previously been recognized for orogenic Au systems; multistaged metal remobilisation along fluid transport pathways is required to explain the extreme isotope variation.

Chapter 3 – *Aseismic Refinement of Orogenic Gold Systems*:

The mechanism that concentrates Au to extremely high "bonanza" grades in small domains within orogenic gold deposits has remained enigmatic for decades. In this chapter it is proposed that Au supersaturation in fluids leads to deposition of Au nanoparticles in quartz-carbonate veins, subsequent pressure-dissolution of vein quartz and carbonate during inter-seismic intervals allows for episodic increase in the Au/quartz ratio, as well as liberation and migration of Au nanoparticles, promoting Au grain growth in favourable textural settings. Repetition of this mechanism over the timescale of deposit formation acts to increase the Au concentration within the lodes.

Chapter 4 – *The first analysis of a telescoped orogenic gold system: Insights from the Fosterville deposit*:

Telescoped ore deposits are those in which early, usually deeper, high-temperature mineralisation and alteration are over-printed vertically by later, usually shallower and lower temperature mineralisation events and their characteristics. There has been little consideration of whether telescoped orogenic ore systems exist, although their mineralogy does vary between deposits with depth of emplacement. The Fosterville deposit is an outstanding example of a telescoped orogenic Au system that changes mineralisation characteristics with depth. Refractory gold hosted in arsenopyrite and pyrite is pervasive throughout the deposit, a narrow window of vein-hosted Au-Sb mineralisation exists from ~800 to 1350 m depth, below which is vein-hosted Au-only mineralisation. Work here suggests that this system represents two separate deposits emplaced in the same locality during mineralisation events that were separated by as much as 60 m.y.

Chapter 5 – *Gold Accumulations in Quartz Driven by Earthquake-Induced Piezoelectricity:*

Quartz is one of the least chemically reactive minerals and yet nearly all Au nuggets globally are found in a quartz veins and not the chemically more reactive host rocks. This chapter suggests that the piezoelectric properties of quartz may provide an overlooked explanation for one of the longest standing questions in geology: how are large vein-hosted gold nuggets formed? Piezoelectricity is a characteristic property observed in a small group of naturally occurring minerals, of which quartz is the only abundant mineral, in which an applied mechanical force generates electrical polarisation on crystal surfaces. This chapter discusses the fundamental concepts of piezoelectricity in the context of an evolving orogenic Au system and will provide the theoretical foundation for the piezopotential of orogenic Au deposit formation.

Chapter 6 – *Synthesis*:

This chapter brings the findings of the individual chapters together and considers them in the context of one holistic system. Orogenic Au deposits are the result of many factors working in tandem, some of which are known well, with others still remaining to be found. It aims to convince the reader of the importance of integrating different scientific sub-disciplines to better understand the gaps of knowledge that remain outstanding in this field of research, some of which may hold significant importance to both academia and industry.

References

Arne, D. C., Bierlin, F., Morgan, J. W., and Stein, H. J., 2001, Re-Os dating of sulphides associated with gold mineralisation in central Victoria, Australia: Economic Geology, v. 96, p. 1455-1459.

Bierlein, F., and McKnight, S., 2005, Possible intrusion-related gold systems in the western Lachlan Orogen, southeast Australia: Economic Geology, v. 100, p. 385-398.

Bierlein, F., and McNaughton, N., 1998, Pb isotope fingerprinting of mesothermal gold deposits from central Victoria, Australia: implications for ore genesis: Mineralium Deposita, v. 33, p. 633-638.

Bierlein, F. P., Arne, D. C., and Cartwright, I., 2004, Stable isotope (C, O, S) systematics in alteration haloes associatedwith orogenic gold mineralisation in the Victorian gold province, SE Australia: Geochemistry: Exploration, Environment, Analysis, v. 4, p. 191-211.

Bierlein, F. P., Arne, D. C., Foster, D. A., and Reynolds, P. R., 2001a, A Geochronological framework for slate belt-hosted gold mineralisation in central Victoria, Australia.: Mineral Deposita, v. 36, p. 741-767.

Bierlein, F. P., Arne, D. C., Keay, S., and McNaughton, N. J., 2001b, Timing relationships between felsic magmatism and mineralisation in the central Victorian gold province, southeast Australia: Australian Journal of Earth Sciences, v. 48, p. 883-899.

Bierlein, F. P., Cartwright, I., and McKnight, S., 2001c, The role of carbonaceous" indicator" slates in the genesis of lode gold mineralisation in the western Lachlan orogen, Victoria, southeastern Australia: Economic Geology, v. 96, p. 431-451.

Bierlein, F. P., Hughes, M., Dunphy, J., McKnight, S., Reynolds, P., and Waldron, H., 2001d, Tectonic and economic implications of trace element, 40Ar/39Ar and Sm–Nd data from mafic dykes associated with orogenic gold mineralisation in central Victoria, Australia: Lithos, v. 58, p. 1-31.

Bierlein, F. P., and Maher, S., 2001, Orogenic disseminated gold in Phanerozoic fold belts—examples from Victoria, Australia and elsewhere: Ore Geology Reviews, v. 18, p. 113-148.

Birch, W. D., 2003, Geology of Victoria.

Cayley, R., Taylor, D., VandenBerg, A., and Moore, D., 2002, Proterozoic–Early Palaeozoic rocks and the Tyennan Orogeny in central Victoria: the Selwyn Block and its tectonic implications: Australian Journal of Earth Sciences, v. 49, p. 225-254.

Cayley, R. A., Korsch, R. J., Moore, D. H., Costelloe, R. D., Nakamura, A., Willman, C. E., Rawling, T. J., Morand, V. J., Skladzien, P. B., and O'Shea, P. J., 2011,

Crustal architecture of central Victoria: results from the 2006 deep crustal reflection seismic survey: Australian Journal of Earth Sciences, v. 58, p. 113-156.

Chappell, B. W., and White, A., 1992, I-and S-type granites in the Lachlan Fold Belt: Earth and Environmental Science Transactions of the Royal Society of Edinburgh, v. 83, p. 1-26.

Connolly, J., and Cesare, B., 1993, C-O-H-S fluid composition and oxygen fugacity in graphitic metapelites: Journal of metamorphic geology, v. 11, p. 379-388.

Cox, S., 2005, Coupling between deformation, fluid pressures, and fluid flow in ore-producing hydrothermal systems at depth in the crust.

Cox, S. F., 1995, Faulting processes at high fluid pressures: an example of fault valve behavior from the Wattle Gully Fault, Victoria, Australia: Journal of Geophysical Research: Solid Earth, v. 100, p. 12841-12859.

Craw, D., 2013, Economic geology: Gilded by earthquakes: Nature Geoscience, v. 6, p. 248.

Elmer, F., Dugdale, A., and Wilson, C., 2008, Application of mineral equilibria modeling to constrain T and X CO2 conditions during the evolution of the Magdala gold deposit, Stawell, Victoria, Australia: Mineralium Deposita, v. 43, p. 759.

Fairmaid, A., Kendrick, M., Phillips, D., and Fu, B., 2011, The origin and evolution of mineralizing fluids in a sediment-hosted orogenic-gold deposit, Ballarat East, Southeastern Australia: Economic Geology, v. 106, p. 653-666.

Foster, D. A., Gray, D. R., Kwak, T. A., and Bucher, M., 1998, Chronology and tectonic framework of turbidite-hosted gold deposits in the western Lachlan Fold Belt, Victoria: 40Ar–39Ar results: Ore Geology Reviews, v. 13, p. 229-250.

Fougerouse, D., Micklethwaite, S., Tomkins, A. G., Mei, Y., Kilburn, M., Guagliardo, P., Fisher, L. A., Halfpenny, A., Gee, M., and Paterson, D., 2016, Gold remobilisation and formation of high grade ore shoots driven by dissolution-reprecipitation replacement and Ni substitution into auriferous arsenopyrite: Geochimica et Cosmochimica Acta, v. 178, p. 143-159.

Gaboury, D., 2013, Does gold in orogenic deposits come from pyrite in deeply buried carbon-rich sediments?: Insight from volatiles in fluid inclusions: Geology, v. 41, p. 1207-1210.

Gaboury, D., and Daigneault, R., 2000, Flat vein formation in a transitional crustal setting by self-induced fluid pressure equilibrium—an example from the Geant Dormant gold mine, Canada: Ore Geology Reviews, v. 17, p. 155-178.

Goldfarb, R., Baker, T., Dube, B., Groves, D. I., Hart, C. J., and Gosselin, P., 2005, Distribution, character and genesis of gold deposits in metamorphic terranes, Society of Economic Geologists.

Goldfarb, R., Groves, D., and Gardoll, S., 2001, Orogenic gold and geologic time: a global synthesis: Ore geology reviews, v. 18, p. 1-75.

Goldfarb, R. J., and Groves, D. I., 2015, Orogenic gold: Common or evolving fluid and metal sources through time: Lithos, v. 233, p. 2-26.

Gray, D., and Foster, D., 2004, Tectonic evolution of the Lachlan Orogen, southeast Australia: historical review, data synthesis and modern perspectives: Australian Journal of Earth Sciences, v. 51, p. 773-817.

Gray, D. R., and Foster, D. A., 1998, Character and kinematics of faults within the turbidite-dominated Lachlan Orogen: implications for tectonic evolution of eastern Australia: Journal of Structural Geology, v. 20, p. 1691-1720.

Groves, D., 1993, The crustal continuum model for late-Archaean lode-gold deposits of the Yilgarn Block, Western Australia: Mineralium deposita, v. 28, p. 366-374.

Groves, D. I., Goldfarb, R. J., Gebre-Mariam, M., Hagemann, S., and Robert, F., 1998, Orogenic gold deposits: a proposed classification in the context of their crustal distribution and relationship to other gold deposit types: Ore geology reviews, v. 13, p. 7-27.

Hannington, M., Harðardóttir, V., Garbe-Schönberg, D., and Brown, K. L., 2016, Gold enrichment in active geothermal systems by accumulating colloidal suspensions: Nature Geoscience, v. 9, p. 299.

Herrington, R., and Wilkinson, J., 1993, Colloidal gold and silica in mesothermal vein systems: Geology, v. 21, p. 539-542.

Hodkiewicz, P., Groves, D. I., Davidson, G. J., Weinberg, R. F., and Hagemann, S., 2009, Influence of structural setting on sulphur isotopes in Archean orogenic gold deposits, Eastern Goldfields Province, Yilgarn, Western Australia: Mineralium Deposita, v. 44, p. 129.

Hofstra, A., Leventhal, J., Northrop, H., Landis, G., Rye, R., Birak, D., and Dahl, A., 1991, Genesis of sediment-hosted disseminated-gold deposits by fluid mixing and sulfidization: Chemical-reaction-path modeling of ore-depositional processes documented in the Jerritt Canyon district, Nevada: Geology, v. 19, p. 36-40.

Hough, M. A., Bierlein, F. P., and Wilde, A. R., 2007, A review of the metallogeny and tectonics of the Lachlan Orogen: Mineralium deposita, v. 42, p. 435-448.

Hughes, M., Phillips, G., and Gregory, L., 1997, Mineralogical domains in the Victorian gold province, Maldon, and Carlin-style potential: Australasian Institute of Mining and Metallurgy Annual Conference, Ballarat, 1997, p. 215-227.

Jowitt, S. M., Keays, R. R., Jackson, P. G., Hoggart, C. R., and Green, A. H., 2012, Mineralogical and geochemical controls on the formation of the Woods point dike swarm, Victoria, Australia: evidence from the morning star dike and implications for sourcing of Au within orogenic gold systems: Economic Geology, v. 107, p. 251-273.

Kaszuba, J. P., Williams, L. L., Janecky, D. R., Hollis, W. K., and Tsimpanogiannis, I. N., 2006, Immiscible CO2-H2O fluids in the shallow crust: Geochemistry, Geophysics, Geosystems, v. 7.

Kerrich, R., and Wyman, D., 1990, Geodynamic setting of mesothermal gold deposits: An association with accretionary tectonic regimes: Geology, v. 18, p. 882-885.

Large, R. R., Bull, S. W., and Maslennikov, V. V., 2011, A carbonaceous sedimentary source-rock model for Carlin-type and orogenic gold deposits: Economic Geology, v. 106, p. 331-358.

Large, R. R., Danyushevsky, L., Hollit, C., Maslennikov, V., Meffre, S., Gilbert, S., Bull, S., Scott, R., Emsbo, P., and Thomas, H., 2009, Gold and trace element zonation in pyrite using a laser imaging technique: Implications for the timing of gold in orogenic and Carlin-style sediment-hosted deposits: Economic Geology, v. 104, p. 635-668.

Micklethwaite, S., Sheldon, H. A., and Baker, T., 2010, Active fault and shear processes and their implications for mineral deposit formation and discovery: Journal of Structural Geology, v. 32, p. 151-165.

Miller, J. M., and Wilson, C. J., 2002, The Magdala lode system, Stawell, southeastern Australia: Structural style and relationship to gold mineralisation across the western Lachlan fold belt: Economic Geology, v. 97, p. 325-349.

Moresi, L., Betts, P. G., Miller, M. S., and Cayley, R. A., 2014, Dynamics of continental accretion: Nature, v. 508, p. 245.

Naden, J., and Shepherd, T. J., 1989, Role of methane and carbon dioxide in gold deposition: Nature, v. 342, p. 793.

Paterson, S. R., Tobisch, O. T., and Morand, V. J., 1990, The influence of large ductile shear zones on the emplacement and deformation of the Wyangala Batholith, SE Australia: Journal of Structural Geology, v. 12, p. 639-650.

Phillips, D., Fu, B., Wilson, C. J., Kendrick, M., Fairmaid, A., and Miller, J. M., 2012, Timing of gold mineralisation in the western Lachlan Orogen, SE Australia: A critical overview: Australian Journal of Earth Sciences, v. 59, p. 495-525.

Phillips, G., and Evans, K., 2004, Role of CO 2 in the formation of gold deposits: Nature, v. 429, p. 860.

Phillips, G., and Powell, R., 2010, Formation of gold deposits: a metamorphic devolatilization model: Journal of Metamorphic Geology, v. 28, p. 689-718.

Phillips, G. N., and Gibb, H., 1993, A century of gold mining at Kalgoorlie, Economic Geology Research Unit, Key Centre in Economic Geology, James Cook ….

Phillips, G. N., and Groves, D. I., 1983, The nature of Archaean gold-bearing fluids as deduced from gold deposits of Western Australia: Journal of the Geological Society of Australia, v. 30, p. 25-39.

Phillips, G. N., and Hughes, M. J., 1996, The geology and gold deposits of the Victorian gold province: Ore Geology Reviews, v. 11, p. 255-302.

Phillips, G. N., and Powell, R., 2011, Origin of Witwatersrand gold: a metamorphic devolatilisation–hydrothermal replacement model: Applied Earth Science, v.

120, p. 112-129.

Phillips, G. N., and Powell, R., 2015, A practical classification of gold deposits, with a theoretical basis: Ore Geology Reviews, v. 65, p. 568-573.

Pilia, S., Rawlinson, N., Cayley, R., Bodin, T., Musgrave, R., Reading, A., Direen, N., and Young, M., 2015, Evidence of micro-continent entrainment during crustal accretion: Scientific reports, v. 5, p. 8218.

Pitcairn, I. K., Craw, D., and Teagle, D. A., 2015, Metabasalts as sources of metals in orogenic gold deposits: Mineralium Deposita, v. 50, p. 373-390.

Pitcairn, I. K., Teagle, D. A., Craw, D., Olivo, G. R., Kerrich, R., and Brewer, T. S., 2006, Sources of metals and fluids in orogenic gold deposits: insights from the Otago and Alpine Schists, New Zealand: Economic Geology, v. 101, p. 1525-1546.

Pope, J., Brown, K., and McConchie, D., 2005, Gold concentrations in springs at Waiotapu, New Zealand: implications for precious metal deposition in geothermal systems: Economic Geology, v. 100, p. 677-687.

Richards, J., and Singleton, O., 1981, Palaeozoic Victoria, Australia: igneous rocks, ages and their interpretation: Journal of the Geological Society of Australia, v. 28, p. 395-421.

Robert, F., Boullier, A. M., and Firdaous, K., 1995, Gold-quartz veins in metamorphic terranes and their bearing on the role of fluids in faulting: Journal of Geophysical Research: Solid Earth, v. 100, p. 12861-12879.

Sandiford, M., and Keays, R. R., 1986, Structural and tectonic constraints on the origin of gold deposits in the Ballarat slate belt, Victoria, Turbidite-hosted gold deposits, 32, Geological Association of Canada Special Paper, p. 15-24.

Sibson, R., Moore, J. M. M., and Rankin, A., 1975, Seismic pumping—a hydrothermal fluid transport mechanism: Journal of the Geological Society, v. 131, p. 653-659.

Sibson, R. H., 1987, Earthquake rupturing as a mineralizing agent in hydrothermal systems: Geology, v. 15, p. 701-704.

Sibson, R. H., Robert, F., and Poulsen, K. H., 1988, High-angle reverse faults, fluid-pressure cycling, and mesothermal gold-quartz deposits: Geology, v. 16, p. 551-555.

Squire, R. J., Stewart, I., and Zang, W. L., 2006, Acritarchs in polydeformed and highly altered Cambrian rocks in western Victoria: Australian Journal of Earth Sciences, v. 53, p. 697-705.

Thomas, H. V., Large, R. R., Bull, S. W., Maslennikov, V., Berry, R. F., Fraser, R., Froud, S., and Moye, R., 2011, Pyrite and pyrrhotite textures and composition in sediments, laminated quartz veins, and reefs at Bendigo gold mine, Australia: Insights for ore genesis: Economic Geology, v. 106, p. 1-31.

Tobisch, O. T., and Paterson, S. R., 1990, The Yarra granite: an intradeformational pluton associated with ductile thrusting, Lachlan Fold Belt, southeastern Aus-

tralia: Geological Society of America Bulletin, v. 102, p. 693-703.

Tomkins, A. G., 2010, Windows of metamorphic sulfur liberation in the crust: Implications for gold deposit genesis: Geochimica et Cosmochimica Acta, v. 74, p. 3246-3259.

Tomkins, A. G., 2013, A biogeochemical influence on the secular distribution of orogenic gold: Economic Geology, v. 108, p. 193-197.

Tomkins, A. G., and Grundy, C., 2009, Upper temperature limits of orogenic gold deposit formation: Constraints from the granulite-hosted Griffin's Find deposit, Yilgarn craton: Economic Geology, v. 104, p. 669-685.

VandenBerg, A., 2000, The Tasman Fold Belt system in Victoria: geology and mineralisation of Proterozoic to Carboniferous rocks, Geological Survey of Victoria.

Voisey, C. R., Maas, R., Tomkins, A. G., Brauns, M., & Brügmann, G., 2019, Extreme Silver Isotope Variation in Orogenic Gold Systems Implies Multistaged Metal Remobilization During Ore Genesis. Economic Geology, 114(2), 233-242.

Voisey, C. R., Willis, D., Tomkins, A. G., Wilson, C. J. L., Micklethwaite, S., Salvemini, F., Bougoure, J., Rickard, W. D. A., 2020, Aseismic Refinement of Orogemic Gold Systems. Economic Geology.

Weatherley, D. K., and Henley, R. W., 2013, Flash vaporization during earthquakes evidenced by gold deposits: Nature Geoscience, v. 6, p. 294.

Wilkinson, J., and Johnston, J., 1996, Pressure fluctuations, phase separation, and gold precipitation during seismic fracture propagation: Geology, v. 24, p. 395-398.

Williams-Jones, A. E., Bowell, R. J., and Migdisov, A. A., 2009, Gold in solution: Elements, v. 5, p. 281-287.

Williams-Jones, A. E., and Norman, C., 1997, Controls of mineral parageneses in the system Fe-Sb-SO: Economic Geology, v. 92, p. 308-324.

Willman, C., Korsch, R., Moore, D., Cayley, R., Lisitsin, V., Rawling, T., Morand, V., and O'Shea, P., 2010, Crustal-scale fluid pathways and source rocks in the Victorian gold province, Australia: Insights from deep seismic reflection profiles: Economic Geology, v. 105, p. 895-915.

Wilson, C. J., Schaubs, P. M., and Leader, L. D., 2013, Mineral precipitation in the quartz reefs of the Bendigo gold deposit, Victoria, Australia: Economic Geology, v. 108, p. 259-278.

Wilson, C. J., Xu, G., and Moncrieff, J., 1999, The structural setting and contact metamorphism of the Wonga gold deposit, Victoria, Australia: Economic Geology, v. 94, p. 1305-1328.

Wyman, D. A., Cassidy, K. F., and Hollings, P., 2016, Orogenic gold and the mineral systems approach: resolving fact, fiction and fantasy: Ore Geology Reviews, v. 78, p. 322-335.

Yu, X., Hou, Z., Qian, Y., and Li, B., 2012, Ore-forming fluids, stable isotopes and

metallogenic epoch of the Fu'an pu molybdenum deposit in the mid-east Jilin Province: Geology and Exploration, v. 48, p. 1151-1162.

Chapter 2

Extreme Ag isotope variation in orogenic gold systems implies multi-staged metal remobilisation during ore genesis

Christopher R. Voisey[1], Roland Maas[2], Andrew G. Tomkins[1], Michael Brauns[3], Gerhard Brügmann[3]

[1]*School of Earth, Atmosphere & Environment, Monash University, Clayton, VIC 3800, Australia*

[2]*School of Earth Sciences, Melbourne University, Melbourne, 3000, Australia*

[3]*Curt-Engelhorn-Zentrum Archäometrie, Mannheim, Germany*

"It's like a black box. How does anyone do this?!"
-Words of a learning man

Abstract

We report the first Ag isotope data for the Paleozoic orogenic Au deposits in the Victorian Goldfields, SE Australia, a world-class province with a historic production of 2,400 tonnes of Au. Despite their relatively uniform geology – similar host rock types, age, mineralisation style – deposits in Victoria show a wide range in $^{107}Ag/^{109}Ag$ ratios in native Au ($\varepsilon^{107}Ag$ -6.6 to +8.3, relative to the NIST SRM 978a Ag standard), comparable to the entire previously known terrestrial range (-9.4 to +5.3). The data show no correlation with mineralisation age or host rock composition, and there is no obvious isotopic link to established 'mantle' or 'crustal' Ag isotope values, implying that source rock signatures are unlikely to be the main control on Ag isotope variations. Instead, it is suggested that the Ag isotopic variation is primarily related to physico-chemical processes, particularly Ag isotope fractionation during redox reactions such as conversion of Ag^0 in native Au to Ag^+ in dissolved $Ag(HS)_2^-$ or sulphide-borne Ag. Repeated $Ag^0 \leftrightarrow Ag^+$ reactions along transport pathways and at sites of ore accumulation could generate a wide range in $\varepsilon^{107}Ag$, and evidence of this range is presented in the data here. Silver isotope fractionation via numerous deposition-dissolution cycles provides a different perspective into large-scale ore genesis that has not previously been recognised for orogenic gold systems; multi-staged metal remobilisation along fluid transport pathways is standard during their formation. Detailed Ag isotope studies have considerable potential for understanding the history of episodic metal addition and within-deposit redistribution.

1. Introduction

Ag is a common trace element in most terrestrial and extra-terrestrial rocks, occurring at ppb level concentrations or higher (Woodland et al., 2005). Ag is composed of two naturally occurring isotopes, ^{109}Ag and ^{107}Ag, with relative abundances of 48.2% and 51.8%, respectively. Variations in the isotopic composition of Ag were first recorded in the 1960's in an iron meteorite (Murthy, 1960) and were scarcely studied in the years following. However, the development of more sophisticated analytical techniques, such as multicollector inductively coupled plasma mass spectrometry (MC-ICP-MS), has sparked a renewed interest in studying Ag isotope systematics. This is due to a reduction in the error in measuring ^{107}Ag/^{109}Ag by approximately an order of magnitude when compared to the traditional method of using thermal ionization mass spectrometry (TIMS) (Carlson and Hauri, 2001; Woodland et al., 2005). The significant difference between the two methods is that the MC-ICP-MS technique allows for adequate correction of the effect of instrumental mass discrimination. The resulting increase in precision means that variations in Ag isotopic compositions of natural materials are now larger than measured uncertainties and can be successfully utilised for studies investigating geological processes.

As Au is mono-isotopic, proxies must be developed to investigate the formation of Au-rich mineral deposits. However, in nature, Au is invariably alloyed with Ag in ore deposits, and they are found in the same minerals (mainly pyrite) in a range of potential source rocks (e.g., (Tomkins, 2010) Their common chalcophile behaviour, and tendency to complex with the same ligands in hydrothermal fluids (Seward et al., 2014), implies that Au and Ag are associated throughout ore genesis, from the source regions to the sites of metal accumulation. Therefore, Ag isotopes are expected to provide a valuable proxy for studying the formation of Au deposits. Previous research has investigated the Ag isotope signatures of Ag-bearing ore minerals from a limited number of mineral deposits to study geological processes related to ore deposition and source region geochemistry (Hauri et al., 2001; Woodland et al., 2005; Chugaev and Chernyshev 2012; Tessalina et al., 2015). Variations in Ag isotopic composition from

these studies are thought to be related to: (i) kinetic or equilibrium isotope fractionation at relatively low temperatures during the physico-chemical processes of ore formation (Tessalina et al. 2015); (ii) natural variations in Ag isotope signatures inherited from protoliths or metal sources (Hauri et al. 2000); and (iii) nuclear volume effects due to s-electron addition during the reduction of Ag^+ into Ag^0 during the precipitation of Ag and Au species (Chugaev and Chernyshev 2012). However, the implications of $^{107}Ag/^{109}Ag$ variations for understanding geological processes remains difficult to interpret and warrants further examination.

The Ag isotope signature of a suite of native Au samples from a broad range of orogenic Au deposits located in central Victoria, Australia, has been investigated using multi-collector inductively coupled plasma mass spectrometry (MC-ICP-MS). The Victorian Goldfields (Fig. 1) are historically one of the richest Au-producing regions on Earth and have been the subject of extensive research over a long period of time. The genesis of Au deposits in this region is thus relatively well understood compared to most Au fields, and the structural history and geological setting for most deposits are relatively simple and broadly comparable. Therefore, this region is well suited to an investigation of the utility of Ag isotopes to ore genesis research. Results presented here exhibit an extreme variation in $^{107}Ag/^{109}Ag$ ratios given the geological context, and consequently provide a different perspective into large-scale orogenic Au ore genesis that has not previously been recognised.

2. Geological Setting

Eastern Australia is composed of a series of geologic terranes, known as the Tasmanides, which were accreted to the Pacific margin of Gondwana during the Paleozoic (VandenBerg et al. 2000; Willman et al. 2010; Phillips et al. 2012). The terranes that make up the Tasman Fold Belt system include the Delamerian, Lachlan, and New England Orogens. The Lachlan Orogen is divided into western, central, and eastern sub-provinces, and the western sub-province is host to most of the orogenic Au mineralisation in Victoria (Fig. 1; Phillips et al. 2012). The Western Lachlan Orogen is

defined by a ~12km thick Cambrian to Silurian turbidite package that overlies a ~25km thick Cambrian basement of oceanic mafic volcanics (Fig. 2) (VandenBerg et al., 2000; Gray & Foster, 2004; Willman et al., 2010). This sub-province is also host to post-tectonic granitic plutons that intruded throughout the Devonian (Paterson et al., 1990; Tobisch & Paterson, 1990; Gray & Foster, 2004). The sedimentary and volcanic rocks have undergone sub-greenschist to lower amphibolite facies metamorphism and were moderately to strongly deformed into dominantly north-south trending chevron folds that are cut by thick-skinned thrust systems (VandenBerg et al., 2000). In Victoria, the Western Lachlan Fold Belt is further sub-divided into three major lithological/structural zones, the Stawell, Bendigo, and Melbourne Zones, which are separated by major north-south striking, high angle reverse faults (VandenBerg et al., 2000; Gray & Foster, 2003; Cayley et al., 2011). Based on seismic data, it has been interpreted that these thrust faults become listric and sub-horizontal at depth, possibly in the vicinity of the turbidite-mafic basement transition (Fig. 2; Cayley et al., 2011).

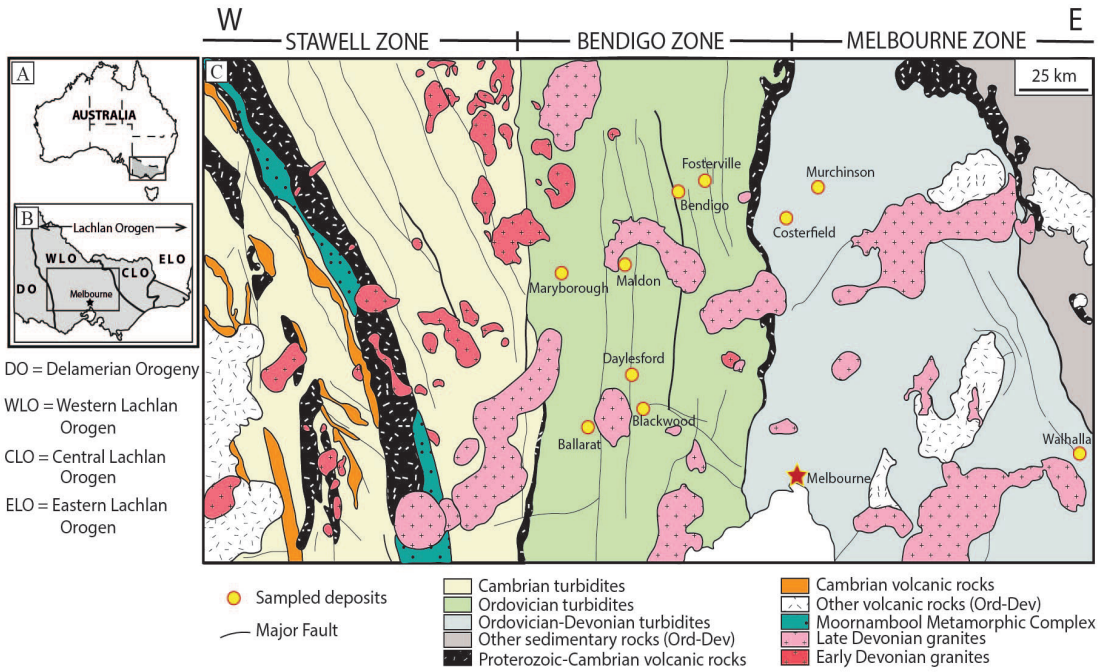

Figure 1: A) Schematic map of Australia with the state of Victoria highlighted in grey, and the position of B indicated. B) The locations of the Lachlan and Delamerian Orogens in a map of Victoria (modified from Willman et al., 2010), and the position of C is indicated. C) Simplified geological map of central Victoria modified from Phillips et al. (2012). Yellow circles indicate the deposits sampled in this study.

The deposits in the Victorian goldfields are clustered along regional north-south trending structures within the thrust faulted chevron fold system (Phillips & Hughes, 1996). The clustering of Au deposits near major fault zones is thought to reflect shallow-level penetration of mid- to lower crustal fluids, which were channellised by these deep seated faults (Hughes & Phillips, 1997). At the deposit scale, ore bodies are associated with second and third order local structures (i.e., upright chevron fold hinges, bedding plane faults, dilational fault offsets and moderate scale reverse faults on a scale of kilometers to tens of kilometers), which acted as traps for mineralising fluids. Ordovician-Silurian sequences of sandstones, siltstones and variably graphitic slates (turbidites) are the host rocks to almost all of the Victorian Au deposits. Most of the Au deposition pre-dates the emplacement of granitic intrusions (Phillips et al. 2012), with the possible exception of the poorly age-constrained Sb-Au mineralisation at two localities (the Fosterville and Costerfield deposits). Au occurs in two main styles: (1) coarse-grained visible native Au (>1 mm) within quartz±ankerite veins associated with brittle-ductile shear zones, saddle reefs, and faults, where Au-free, coarse-grained arsenopyrite (1-2 cm) and pyrite (1-5 mm) are disseminated in the wall rocks (e.g. Bendigo), and (2) refractory Au contained in fine-grained arsenopyrite (0.2-3 mm) and arsenian pyrite crystals (< 1 mm) disseminated throughout the wall rock proximal to quartz±ankerite veins (e.g. Fosterville) (Hughes & Phillips, 2015).

3. Methodology

The samples used in this study are native Au grains from ten orogenic Au deposits hosted in Paleozoic rocks of the western Lachlan Fold Belt in Victoria, SE Australia (Fig. 1). The Au samples were sourced from collections held at the Museum of Victoria and from Fosterville Gold Mine. Following inspection under a binocular microscope, the specimens were cleaned/sectioned as required using a steel scalpel.

Ag isotopic compositions were measured at the Curt-Engelhorn-Zentrum Archäometrie (CEZ) in Mannheim, Germany. Au grains (typically 1-10 mg) were weighed into Savillex beakers and dissolved with 1 ml of aqua regia (12 hrs, 80°C).

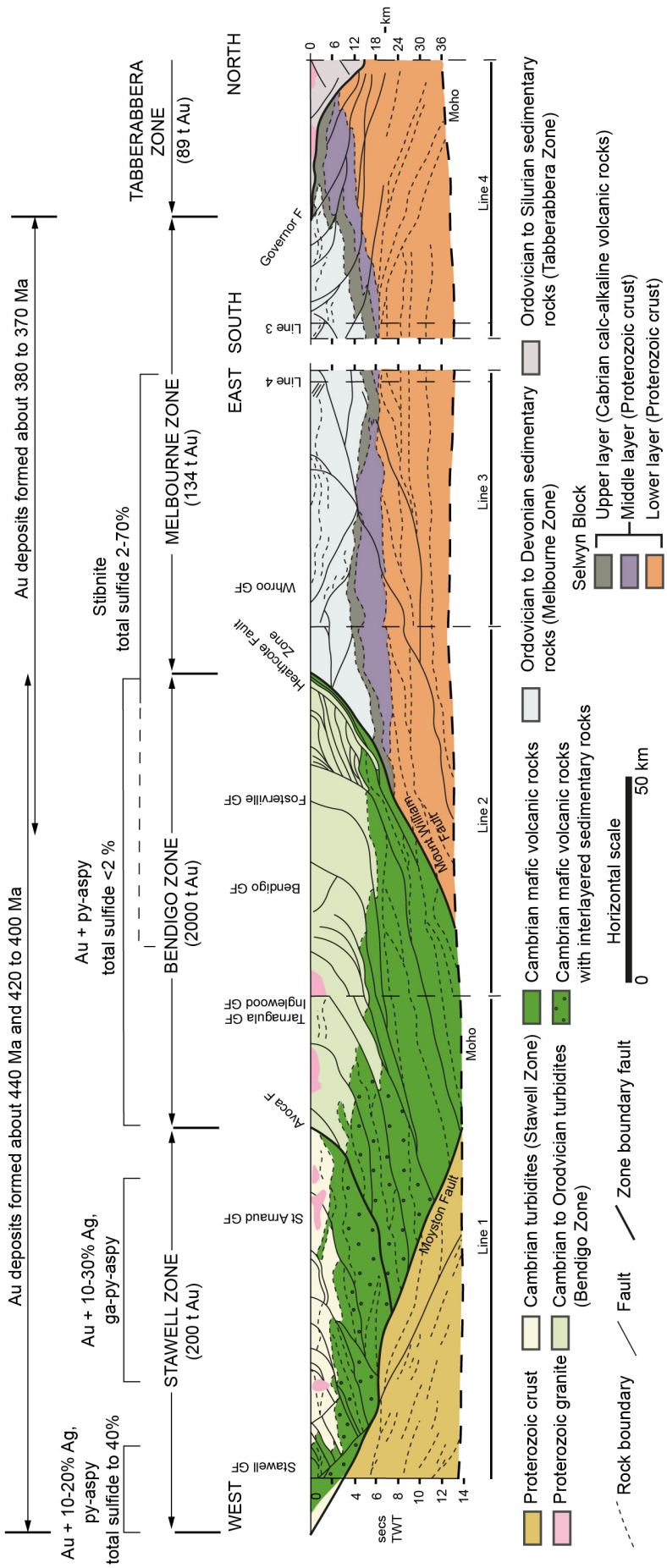

Figure 2: Interpreted cross section of the Western Lachlan Fold Belt via seismic lines. From Willman et al. (2010).

After evaporation, samples were re-dissolved in 0.5 ml of concentrated HCl. At this stage, a small split of each sample solution was used to determine the concentrations of Ag, Au, Cu and Pd in each sample by quadrupole ICP-MS. The remaining sample solution was used for high-precision Ag isotope ratio mass spectrometry. Ag was purified using a 2-step ion exchange column procedure. On column 1, Au (and some other matrix elements, notably Pd) were removed by passing the sample over a bed of anion resin (AG1-X8, 100-200 mesh, Cl- form, resin bed 3x28 mm, ~0.2 ml resin volume) in 6M HCl. In strong HCl, Au and Pd are strongly extracted onto the resin while Ag passes through the column, providing a reliable and efficient means to remove most of the (largely Au) matrix. Column 2 (Triskem TBP resin, 50-100 µm, 0.2 ml above a 0.075 ml bed of Eichrom prefilter medium, total resin bed length ~39 mm in a 3 mm inner diameter column) was used to further purify the Ag and convert Ag from chloride to nitrate form, a step considered crucial to avoid Ag loss as AgCl at very low HCl concentrations (e.g. Woodland et al., 2005, Schönbächler et al., 2007). Triskem TBP resin was chosen for the Ag-in-Au matrix materials studied here because it produces clean Ag fractions with consistently high Ag yields. For this purpose, a very small fraction of the 6M HCl eluate from column 1, containing a few µg of Ag, was diluted to 0.5M/L, loaded onto column 2 and washed through the resin with several small volumes of water. Ag was eluted in 0.31M (2%) HNO_3. Ag yields were measured after column 1 and column 2 using quadrupole ICPMS with HCl- and HNO_3-based calibration standards, respectively, and were typically ≥99%.

Silver isotope analyses were carried out on a Thermo Finnigan Neptune Plus MC-ICPMS. Prior to analysis, Ag fractions were adjusted to ~200-300 ppb Ag and doped with SRM3138-Pd, to generate Pd/Ag near 2 ($^{108}Pd/^{107}Ag$ ~ 1). This Ag-Pd mix was introduced to the MC-ICPMS using a self-aspirating nebuliser and cyclonic spray chamber (uptake rate 0.05 ml/min), which produced ^{107}Ag signals of 5-8 x10^{-11} A, equivalent to a sensitivity near 50V/ppm Ag. Data for unknowns were collected in 3 blocks of eighty 8.4 second integrations while data for Pd-doped standard Ag (SRM978a) were collected in 1 block of ninety 8.4 second integrations. Samples were

Table 1. Silver Isotope and Elemental Compositions: Paleozoic Orogenic Gold from Victoria, Australia

Sample ID	Description	Location	Au (wt %)	Ag (wt %)	Cu (ppm)	Pd (ppm)	ε^{107}Ag	±2 se
M45071	Massive disseminated free Au in qtz-ank vein	Bendigo	92.07	7.93	18	<0.1	–2.7	0.01
M43937	Fracture-hosted visible Au grains (3–8 mm) in laminated qtz vein with minor (3%) subhedral py	Bendigo	88.88	11.12	12	0.34	–3.3	0.1
M24258	Fracture-hosted visible Au grain (~2 mm) in qtz vein	Bendigo	92.28	7.72	53	<0.1	–3.8	0.03
M7864	Massive free Au coating vuggy surface in qtz vein	Mount Barker, Bendigo	96.2	3.79	88	0.1	–2.9	0.05
M7866	Free Au grain (~4 mm) in qtz vein	Mount Barker, Bendigo	86.65	13.35	17	<0.1	–3.4	0.06
M52063	Free Au grain (~3 mm) in qtz vein along pyritized black slate host rock	Kangaroo Flat, Bendigo	96.92	3.06	188	0.53	–2.3	0.04
M11078	Fine-grained (<1 mm) free Au disseminated within vuggy surface in qtz vein	Ballarat	96.26	3.73	114	<0.1	–1.6	0.05
M39912	Free Au grains (~2 mm) in qtz vein	Canadian Gully, Ballarat	99.3	0.67	248	<0.1	0.95	0.08
M38399	Fracture-hosted visible Au grains (1–4 mm) in qtz vein	Blackwood	95.44	4.55	110	<0.1	–0.66	0.01
M17680	Native Au grains (2-4 mm) disseminated along carbonaceous wall-rock selvage in qtz vein	Cornish mine, Daylesford	95.42	4.57	129	<0.1	–0.03	0.03
M39933	Fracture-hosted visible Au grain (~3 mm) in qtz vein	Wombat Hill, Daylesford	87.03	12.97	9	<0.1	–2	0.05
M25038	Fine-grained free Au (~1 mm) grain in qtz vein	Charleys Hope, Maldon	96.93	3.07	49	<0.1	–0.19	0.06
M42560	Fine-grained (<1 mm) native Au disseminated on mlc in qtz vein with coare-grained (~1 cm) subhedral py	Maryborough	99.14	0.82	400	<0.1	4.5	0.05
M18738	Free Au grains (~3 mm) in qtz vein	Maryborough	95.45	4.54	82	<0.1	–1.3	0.02
KH002	Fracture-hosted visible Au grains (2–5 mm) in laminated qtz vein	Fosterville	96.67	3.32	35	<0.1	–4.7	0.04
M38375	Fine-grained (<1–2 mm) native Au disseminated within massive stb (~80%) and qtz vein	South Costerfield shaft	99.56	0.43	72	<0.1	8.3	0.03
M39880	Fracture-hosted visible Au grain (5 mm) in qtz vein	Murchison, Rushworth	96.7	3.29	87	0.11	–1.8	0.02
M22977	Massive fracture-hosted native Au (2–7 mm) in drusy qtz vein	Long Tunnel, Walhalla	92.45	7.55	66	<0.1	–6.6	0.05

Abbreviations: ank = ankerite, mlc = malachite, py = pyrite, qtz = quartz
2 se is the standard error of the sample mean in ε units

measured in the sequence: blank – standard – blank – unknown – blank – standard, with 5 minute wash-outs following each standard or unknown. Measured signals were corrected for baselines using the preceding blank analysis (which showed only modest memory increase - ca. 1 mV at masses 107 and 109 - over a 20 hr analytical session), and Pd signals were corrected for (typically negligible) interference from ^{106,108}Cd. The resulting ^{107}Ag/^{109}Ag, ^{108}Pd/^{105}Pd, ^{106}Pd/^{105}Pd and ^{110}Pd/^{105}Pd ratios were corrected for instrumental mass bias by internal normalization to ^{108}Pd/^{105}Pd=1.18899 (Kelly and Wasserburg, 1978) using the exponential law (Russell et al., 1978; Baxter et al., 2006). The average Pd-corrected ^{107}Ag/^{109}Ag for SRM978a measured in 18 sessions over 5 months is 1.07988±0.00010 (2sd), indistinguishable from the averages given in Schönbächler et al. (2007, 2008). However, while normalization to ^{108}Pd/^{105}Pd removes the bulk of the instrumental mass bias in both elements, mass bias in Ag and Pd is not necessarily identical and potential differences may also be affected by drift. For this reason, mass bias-corrected ^{107}Ag/^{109}Ag in unknowns was normalised to the average of the mass bias-corrected ^{107}Ag/^{109}Ag in bracketing runs of SRM978a-Ag. This combination of Pd doping and standard-sample bracketing (SSB) was used in previous studies (e.g. Woodland et al., 2005; Schönbächler et al., 2007, 2008; Luo et al., 2010; Desaulty et al., 2011;

Mathur et al., 2018). $^{107}Ag/^{109}Ag$ results for unknowns are reported as $\varepsilon^{107}Ag$ values (1ε = 1 part in 10000) calculated relative to the mean $^{107}Ag/^{109}Ag$ for the bracketing runs of SRM978a. Again, this follows established procedure although it is noted that more recent studies (e.g. Desaulty et al., 2011, 2013; Mathur et al., 2018; Argapadmi et al., 2018) report their Ag isotope results as $\varepsilon^{109}Ag$ or $\delta^{109}Ag$, a more intuitive notation which readily correlates isotopically 'heavy Ag' with positive $\varepsilon^{109}Ag$ or $\delta^{109}Ag$. Internal precisions for Pd-normalized $^{107}Ag/^{109}Ag$ in a single MC-ICPMS analysis range from ±1 to 10 ppm (2se, see also Table 1), reflecting the large number of scans (n=240) that make up a single isotopic run and the Ag signal in the mass spectrometer. The external precision achieved using combined Pd-doping and SSB was assessed from multiple analyses of homogeneous Ag samples. The average $\varepsilon^{107}Ag$ for ten splits of SRM8978a processed through the chemistry and analysed as unknowns with the Victorian Au samples is -0.07±0.15 (2sd, n=10, see Table 2), identical to the long-term average of -0.07±0.16 (2sd, n=18) in the CEZ laboratory. Likewise, seven splits of the CEZAg Au nugget solution processed through the column chemistry yield an average $\varepsilon^{107}Ag$ = -0.44±0.13 (2sd, n=7, see Table 2), again virtually identical to the long-term average (-0.43±0.15, 2sd, n=18) reported for this new standard at CEZ. These results suggest an external precision for $\varepsilon^{107}Ag$ around ±0.20, or 20 ppm, consistent with external precisions reported in other studies (e.g. Schönbächler et al., 2008; Mathur et al., 2018).

Table 2. Ag isotope results for the CEZAg and SRM978a standards.

Sample no.	CEZAg ($\varepsilon^{107}Ag$)	±2se	SRM978a ($\varepsilon^{107}Ag$)	±2se
1	–0.443	0.04	–0.074	0.044
2	–0.362	0.081	–0.096	0.032
3	–0.36	0.048	–0.032	0.058
4	–0.465	0.028	–0.056	0.034
5	–0.537	0.032	0.031	0.041
6	–0.471	0.02	–0.188	0.099
7	–0.428	0.079	–0.187	0.063
8			–0.003	0.056
9			0.009	0.053
10			–0.131	0.033
Average	–0.438		–0.073	
±2sd	0.126		0.156	

CEZAg is an in-house Au nugget solution standard at the Curt-Engelhorn-Zentrum Archäometri

Results

The Ag isotopic compositions and concentrations of Au, Ag, Cu and Pd for Au grains from 10 Paleozoic Au deposits in Victoria are shown in Table 1. Silver and Cu contents in the Au grains range from 0.43 to 13.35 wt%, and from 9 to 400 ppm, respectively, while Pd was only detectable in 3 samples at <1 ppm. ε^{107}Ag ranges from -6.6 to +8.3, i.e. a total variation of 14.9 ε-units. This is comparable to the total range of ε^{107}Ag (–9.4 to +5.3) for terrestrial Ag reported in other studies and extends the known range to 17.7 ε units (Fig.3). Most of the 18 samples listed in Table 1 have ε^{107}Ag that cluster between -4 and +1, with ε^{107}Ag outside this range recorded for Fosterville (-4.7), Maryborough (+4.5), Walhalla (-6.6) and Costerfield (+8.3; Fig. 3).

In order to provide a broad sampling of Victorian Paleozoic orogenic Au deposits for this pilot study, most of the deposits analysed here are represented by just a single Au sample. Multiple samples were analysed for Bendigo (ε^{107}Ag -2.3 and -3.8), Ballarat (-1.6 and +0.95) and Maryborough (-1.3 and +4.5, Fig. 4), i.e. showing isotopic ranges of 1.5, 2.55 and 5.8 ε^{107}Ag units.

5. Discussion

5.1 Isotopic Inheritance

It has been suggested that Ag isotope signatures in ore minerals may be inherited from the Ag sources (Hauri et al. 2000; Chugaev and Chernyshev 2012; Tessalina et al. 2015), much like Pb isotope variations are thought to reflect the sources of the Pb (e.g. Standish et al., 2013; Kamenov et al., 2013). This also predicts that isotopic variability within a single Ag-bearing ore deposit could reflect multiple Ag sources, assuming that isotopic fractionation on the pathway from source to ore mineral are negligible relative to the range of ^{107}Ag/^{109}Ag in the source rocks. Resolvable Ag isotope variations are indeed known from common crustal rock types (Fig. 3) (Hauri et al. 2000; Woodland et al. 2005; Schönbächler et al. 2007; 2010). Distinct ranges of ε^{107}Ag values have been reported for different deposit types and are possibly related to different source rocks

(Fig. 3) (Tessalina et al. 2015).

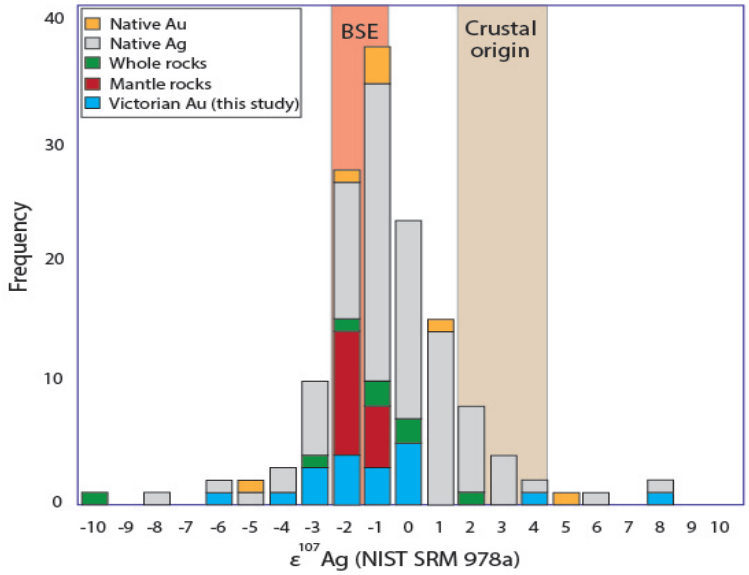

Figure 3: Frequency distribution histogram of Ag isotopic compositions in terrestrial materials from this study (blue) as well as Hauri et al., (2000); Woodland et al., (2005); Schönbächler (2007); Schönbächler et al. (2010); Chugaev and Chernyshev, (2012); Mathur et al., (2018). Bulk silicate Earth (BSE) is defined by Schönbächler et al. (2010) and crustal origin is defined by Tessalina et al., (2015). Epsilon units are relative to the NIST SRM 978a Ag isotope standard.

If inheritance of $^{107}Ag/^{109}Ag$ from source rocks is the major control on Ag isotope variability in hydrothermal mineral deposits, one would expect small $\varepsilon^{107}Ag$ ranges in genetically similar groups of deposits. The orogenic Au deposits in the Bendigo Zone all share similar settings (e.g. age, host rocks, structure, and potential – basaltic or shale derived – Au-Ag sources) and should, thus, show little variation in $\varepsilon^{107}Ag$. The large range in $\varepsilon^{107}Ag$ (-6.6 to +8.3) observed for the analysed Au grains from these deposits suggests that inheritance is not the major control on $^{107}Ag/^{109}Ag$ in the hydrothermal Au. This is made evident by gold samples from the Walhalla and Fosterville deposits, which have significantly lower $\varepsilon^{107}Ag$ values (-6.6 and -4.7 respectively) than the Bulk Silicate Earth (BSE) range. The BSE value of -2.2 comes from unaltered mantle-derived igneous rocks (Schönbächler et al. 2010), and it is expected that the Cambrian basaltic basement below Victoria would have this value. Similarly, the Costerfield gold sample has a $\varepsilon^{107}Ag$ value (+8.3) significantly higher than the "crustal origin" range, supposedly an analogue for the Ordovician turbidites in Victoria (Tessalina et al., 2015) (Fig. 3). Large intra-deposit variations such as those for Maryborough (two native Au samples differ

by 5.8 ε units) are also difficult to explain with simple isotopic inheritance. Therefore, it is suggested that physico-chemical fractionation of Ag isotopes during ore-forming processes are a major control on ε^{107}Ag in the orogenic Au deposits of Victoria.

5.2 The Nuclear Volume Effect

While systematic studies of Ag isotopic fractionation in natural and experimental settings are still rare (Mathur et al., 2018), helpful insights can be gained from other, better-studied heavy isotope systems. It has been shown that isotopic fractionation mechanisms important in relatively heavy elements differ from those that affect the low-mass elements such as H, C, N, O and S (Schauble, 2007). Heavy element isotope fractionation is not dominated by mass-dependant mechanisms because the differences in zero-point vibrational energies that drive these reactions are smaller than in the lighter elements. As a result, natural isotopic fractionation in heavy elements is more limited than in the light elements. For example, ^{203}Tl/^{205}Tl and ^{202}Hg/^{198}Hg show total variations of 1.8-2.0 and 3-5 ‰, respectively, in seafloor hydrothermal systems (Rehkämper et al., 2004; Smith et al., 2005). Such variations have been attributed to relative differences in the contraction of s-orbitals in nuclei of different ionic charge, the so-called nuclear

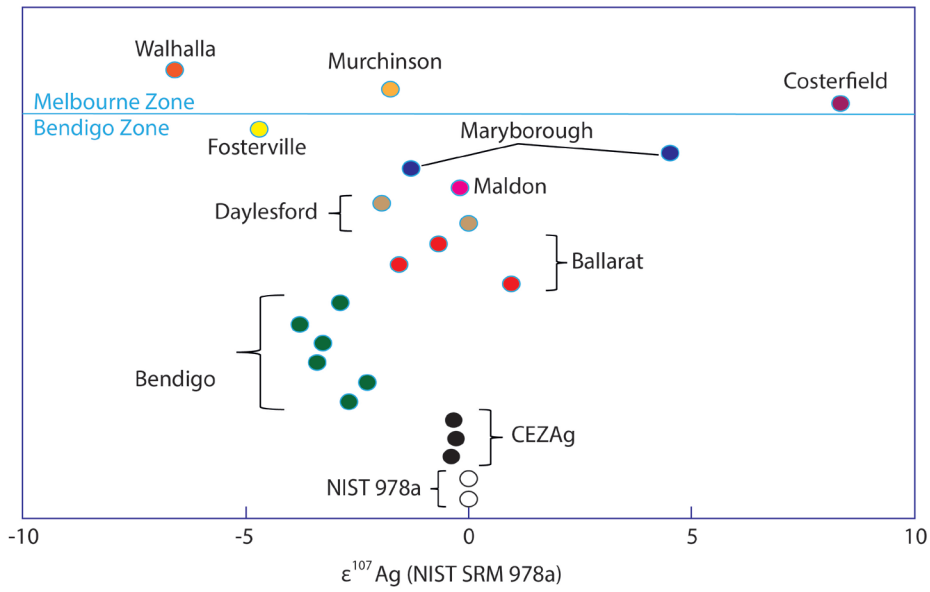

Figure 4: ε107Ag values and corresponding locations for Victorian gold samples and standards discussed in this study. Ag isotopic compositions of Au samples relative to NIST 978a. CEZAg is an in house Au nugget solution standard at the Curt-Engelhorn-Zentrum Archäometrie.

volume effect (Schauble, 2007). The nuclear volume effect predicts heavy isotope enrichment in the more oxidised forms of an element, e.g. for Tl^{3+} and Hg^{2+} compared to the more reduced Tl^{+} and Hg^{0}. The calculations predict nuclear volume -related isotopic fractionations of ~10 ‰ per amu for Tl and Hg, decreasing to 2‰ per amu for Ru and 0.2‰ per amu for S. Oxidation state, or s-orbital electron density, is thus a potentially significant control on isotope fractionation in the heavy elements, including Ag.

Silver occurs as Ag^{0} and Ag^{+}, and s-electron occupational changes between these species (i.e., Ag^{0} [Kr]4d105s1→ Ag^{+} [Kr]4d105s0) should lead to Ag^{109} enrichment in the oxidized Ag. Indeed, this was shown to be the case in leach experiments using native Ag (Mathur et al., 2018). In hydrothermal solutions, Ag is thought to be present as Ag^{+} (Migdisov and William-Jones, 2013; Pokrovski et al., 2013a) while deposition occurs as Ag^{+} in sulphides and sulfosalts, or as Ag^{0} in native metal alloys such as Au and electrum. The reduction associated with deposition of dissolved Ag^{+} as Ag^{0} in Au grains should produce ^{109}Ag enrichment (lower $^{107}Ag/^{109}Ag$) in the residual hydrothermal fluid relative to the Au. Furthermore, cogenetic mineral phases containing Ag in the different oxidation states (e.g., co-precipitating sulphides and native metal) should show systematic Ag isotope fractionation (Fig.5). This co-precipitation of Ag in metal and in sulphide might create differences between deposits given their different mineralogies. For example, coexisting native Ag (Ag^{0}) and pyrite (with trace Ag^{+}) from Pibram (Czech Republic) have $\varepsilon^{107}Ag$ of +1.9 and -0.8, respectively, a difference of 2.7 ε units (Woodland et al., 2005). Based on interpolation of the data for Tl, Hg, and Ru (Schauble, 2007), the total equilibrium fractionation of ^{107}Ag and ^{109}Ag is predicted to be ~2-4 ε (Chugaev and Chernyshev, 2012), consistent with the Pibram results. It is concluded that nuclear volume effects associated with Ag oxidation state changes are likely to be a major control on $^{107}Ag/^{109}Ag$ fractionation in Ag-bearing minerals.

The nuclear volume effect could also explain the Ag isotope variation observed in the genetically similar orogenic Au deposits of Victoria, such as the relatively modest variations (1.5 and 1.55 ε units) observed in data for Bendigo and Ballarat (Table 1, Fig.4). $\varepsilon^{107}Ag$ in the two Au grains from Maryborough differs by 5.8 ε-units and have

distinctly different mineralogies. Sample M18738 (ε^{107}Ag -1.3) contains native Au in quartz with no other Ag-bearing phases, while M42560 (ε^{107}Ag +4.5) contains quartz with native Au, pyrite and malachite. Silver is both chalcophile and aurophile and would be expected to partition into pyrite and chalcopyrite (later weathered to malachite) as oxidized Ag^+ and into native Au as Ag^0. The oxidized Ag in the sulphides should be enriched in ^{109}Ag compared to the reduced Ag in the native Au, producing higher ε^{107}Ag in the sulphide-bearing sample M42560. This suggests that nuclear volume effects during redox reactions may be the main driver behind Ag-isotopic fractionation.

5.3 Physio-chemical Fractionation in Ore Deposit Environments

The interpretation of ^{107}Ag/^{109}Ag in hydrothermal Au deposits may be further complicated by other physio-chemical processes, such as boiling/phase separation, multistage ore paragenesis, and remobilisation. The effects of boiling and other vapour-liquid or liquid-liquid phase separations are commonly observed in shallow hydrothermal environments, such as porphyry and epithermal deposits (Heinrich et al., 1999; Cooke and Simmons, 2000). Coexisting vapour and liquid phases produced by boiling can carry ore-forming elements and stable isotope compositions are known to fractionate (Leeman et al., 1992; Truesdell et al., 1978; Giggenbach and Stewart, 1982). For example, significant fractionation of Hg isotopes in epithermal systems in Nevada was attributed to boiling (Smith et al., 2005). It was shown that Hg^0 partitioned into a vapour phase during fluid ascent, and continued diffusion of Hg between the coexisting liquid and vapour phases enriched the vapour in ^{198}Hg, leaving the residual liquid enriched in ^{202}Hg. Shallow parts of these epithermal systems appear to be dominated by vapour-borne Hg (δ^{202}Hg = -3.5‰) while deeper parts are dominated by the fluid-borne Hg (δ^{202}Hg = +2.1‰), producing a total range of 5.6‰. This isotopic gradient is larger than the variations in low-temperature deposits that did not boil (δ^{202}Hg ranges of 1.3 to 1.9‰). Likewise, experimental data on Cu isotope partitioning between coexisting vapour and liquid phases show light Cu (^{63}Cu) enrichment in the vapour phase in conditions typical of shallow porphyry environments (Rempel

et al., 2012). These results may be equally applicable to Ag isotopes: modelling by Migdisov and Williams-Jones (2012) has shown that Ag solubility in vapour is significant in magmatic-hydrothermal systems, implying the potential for Ag isotope fractionation during phase separation.

5.4 Ag isotope constraints on orogenic Au deposition in the Victorian Goldfields

Mineralisation in orogenic Au deposits is thought to be episodic and linked to earthquake-induced fault-valve processes (Sibson et al., 1988; Cox, 1995; Micklethwaite et al., 2010; Weatherley and Henley, 2013; Peterson and Mavrogenes, 2014). This is supported, for example, by cyclic changes in trace element and $\delta^{34}S$ in pyrites from the Porgera Au-Ag deposit in Papua New Guinea. Single Porgera pyrites record repeated high-Au/negative $\delta^{34}S$ (−11.98‰ ± 0.43‰) and low-Au/positive $\delta^{34}S$ (+0.34‰ ± 0.45‰) zones which are thought to be related to rapid Au deposition during pressure release, due to fault failure, followed by the deposition of a more rock-buffered (Au-poor) fluid from adjacent wallrock as the fracture seals (Peter-

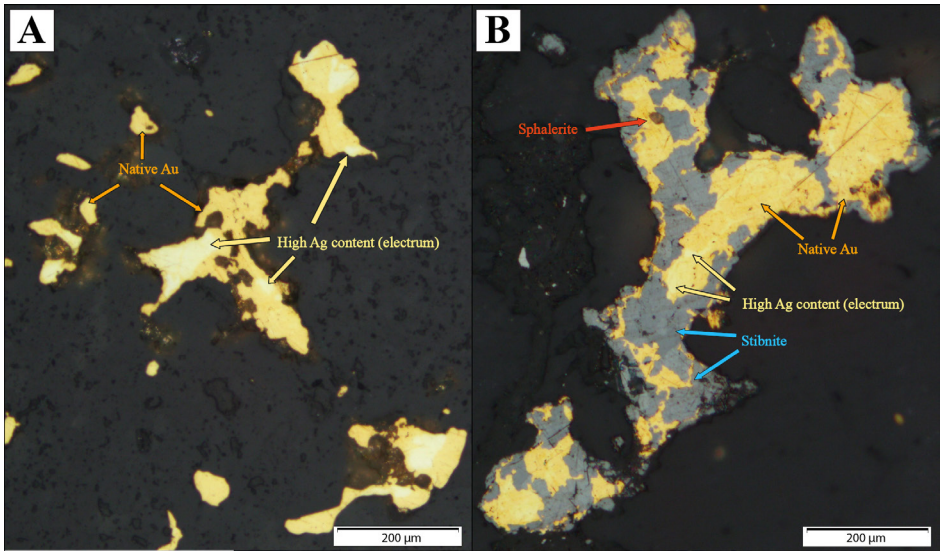

Figure 5: A) Photomicrograph of a polished thin section showing zones of high Ag content within native Au grains from the Fosterville gold mine, Victoria, Australia. Areas of high Ag content are pale yellow to white in colour and zoning is patchy and irregular. Plane polarized reflected light. B) Photomicrograph of a polished thin section showing intergrown anhedral sphalerite, stibnite and native Au from the Fosterville gold mine, Victoria, Australia. The gold grains contain fine irregular zones of high Ag content (pale yellow to white). Plane polarized reflected light.

son and Mavrogenes, 2014). Orogenic Au mineralisation in Victoria is thought to be sourced from deeply-buried metabasalts and/or black shales within a large crustal region undergoing metamorphism (e.g. Tomkins, 2010; Elmer et al. 2006). Auriferous metamorphic fluids are then transported upwards via crustal-scale fault networks during earthquakes, for 10s of kms, from upper amphibolite facies rocks in the source to the lower greenschist facies rocks which host the deposits (Sibson et al., 1988; Cox et al., 1995; Micklethwaite et al., 2010), where Au and sulphides are precipitated in response to changing fluid conditions (e.g., Evans et al., 2006; Bateman & Hagemann 2004; Möller & Kersten 1994). Apart from geochronological evidence for multiple mineralisation stages spaced 10s of M.y. apart (e.g., Bierlein et al., 2001; Phillips et al., 2012; Fairmaid et al., 2018), there is textural and mineral-chemical evidence for remobilisation of Au within deposits (e.g., Fougerouse et al., 2016). For example, Au grains from several deposits show zoning in Ag content (Fig. 5) and - by analogy with observations like those from Porgera - preserve evidence for numerous cycles of Au-Ag remobilisation and mineralisation. Evidence for multiple remobilisation events in the Au deposits themselves may imply that remobilisation also occurs along deeper parts of the fault-hosted fluid pathways. A step-wise remobilisation and reprecipitation process may act to migrate, and upgrade, Au and Ag during fluid ascent, with implications for Ag isotope compositions. In multiple dissolution-precipitation cycles, dissolution of Ag-bearing native Au should produce dissolved $Ag^{1}Cl$ or $Ag^{1}(HS)_2^-$ which, according to the nuclear volume effect, should be enriched in ^{109}Ag relative to the original native Au (Seward et al., 2014; Mathur et al., 2018). Numerous remobilisation events involving native Au should cause fertile fluids to become progressively ^{109}Ag-rich (lower $\varepsilon^{107}Ag$), leaving behind ^{109}Ag-depleted (high $\varepsilon^{107}Ag$) Au residua at depth. This could produce vertical Ag isotopic gradients, or zonation, in orogenic gold systems, with ^{109}Ag-enriched Au in its uppermost parts and ^{109}Ag-depleted Au left at depth. This may explain the more extreme $\varepsilon^{107}Ag$ values recorded in this study, i.e. strongly negative (^{109}Ag-enriched) $\varepsilon^{107}Ag$ as observed for Au nuggets from Fosterville and Walhalla (-4.7 and -6.6), and the strongly positive (^{109}Ag-depleted) $\varepsilon^{107}Ag$ for

Costerfield (+8.3).

6. Conclusions

The large range of $^{107}Ag/^{109}Ag$ in 18 native Au grains from 440-370 Ma orogenic Au deposits in Victoria strongly contrasts with the narrow ranges in mineralisation styles, host rocks and tectonic setting of these deposits. While there is some clustering of measured $\varepsilon^{107}Ag$ around the composition of mantle-derived (basaltic) Ag (Fig.3), the diversity of isotopic compositions seems to preclude simple isotopic links to particular source rocks (basalts, black shales, turbidites, granites). It is likely that source signatures were variably modified by transport- and deposition-related processes capable of producing Ag isotopic fractionation, such as (i) physico-chemical processes related to ore formation (e.g., phase separation, boiling, etc.); and (ii) nuclear volume fluctuations due to s-electron addition/removal during redox reactions involving Ag^{+} $\leftrightarrow$ Ag^{0} along transport pathways and at the sites of ore accumulation. Although mass-dependant (kinetic) isotope fractionation cannot be ruled out, it's contribution may be restricted for the Ag isotope system and we consider the data here to be best explained by processes (i) and (ii). Further studies of the effects of temperature, redox, ligand and mineral speciation on the fractionation of Ag isotopes are clearly needed, as is a better understanding of the diversity in crustal Ag isotope reservoirs. The remobilisation model proposed here is consistent with the inferred episodic nature of fluid transport within orogenic Au systems during their formation, and with macroscopic and microscopic evidence for reworking. If, as the model implies, Ag isotopic heterogeneity exists on the large scale, it may also be recorded at the grain scale. Spatially-resolved Ag isotope work in Au grains would be useful to further explore this aspect of the model suggested for the ore genesis of orogenic Au deposits in the Victorian Goldfields.

Acknowledgments

The authors wish to thank Braden Verity, Simon Hitchman, Nathan Phillips and the geological team at the Fosterville Gold Mine for their assistance and advice. We would also like to thank Rob Duncan and the Geological Survey of Victoria for their partnership in this endeavour. We would like to show our appreciation towards Museum Victoria for their kind donation of samples from their collections which made this study possible. Finally, thanks to Dr. Nicholas Hunter for providing stimulating discussion regarding sample textures. This project was funded by the ARC Linkage grant (LP150100717).

References

Argapadmi, W., Toth, E. R., Fehr, M. A., Sehonbachler, M., and Heinrich, C. A., 2018, Silver Isotopes as a Source and Transport Tracer for Gold: A Reconnaissance Study at the Sheba and New Consort Gold Mines in the Barberton Greenstone Belt, Kaapvaal Craton, South Africa: Economic Geology, v. 113, p. 1553-1570.

Bateman, R., and Hagemann, S., 2004, Gold mineralisation throughout about 45 Ma of Archaean orogenesis: protracted flux of gold in the Golden Mile, Yilgarn craton, Western Australia: Mineralium Deposita, v. 39, p. 536-559.

Bierlein, F. P., Arne, D. C., Foster, D. A., and Reynolds, P. R., 2001, A Geochronological framework for slate belt-hosted gold mineralisation in central Victoria, Australia.: Mineral Deposita, v. 36, p. 741-767.

Carlson, R. W., and Hauri, E. H., 2001, Extending the 107Pd-107Ag chronometer to low Pd/Ag meteorites with multicollector plasma-ionization mass spectrometry: Geochimica et Cosmochimica Acta, v. 65, p. 1839-1848.

Cayley, R. A., Korsch, R. J., Moore, D. H., Costelloe, R. D., Nakamura, A., Willman, C. E., Rawling, T. J., Morand, V. J., Skladzien, P. B., and O'Shea, P. J., 2011, Crustal architecture of central Victoria: results from the 2006 deep crustal reflection seismic survey: Australian Journal of Earth Sciences, v. 58, p. 113-156.

Chugaev, A. V., and Chernyshev, I. V., 2012, High-noble measurement of 107Ag/109Ag in native silver and gold by multicollector inductively coupled plasma mass spectrometry (MC-ICP-MS): Geochemistry International, v. 50, p. 889-910.

Cooke, D. R., and Simmons, S. F., 2000, Characteristics and Genesis of Epithermal Gold Deposits, *in* Hagemann, S. G., and Brown, P. E., eds., Gold in 2000, Society of Economic Geologists.

Cox, S. F., 1995, Faulting processes at high fluid pressures: An example of fault valve behavior from the Wattle Gully Fault, Victoria, Australia: Journal of Geophysical Research: Solid Earth, v. 100, p. 12841-12859.

Desaulty, A.-M., Telouk, P., Albalat, E., and Albarède, F., 2011, Isotopic Ag–Cu–Pb record of silver circulation through 16th–18th century Spain: Proceedings of the National Academy of Sciences, v. 108, p. 9002-9007.

Elmer, F., White, R., and Powell, R., 2006, Devolatilization of metabasic rocks during greenschist–amphibolite facies metamorphism: Journal of Metamorphic Geology, v. 24, p. 497-513.

Evans, K. A., Phillips, G. N., and Powell, R., 2006, Rock-buffering of auriferous fluids in altered rocks associated with the Golden Mile-style mineralisation, Kalgoorlie gold field, Western Australia: Economic Geology, v. 101, p. 805-817.

Fairmaid, A. M., Phillips, D., and Wilson, C. J. L., 2017, Episodic gold mineralisation correlated with discrete structural events at Ballarat East, southeast Australia: Ore Geology Reviews, v. 91, p. 541-558.

Fougerouse, D., Micklethwaite, S., Tomkins, A. G., Mei, Y., Kilburn, M., Guagliardo, P., Fisher, L. A., Halfpenny, A., Gee, M., and Paterson, D., 2016, Gold remobilisation and formation of high grade ore shoots driven by dissolution-reprecipitation replacement and Ni substitution into auriferous arsenopyrite: Geochimica et Cosmochimica Acta, v. 178, p. 143-159.

Giggenbach, W., and Stewart, M., 1982, Processes controlling the isotopic composition of steam and water discharges from steam vents and steam-heated pools in geothermal areas: Geothermics, v. 11, p. 71-80.

Gray, D., and Foster, D., 2004, Tectonic evolution of the Lachlan Orogen, southeast Australia: historical review, data synthesis and modern perspectives: Australian Journal of Earth Sciences, v. 51, p. 773-817.

Hauri, E., Carlson, R., and Bauer, J., 2000, The timing of core formation and volatile depletion in solar system objects from high-precision 107Pd-107Ag isotope systematics: Lunar and Planetary Science Conference, 2000.

Heinrich, C. A., Gunther, D., Audétat, A., Ulrich, T., and Frischknecht, R., 1999, Metal fractionation between magmatic brine and vapor, determined by microanalysis of fluid inclusions: Geology, v. 27, p. 755-758.

Hughes, M., and Phillips, G., 2015, Mineralogical domains within gold provinces: Applied Earth Science, v. 124, p. 191-204.

Hughes, M., Phillips, G., and Gregory, L., 1997, Mineralogical domains in the Victorian gold province, Maldon, and Carlin-style potential: Australasian Institute of Mining and Metallurgy Annual Conference, Ballarat, 1997, p. 215-227.

Kamenov, G. D., Melchiorre, E. B., Ricker, F. N., and DeWitt, E., 2013, Insights from Pb isotopes for native gold formation during hypogene and supergene processes at Rich Hill, Arizona: Economic Geology, v. 108, p. 1577-1589.

Kelly, W. R., and Wasserburg, G., 1978, Evidence for the existence of 107Pd in the early solar system:

Geophysical Research Letters, v. 5, p. 1079-1082.

Leeman, W. P., Vocke, R. D., and McKibben, M. A., 1992, Boron isotopic fractionation between co-existing vapor and liquid in natural geothermal systems: 7th International symposium on waterrock interaction proceedings, 1992, p. 1007-1010.

Luo, G., Kump, L. R., Wang, Y., Tong, J., Arthur, M. A., Yang, H., Huang, J., Yin, H., and Xie, S., 2010, Isotopic evidence for an anomalously low oceanic sulfate concentration following end-Permian mass extinction: Earth and Planetary Science Letters, v. 300, p. 101-111.

Mathur, R., Arribas, A., Megaw, P., Wilson, M., Stroup, S., Meyer-Arrivillaga, D., and Arribas, I., 2018, Fractionation of silver isotopes in native silver explained by redox reactions: Geochimica et Cosmochimica Acta, v. 224, p. 313-326.

Micklethwaite, S., Sheldon, H. A., and Baker, T., 2010, Active fault and shear processes and their implications for mineral deposit formation and discovery: Journal of Structural Geology, v. 32, p. 151-165.

Migdisov, A. A., and Williams-Jones, A., 2013, A predictive model for metal transport of silver chloride by aqueous vapor in ore-forming magmatic-hydrothermal systems: Geochimica et Cosmochimica Acta, v. 104, p. 123-135.

Möller, P., and Kersten, G., 1994, Electrochemical accumulation of visible gold on pyrite and arsenopyrite surfaces: Mineralium Deposita, v. 29, p. 404-413.

Murthy, V. R., 1960, Isotopic composition of silver in an iron meteorite: Physical Review Letters, v. 5, p. 539.

Paterson, S. R., Tobisch, O. T., and Morand, V. J., 1990, The influence of large ductile shear zones on the emplacement and deformation of the Wyangala Batholith, SE Australia: Journal of Structural Geology, v. 12, p. 639-650.

Peterson, E. C., and Mavrogenes, J. A., 2014, Linking high-grade gold mineralisation to earthquake-induced fault-valve processes in the Porgera gold deposit, Papua New Guinea: Geology, v. 42, p. 383-386.

Phillips, D., Fu, B., Wilson, C. J., Kendrick, M., Fairmaid, A., and Miller, J. M., 2012, Timing of gold mineralisation in the western Lachlan Orogen, SE Australia: A critical overview: Australian Journal of Earth Sciences, v. 59, p. 495-525.

Phillips, G. N., and Hughes, M. J., 1996, The geology and gold deposits of the Victorian gold province: Ore Geology Reviews, v. 11, p. 255-302.

Pokrovski, G. S., Borisova, A. Y., and Bychkov, A. Y., 2013, Speciation and transport of metals and metalloids in geological vapors: Reviews in Mineralogy and Geochemistry, v. 76, p. 165-218.

Rehkämper, M., Frank, M., Hein, J., and Halliday, A., 2004, Cenozoic marine geochemistry of thallium deduced from isotopic studies of ferromanganese crusts and pelagic sediments: Earth and Planetary Science Letters, v. 219, p. 77-91.

Rempel, K. U., Liebscher, A., Meixner, A., Romer, R. L., and Heinrich, W., 2012, An experimental study of the elemental and isotopic fractionation of copper between aqueous vapour and liquid to 450 C and 400 bar in the CuCl–NaCl–H2O and CuCl–NaHS–NaCl–H2O systems: Geochimica et Cosmochimica Acta, v. 94, p. 199-216.

Schauble, E. A., 2007, Role of nuclear volume in driving equilibrium stable isotope fractionation of mercury, thallium, and other very heavy elements: Geochimica et Cosmochimica Acta, v. 71, p. 2170-2189.

Schönbächler, M., Carlson, R., Horan, M., Mock, T., and Hauri, E., 2010, Heterogeneous accretion and the moderately volatile element budget of Earth: Science, v. 328, p. 884-887.

Schönbächler, M., Carlson, R. W., Horan, M. F., Mock, T. D., and Hauri, E. H., 2007, High precision Ag isotope measurements in geologic materials by multiple-collector ICPMS: an evaluation of dry versus wet plasma: International Journal of Mass Spectrometry, v. 261, p. 183-191.

Seward, T., Williams-Jones, A., and Migdisov, A., 2014, 13.2 The Chemistry of Metal Transport and Deposition by Ore-Forming Hydrothermal Fluids: Treatise on Geochemistry. second ed. Elsevier, Oxford, p. 29-57.

Sibson, R. H., Robert, F., and Poulsen, K. H., 1988, High-angle reverse faults, fluid-pressure cycling, and mesothermal gold-quartz deposits: Geology, v. 16, p. 551-555.

Smith, C. N., Kesler, S. E., Klaue, B. r., and Blum, J. D., 2005, Mercury isotope fractionation in fossil hydrothermal systems: Geology, v. 33, p. 825-828.

Standish, C., Dhuime, B., Chapman, R., Coath, C., Hawkesworth, C., and Pike, A., 2013, Solution and laser ablation MC-ICP-MS lead isotope analysis of gold: Journal of Analytical Atomic Spectrometry, v. 28, p. 217-225.

Tessalina, S. G., Rankenburg, K., Naumo, v. E., Goryachev, N. A., and Savva, N. E., 2015, The Ag Isotope Systematics in Native Silver from Some Hydrothermal Deposits: Toward a New Tool for Mineral Deposits Studies.: Mineral resources in a sustainable world, 13th SGA Biennial meeting Proceedings, Nancy, France, v. 2, p. 647-650.

Tobisch, O. T., and Paterson, S. R., 1990, The Yarra granite: an intradeformational pluton associated with ductile thrusting, Lachlan Fold Belt, southeastern Australia: Geological Society of America Bulletin, v. 102, p. 693-703.

Tomkins, A. G., 2010, Windows of metamorphic sulfur liberation in the crust: Implications for gold deposit genesis: Geochimica et Cosmochimica Acta, v. 74, p. 3246-3259.

Truesdell, A., Rye, R., Pearson Jr, F., Olson, E., Nehring, N., Whelan, J., Huebner, M., and Coplen, T., 1979, Preliminary isotopic studies of fluids from the Cerro Prieto geothermal field: Geothermics, v. 8, p. 223-229.

VandenBerg, A., 2000, The Tasman Fold Belt system in Victoria: geology and mineralisation of Proterozoic to Carboniferous rocks, Geological Survey of Victoria.

Weatherley, D. K., and Henley, R. W., 2013, Flash vaporization during earthquakes evidenced by gold deposits: Nature Geoscience, v. 6, p. 294.

Willman, C., Korsch, R., Moore, D., Cayley, R., Lisitsin, V., Rawling, T., Morand, V., and O'Shea, P., 2010, Crustal-scale fluid pathways and source rocks in the Victorian gold province, Australia: Insights from deep seismic reflection profiles: Economic Geology, v. 105, p. 895-915.

Woodland, S., Rehkämper, M., Halliday, A. N., Lee, D.-C., Hattendorf, B., and Günther, D., 2005, Accurate measurement of silver isotopic compositions in geological materials including low Pd/Ag meteorites: Geochimica et cosmochimica acta, v. 69, p. 2153-2163.

Chapter 3

Aseismic Refinement of Orogenic Gold Systems

Christopher R. Voisey[1], David Willis[2], Andrew G. Tomkins[1], Christopher J. L.Wilson[1], Steven Micklethwaite[1], Filomena Salvemini[3], Jeremy Bougoure[4], William D. A. Rickard[5]

[1]*School of Earth, Atmosphere & Environment, Monash University, Clayton, VIC 3800, Australia*

[2]*Department of Earth & Environmental Sciences, University of Kentucky, Lexington, KY 40506-0053, United State of America*

[3]*Australian centre for neutron Scattering, ANSTO, Lucas Heights, New South Wales, 2234, Australia*

[4]*Centre for Microscopy, Characterisation & Analysis, University of Western Australia, Perth, Western Australia, 6009, Australia*

[5]*John de Laeter Centre, Curtin University, Bentley, Western Australia, 6845, Australia*

"I'm not crazy!"
- Words of an obsessed man

Abstract

Orogenic Au deposits have contributed the majority of Au recovered globally throughout history. However, the mechanism that concentrates Au to extremely high "bonanza" grades in small domains within these deposits remains enigmatic. The volume of fluid required to provide extreme Au endowments in localized occurrences are not reflected in field observations (e.g., in the extent of quartz veining or hydrothermal alteration). Detailed optical, scanning and transmission electron microscopy, nanoscale secondary ion mass spectrometry, as well as 3-D neutron tomography have been used to investigate the processes responsible for development of anomalously high-grade ore (upwards of 3% Au) found in quartz veins at Fosterville gold mine (Victoria, Australia). Distinct textural settings of visible Au include: (i) Au concentrated along pressure-solution seams (PSS) associated with wall-rock selvages; (ii) as nano- to micro-scale "dusty gold seams" parallel to PSS; and (iii) in micro-scale tension fractures perpendicular to stylolitic seams. The distribution of Au in arsenopyrite and pyrite hosted within PSS changes as a function of the extent of deformation. Sulphides in highly deformed PSS exclusively host Au as nano- to micro-metre sized clusters within features associated with corrosion and brittle failure, whereas sulphides in mildly deformed PSS have Au bound in the crystal structure. It is proposed that Au supersaturation in fluids introduced during seismic periods led to the deposition of abundant Au nanoparticles in quartz-carbonate veins. Subsequent pressure-dissolution of vein quartz and carbonate during inter-seismic intervals allowed for episodic increase in the gold/quartz ratio, and permitted liberation and migration of Au nanoparticles, promoting gold grain growth in favourable textural settings. Galvanic corrosion and brittle fracturing of auriferous sulphides during the inter-seismic period allowed additional remobilisation and/or enrichment of sulphide-hosted Au. Repetition of this mechanism over the time scale of deposit formation acted to concentrate Au within the lodes. This Au ore upgrading model, referred to as "aseismic refinement", provides a new insight for the genesis of ultra-rich Au mineralisation and, based on textures reported from many Au deposits, may be a globally significant component in the formation of orogenic Au deposits.

Chapter 3

1. Orogenic Gold Systems

Orogenic Au deposits, also known as “mesothermal” or “lode-Au” deposits, are a distinct family of mineral deposits that are responsible for ~30% of the Au recovered globally through history - if their derived placer deposits are considered (Phillips and Powell, 2011; Phillips, 2013). This family of Au deposits formed in distinct periods across much of the Earth’s geological history, with peaks of formation in the late Archean cratons, Paleoproterozoic mobile belts, and Phanerozoic orogenic fold and thrust belts (Goldfarb et al., 2001; Tomkins, 2013). Forming during convergent tectonics, these wide-spread hydrothermal systems are hosted in rocks of variable metamorphic grade involving mid- to upper-crustal temperatures and pressures between 200-650 °C and 1-5 kbar (Groves, 1993; Tomkins and Grundy, 2009). Under these conditions, the abundant episodic quartz-carbonate veining found in these deposits indicates formation from fluids that attained supralithostic pressures numerous times during deposit formation (Sibson, 1975; Cox, 1995). These seismic pumping or fault-valving events have been a primary focus of research on orogenic Au deposits and are widely considered a vital component of their formation. However, processes that occur during the inter-seismic intervals between these failure events have been almost entirely overlooked with respect to their significance for the genesis of Au ore.

It has been shown that hydrothermal fluids that are enriched in H_2S, with ideal intermediate fO_2, and circum-neutral pH can carry Au in concentrations on the order of 10s to 100s of ppb, increasing to as high as ppm levels at elevated temperatures and pressures (Williams-Jones et al., 2009). But for very-high-grade Au occurrences, which in these deposits can locally exceed several percent, identifying the mechanism that so effectively concentrates Au from such modest concentrations in solution remains a long-standing problem. The volume of fluid required to provide such extreme localized endowments of Au are not reflected in field observations; for example, the extent of quartz veining and hydrothermal mineral alteration is not distinctly different to low grade ores. It is possible that large accumulations of native Au may form from gradual enrichment by ongoing precipitation on an initial Au “nucleus” over a

prolonged period. This would require that the gold nucleus remains, or is periodically, exposed to fluids throughout numerous infiltration events to allow for a gradual accumulation. This requirement is unlikely to be satisfied given that laminated quartz veins in orogenic systems form incrementally (Robert, 1995), whereby each stage of quartz growth effectively acts as a barrier between later fluid pulses and existing Au particles. Those focusing on the structural evolution of these systems specifically refer to quartz growth sealing up a periodically permeable system (Sibson et al., 1988; Cox et al., 1991). An alternative process proposed for carrying elevated concentrations of Au is the suspension of Au nanoparticles in a fluid that is saturated (or supersaturated) with respect to Au, or as a stable colloidal solution. Suspensions of Au nanoparticless have been observed to carry substantial concentrations of Au and can be stable during transport in geological conditions (e.g., Reich et al., 2006; Hough et al. 2011; Hannington et al., 2016; Saunders and Burke, 2017). However, most research on Au nanoparticles is focused on epithermal and Carlin-type ores and, with the exception of the novel study by Herrington and Wilkinson (1993), the significance of Au nanoparticle suspensions in the formation of vein-hosted orogenic Au deposits has not been considered.

Here, samples of anomalously high-grade (upwards of ~30,000 g/tonne Au) Au ore hosted in quartz-carbonate veins from Fosterville were examined to investigate how extremely rich localized occurrences of Au might form. A petrographic study combining optical, scanning and transmission electron microscopy was conducted to constrain the textural settings and nature of Au. Additionally, 3D neutron tomography was used to examine the spatial distribution of Au grains with respect to vein textures and nanoscale secondary ion mass spectrometry (nanoSIMS) was used to map the distribution of Au in pyrite and arsenopyrite in these settings. Textural features suggest that a combination of pressure-dissolution and self-assembly of Au nanoparticles during inter-seismic periods were important in forming the highest-grade Au lodes located at Fosterville. A naturally occurring ore refining model for the formation of ultra-high-grade Au ores and vein-hosted Au nuggets is proposed for orogenic settings.

1.1 Geological Setting & Sampling

The Fosterville Gold Mine, which is hosted by Ordovician turbidites of the Bendigo Zone within the western Lachlan Orogen (Gray et al., 2004), is located ~135 km north of Melbourne, Australia (Fig. 1). These sedimentary sequences have undergone greenschist facies metamorphism and were deformed into dominantly north-south trending chevron folds that are cut by thick-skinned thrust systems (VandenBerg et al., 2000). The majority of the Au deposits in the Bendigo Zone (containing ~2000 t Au; Moore, 2007) contain visible Au in quartz veins associated with brittle-ductile fault zones, saddle reefs, and en échelon vein networks (e.g., the Bendigo deposit, Wilson et al., 2013). The Fosterville deposit differs in that it contains three distinct mineralisation styles, (i) at all levels in the deposit, Au hosted in fine-grained arsenopyrite and pyrite crystals disseminated throughout metasedimentary wall rocks proximal to veining and major faulting; and (ii) at intermediate depths, visible free Au in quartz-carbonate veins variably associated with moderately abundant stibnite mineralisation, and (iii) at deeper levels, visible free Au in quartz-carbonate veins with minimal stibnite. All of these are associated with complex splay faulting focused on a shallowly south plunging anti-

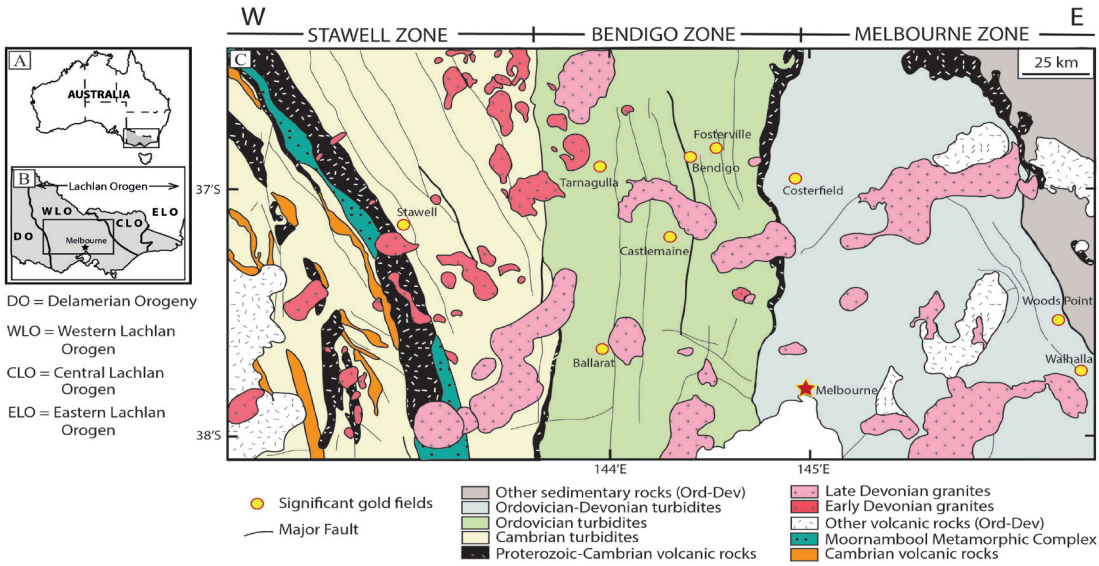

Figure 1: A) Schematic map of Australia with the state of Victoria highlighted in grey. Position of B is indicated. B) Inset map of Victoria and part of New South Wales showing the locations of the Lachlan Orogen and the Delamerian Orogen modified from Willman et al. (2010). Position of C is indicated. C) Simplified geological map of central Victoria modified from Phillips et al. (2012). Infilled circles show major goldfields.

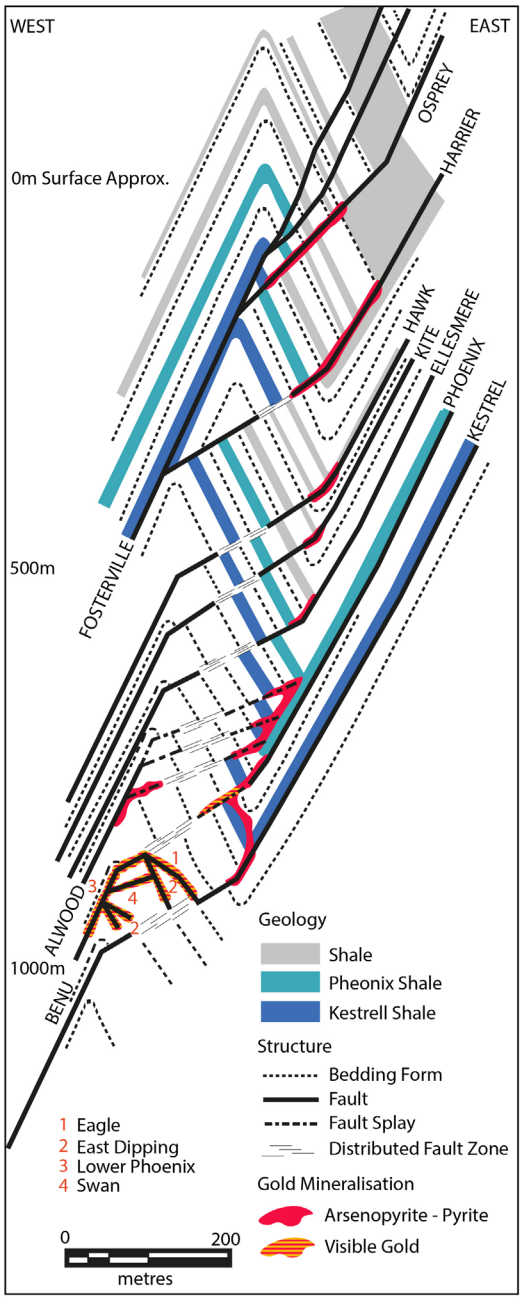

Figure 2: Schematic cross section of the Fosterville gold deposit, Victoria, Australia, adapted from Hitchman et al., (2018). Proportion of gold-bearing arsenopyrite increases towards mineralised quartz veins and along bedding discordant fault intersections. Visible vein-hosted gold grades are highest on west-dipping high-order linkage faults (faults labelled with numbers) at and below the Eagle Zone -e.g., Swan (4).

cline-syncline pair (Fig. 2). Sulphide-hosted Au mineralisation is found ubiquitously throughout the deposit, whereas visible Au is only present deeper in the system (>800 m depth from surface) (Fig. 2).

Disseminated sulphide-hosted Au ore is the volumetrically dominant Au mineralisation style at Fosterville, with average grades of 5-10 g/t Au and individual assays of up to 60 g/t Au (Hitchman et al., 2018). This mineralisation is structurally controlled by discordant bedding-fault relationships and forms as a selvage to quartz-carbonate veining (Fig. 2) (Leader et al., 2012). Sulphide ore shoots are typically 4-15 m wide, 50-150 m in dip extent and 300 – 2500 m in length down-plunge (Hitchman et al., 2018). Arsenopyrite occurs as fine-grained acicular needles (0.05-6 mm in length) that are either aligned with north-south trending cleavage or with no preferred orientation. Auriferous pyrite crystals occur as pyritohedrons between 0.1-2 mm in size. Gold contents in arsenopyrite range from 100-1000 ppm and pyrite contains between 10-100 ppm Au (Roberts et al., 2003). This sulphide mineralisation is variably overprinted by visible Au ± stibnite mineralisation at depths greater than 800m from the surface.

Visible gold found in the Eagle Zone and below (Fig. 2) averages grades of 15 g/t Au with individual assays over 1% Au and as high as 3% Au. Visible gold occurs as disseminated grains in quartz with sizes typically 0.01 – 3 mm, loosely arranged in planar accumulations parallel to their host vein orientation. In the Eagle Zone, visible Au contributes ~40% of the contained Au, and contributes ~10% of the total mineral resource at Fosterville (Hitchman et al., 2018). Areas with stibnite mineralisation may contain disseminated visible Au (<3 mm), although the grade is highly variable. The stibnite mineralisation appears to have replaced and infilled earlier quartz-carbonate veins, or occur as massive stibnite-quartz breccias along fault margins (Hitchman et al., 2018). Gold and stibnite can also be found in variably sized quartz crystal-lined vugs (1-5 cm) within quartz-carbonate veins.

2. Methodology

For this study, samples of vein-hosted Au from Fosterville's highest-grade ores were chosen. The samples consist of abundant visible Au in quartz-carbonate veins from reverse splay faults in the Eagle Zone (Fig. 2). These veins contain numerous stylolites defined by pressure-dissolved wall rock selvages, which are also host to high-grade auriferous sulphide mineralisation.

The suite of samples were prepared as 30µm thick polished thin sections for optical and scanning electron microscopy (SEM). SEM imaging was carried out at the Monash Centre of Electron Microscopy using a JOEL 7001 FEG-SEM as a first order examination of Au distribution and vein textures. Images were taken using a backscattered electron (BSE) detector with an acceleration voltage of 15.0 kV at a working distance of 9.1 mm and a probe current of 1.5 nA.

To inspect the extent of episodic quartz growth and pressure-dissolution with respect to Au distribution, cathodoluminescence (CL) and elemental mapping was conducted using a JOEL 8500F electron probe microanalyser (EPMA) at the Commonwealth Scientific and Industrial Research Organisation Microbeam Laboratory, Clayton. These maps were collected at an acceleration voltage of 25 kV and a probe current

of 40 nA. Both CL and elemental images were gathered with a 10 µm step size and a 30 ms dwell time per pixel.

Neutron tomography was conducted on the suite of Au-rich samples at the Australian Centre for Neutron Scattering to map the 3D distribution of Au with respect to vein microstructures. Using the DINGO instrument (Garbe, 2015), the high spatial resolution configuration (with the ratio of collimator-detector length, L, to inlet collimator diameter, D, equal to 1000), corresponding to a pixel size of 27 µm, was chosen. During the measurement, projections were obtained by rotating the sample around its vertical axis for 1339 angles equiangularly spaced from 0° to 360°. At each step the samples were exposed to the neutron beam for a period of 60s. The portion of the beam transmitted through the sample is converted into visible light using a 50µm thick 6LiF/ZnS scintillator, which is then guided via a mirror to an Andor DW434 CCD camera with 1024 x 1024 pixels. The data sets were reconstructed with the Octopus package (Dierick et al. 2004), and ANU Vizlab's Drishti software was used for visualization, analysis, and full three-dimensional image reconstruction.

Transmission electron microscopy (TEM) and focused ion beam - scanning electron microscopy (FIB-SEM) was conducted at the John de Laeter Centre, Curtin University, to investigate the nature of sub-micron Au particles within quartz. Images of sample F7B1 were acquired from a polished thin section with a thin carbon coating using a Tescan Lyra 3 FIB-SEM operated at acceleration voltage of 10 kV using secondary electron (SE) and BSE detectors. In some cases, the images were complemented by spot and area chemical analysis collected using energy-dispersive x-ray spectroscopy (EDS). The Tescan Lyra 3 FIB–SEM was used to produce site-specific lift out of a lamella. A region containing submicron Au particles (identified by EDS) approximately 10 µm wide was lifted out and mounted onto a copper grid. The lamella was then thinned to approximately 100 nm, followed by a low voltage (2 kV) "clean up" routine to remove surface damage.

The electron transparent lamella was used for transmission electron microscopy

(TEM) analysis on an FEI Talos FS200X G2 TEM/scanning TEM (STEM) microscope operated at 200 kV and equipped with a Super-X EDS system. High Angle Angular Dark Field (HAADF) imaging in STEM mode was used for imaging the Au grains.

High-resolution elemental mapping of pyrite and arsenopyrite crystals hosted in a wall-rock selvage in quartz was carried out using the Cameca NanoSIMS 50L at the Centre for Microscopy, Characterisation and Analysis (CMCA) at The University of Western Australia. Sulphide grains showing various degrees of pressure-dissolution were targeted for analysis to investigate the mineral geochemistry of sulphide-hosted Au ores during progressive deformation. The crystals of interest were removed from the hand sample specimen using a handheld rotary tool and were then prepared as a one-inch polished resin mount and carbon coated (approx. 15 nm). NanoSIMS measurements were performed with a Cs^+ primary beam, using a spot size of approximately 100 nm, impact energy of 16 keV, and a beam current of 10 pA. The instrument was operated in multicollector mode, allowing for detection of seven ion species in tandem (^{34}S, $^{54}Fe^{32}S$, $^{60}Ni^{32}S$, $^{75}As^{32}S$, ^{123}Sb, ^{130}Te and ^{197}Au). Secondary ion images were obtained by rastering the primary ion beam across areas measuring 50 x 50 μm, at a resolution of 512 x 512 pixels (each pixel measuring approximately 97 nm), with dwell time of 40 ms per pixel. The sample surface was presputtered with the primary ion beam (using 250 pA beam current) to 1.5 e17 ions/cm^2 in order to remove surface contamination and implant Cs^+ ions into the samples to reach a steady-state of ion emission. In all experiments an electron flood gun was used to minimize sample charging effects.

3. Gold Textures

Photographs show the distribution of variably sized Au grains along planes parallel to wall rock selvages and pressure solution seams, giving rise to a “dusty Au” seam texture (Fig. 3A, B, C). Photomicrographs reveal that Au grains are rounded to sub-round and are hosted within quartz crystals and along quartz grain boundaries, with many Au grains smaller than one micron in diameter (Fig. 3D, E). Cathodoluminescence imaging of sample F7B1 highlights multiple generations of quartz growth,

brecciation, fracturing, and neo-crystallization (Fig. 4A). Fine-grained quartz adjacent to these stylolitic pressure solution seams appear reprecipitated. These areas of secondary quartz have high porosity and are spatially associated with the distribution of fine-grained Au seen in the element maps (Fig. 4B). SEM images of the same sample reveal that Au mineralisation is nano-particulate in nature along porous areas, as well as within quartz crystals (Fig. 4C, D).

A fine-grained Au-rich seam found parallel and adjacent to the stylolitic selvage

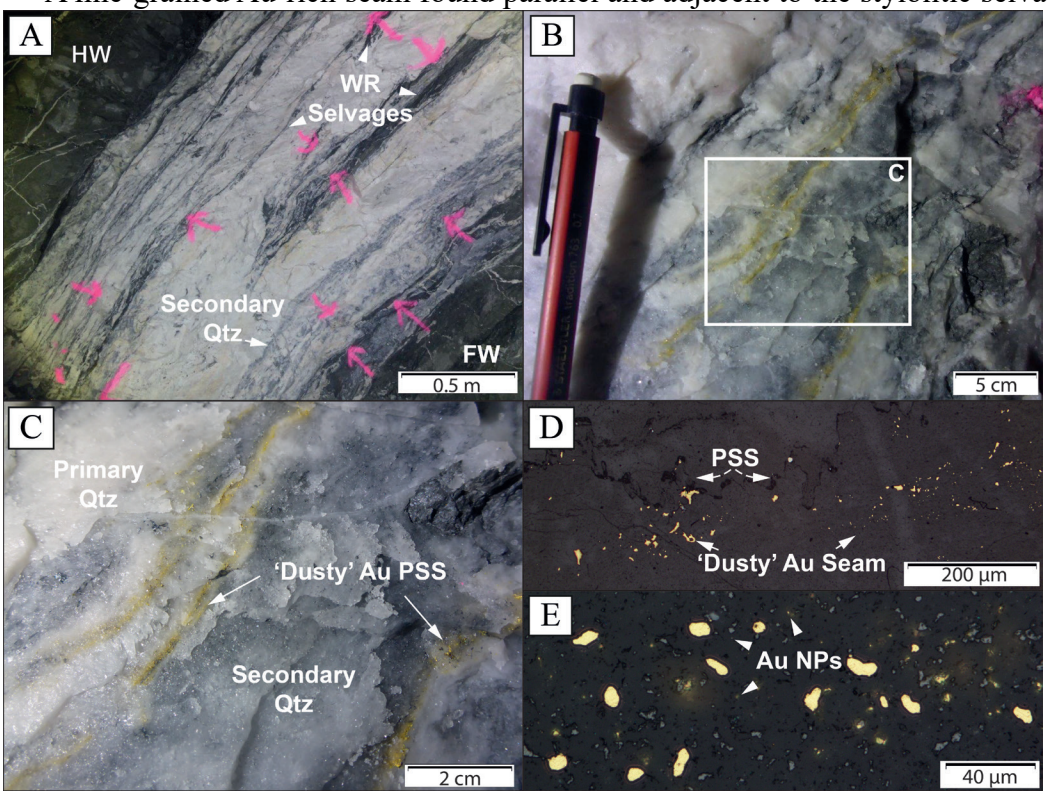

Figure 3: A) Photograph of laminated quartz vein from the Lower Phoenix fault at Fosterville. Pink arrows point towards areas of visible Au mineralisation. B) Photograph of 'dusty Au' pressure-solution seams forming parallel to stylolitized wall rock selvages. C) Photograph of area outlined in (B) of 'dusty Au' seams with grey reprecipitated secondary quartz between pressure-solution seams (PSS). D) Photomicrograph of sample F7B1 showing fine-grained Au seams formed parallel to a stylolitic wall rock selvage. E) Photomicrograph of D at higher magnification revealing sub-micron sized Au particles.

in sample F7B1 was the target for FIB-SEM to detect the presence of nanoparticulate Au (Fig. 5). The target area for the TEM sample foil is highlighted in Fig. 5C; the sub-micron Au particles of interest are noted in Fig. 5B. Bright-field TEM images of the sample foil (Fig. 6) how 3 notable Au grains (black) situated between variably de-

formed crystals of quartz (shades of grey). One grain is a hexagonal Au microplate ~2 µm (Fig. 6A), another is a 300 nm Au particle exhibiting crystal twinning and internal deformation (Fig. 6B), and the third is a sub-rounded 100 nm Au particle (Fig. 6 C). EDS spectra reveal that the particles are almost pure Au (Cu spectra being an artefact from the Cu grid used to mount the sample foil; Fig. 6D).

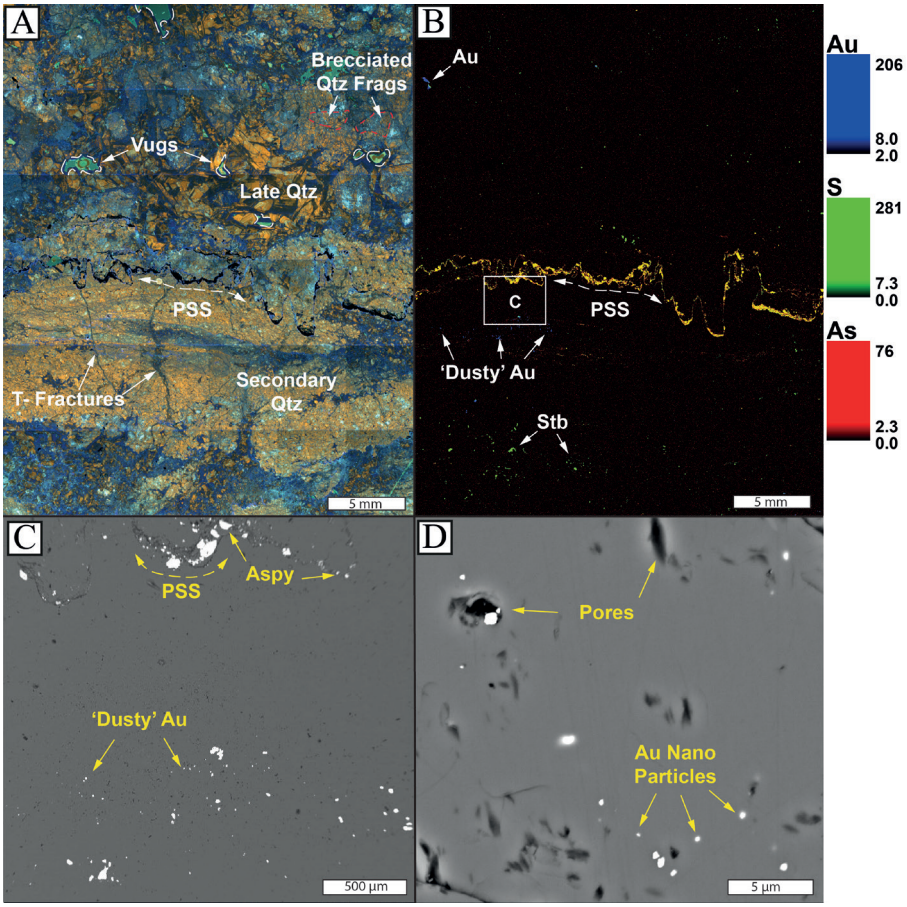

Figure 4:A) Cathodoluminescence image of sample F7B1, a Au-bearing quartz vein with pressure-dissolved wall rock selvage. Different colours exhibit multiple generations of quartz mineralisation, highlighting brecciation, reprecipitated, and fracturing events. Fine-grained reprecipitated quartz occurs along the wall rock selvage pressure-solution seam (PSS). Late stage quartz growth exhibits prismatic zoning and crystallizes into open void space forming vugs. B) Elemental map of the same area as (A) highlighting the distribution of Au, Sb and S within the sample. Au occurs as fine particles disseminated throughout porous, secondary reprecipitated quartz. PSS is highlighted by arsenopyrite (Aspy) contents of the wall rock selvage. Disseminated stibnite (Stb) occurs in lower parts of the sample. C) SEM image of the square outlined in (B) of the 'dusty Au' seams associated with PSS within secondary quartz. D) SEM image of (C) at higher magnification revealing nano particles of Au within quartz grains and accumulated within the porous domains of secondary quartz.

Gold grains are more abundant in and along pressure-dissolved (stylolitized) wall-rock selvages. False-coloured 3D reconstruction of these Au-rich veins from neutron computed tomography shows the three-dimensional distribution of isosurfaces of Au corresponding with these features (Fig. 7A). This 3D reconstruction shows that the highest concentration of Au in this sample occurs along the pressure-dissolved wall-rock selvage, and moderately abundant fine-to medium-grained Au is dispersed throughout the vein. Photographs of similar samples show that accumulations of abundant fine-grained Au grains preferentially occur in stylolitized wall rock selvages (Fig. 7B, C).

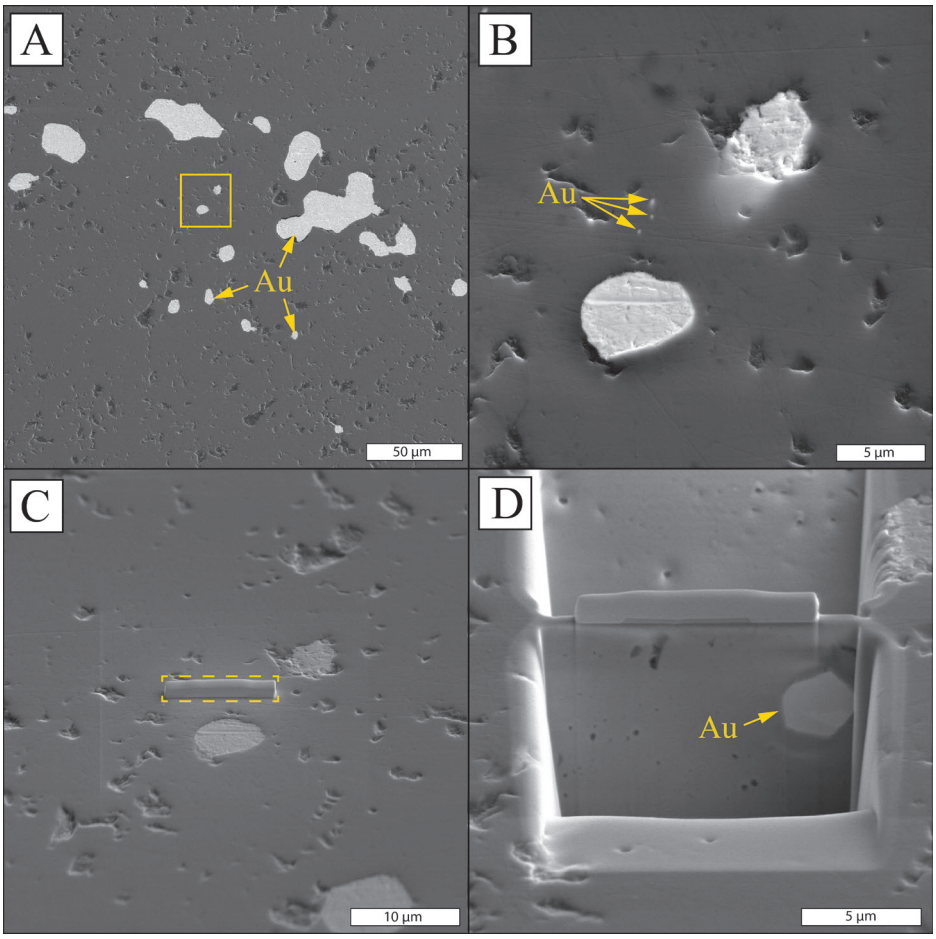

Figure 5:A) SEM image of the of the 'dusty Au' seams in sample F7B1 that was the area of interest for study. B) SEM image of the square outlined in (A) with arrows pointing towards the target Au particles for FIB milling. C) SEM image highlighting the area of the FIB lamella before extraction. D) Cross sectional SEM image of the FIB lamella before clean-up polishing revealing a hexagonal Au nanoplate.

An additional textural setting of Au is within tension microfractures that are commonly found perpendicular to and intersecting pressure soltuion seams in quartz veins (Fig. 8). Neutron tomography reconstructions show that the most Au rich domain in sample F5 is one of these tension fractures (Fig. 8 A). In situ photographs of a tension fracture perpendicular to a pressure-dissolved wall rock selvage shows that coarse-grained Au is periodically distributed along the fracture surface (Fig. 8 B). Other photomicrographs of a tension fracture associated with wall-rock pressure solution seams shows that Au is enriched at the termination points of the fracture.

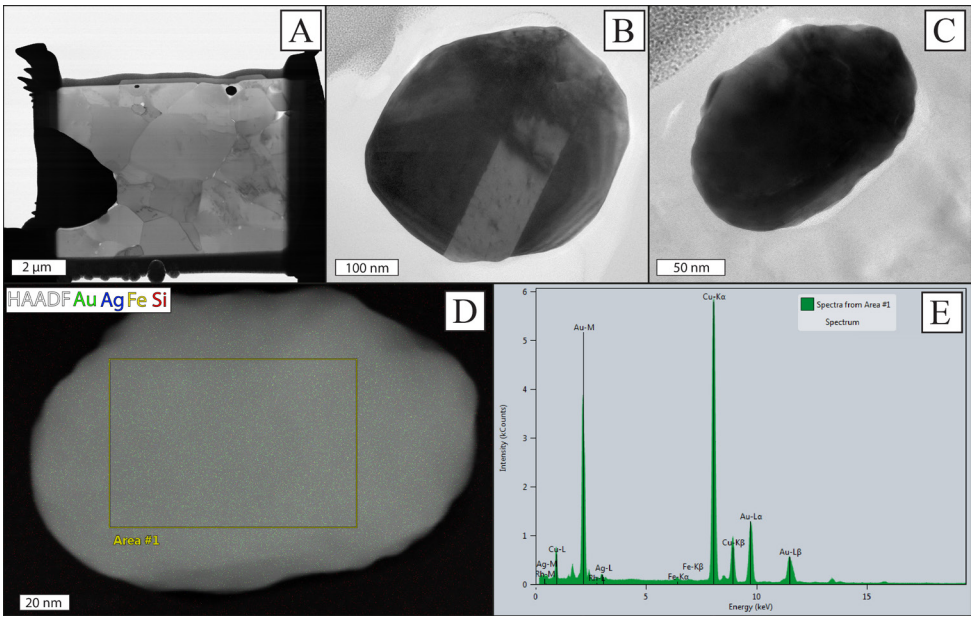

Figure 6:A) Bright-field TEM image of the FIB lamella from Fig. 5. Au particles appear black due to their heavy atomic composition. The sample contains 3 notable Au grains; bottom left, top left and top right. B) Bright-field TEM image of the top right rounded 300 nm Au particle exhibiting crystal twinning and internal deformation. C) Bright-field TEM image of the top left sub-rounded 100 nm Au particle. D) EDS elemental map overlayed on HAADF image of Au particle from (C). Area #1 shows EDS chemical analyses area. E) EDS chemical spectra from (D) showing that the particle is almost pure Au. Cu spectra are from the copper grid that the sample lamella is mounted on.

NanoSIMS results reveal element distributions and textural settings of auriferous sulphides across one variably deformed (pressure-dissolved) wall-rock selvage (Fig. 9). Although a suite of seven ion species were analysed (^{34}S, $^{54}Fe^{32}S$, $^{60}Ni^{32}S$, $^{75}As^{32}S$, ^{123}Sb, ^{130}Te and ^{197}Au), only those with considerable concentration and/or a relationship with Au content are displayed. Arsenopyrite from the least deformed area of the selvage is an

idiomorphic acicular needle ~200 µm in length (Fig. 9B). There is no detectable compositional zoning with respect to Fe, S, or As, and Au appears to be lattice bound as it mimics crystal zoning. Arsenopyrites from the moderately deformed area of the selvage are subhedral with irregular grain boundaries and contain minor brittle fractures (Fig. 9C). No compositional zoning with respect to Fe, S, or As was observed, but Au has two apparent textural settings. In one setting Au mimics crystal zoning near the interior of the crystal, whereas near the irregular grain boundary Au appears fracture-hosted in relatively higher concentrations. Small inclusions of stibnite are present sporadically in micro-porosity throughout the crystal. Pyrite and arsenopyrite that are cataclastic contain nano- to micro-clusters of Au that are associated with fractures, irregular grain boundaries, and porosity (Fig. 9D, E). Pyrite shows compositional zoning with respect to As concentration and Au-bearing fractures that crosscut the crystal appear to be As-

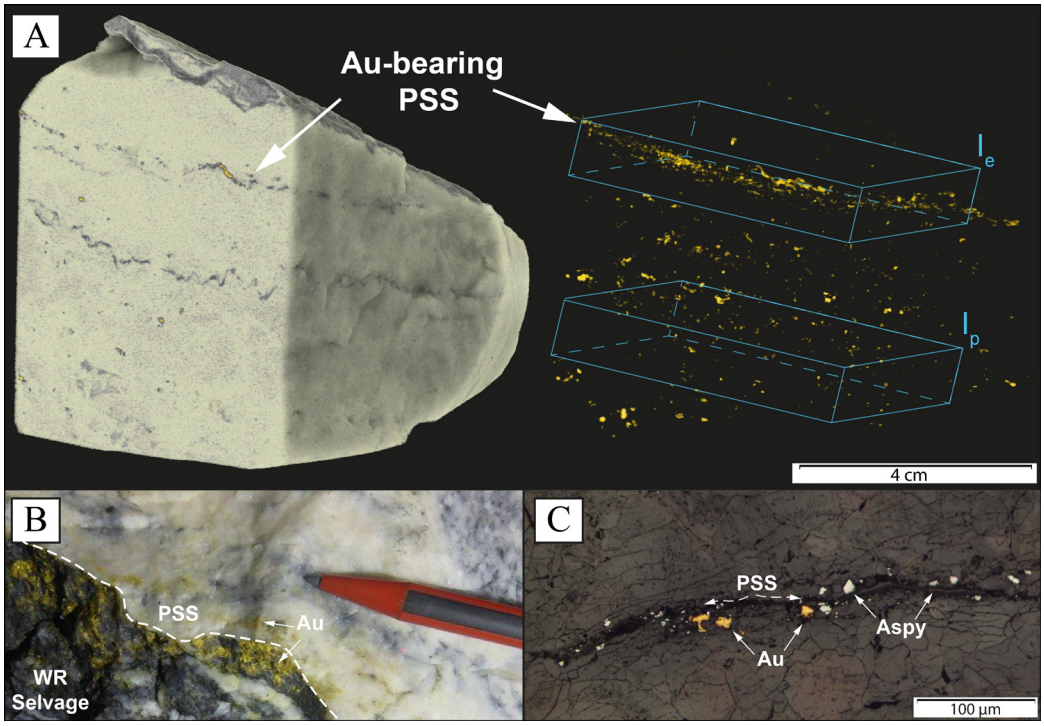

Figure 7: A) False-coloured 3D reconstruction from neutron computed tomography showing the three-dimensional distribution of Au in sample F7B1. The highest concentration of Au occurring along wall rock selvage PSS with other fine-to medium-grained Au disseminated throughout quartz. Blue rectangles are volumes selected for relative mass balance calculations (see text). B) Photograph of finely disseminated Au accumulated along wall rock selvage PSS, taken underground at Fosterville Gold Mine. C) Photomicrograph of Au and arsenopyrite within wall rock PSS.

rich. Gold within this pyrite grain is clearly fracture-hosted, but appears to preferentially occur in sites adjacent to As-enriched zones (Fig. 9D). Arsenopyrite in this setting shows no apparent zoning in Fe or S, but margins along grain boundaries and pore spaces have a thin film of Sb enrichment. Gold in this sample is present exclusively as clusters within porosity networks (Fig. 9E).

All textural settings of Au observed from high-grade Fosterville samples include sub-micron to nanometre sized particles (Figs. 4, 5, 6, 7, 8, 9). As such, our understanding of the genesis of this deposit requires explanations consistent with the generation, transport and behaviour of Au nanoparticles.

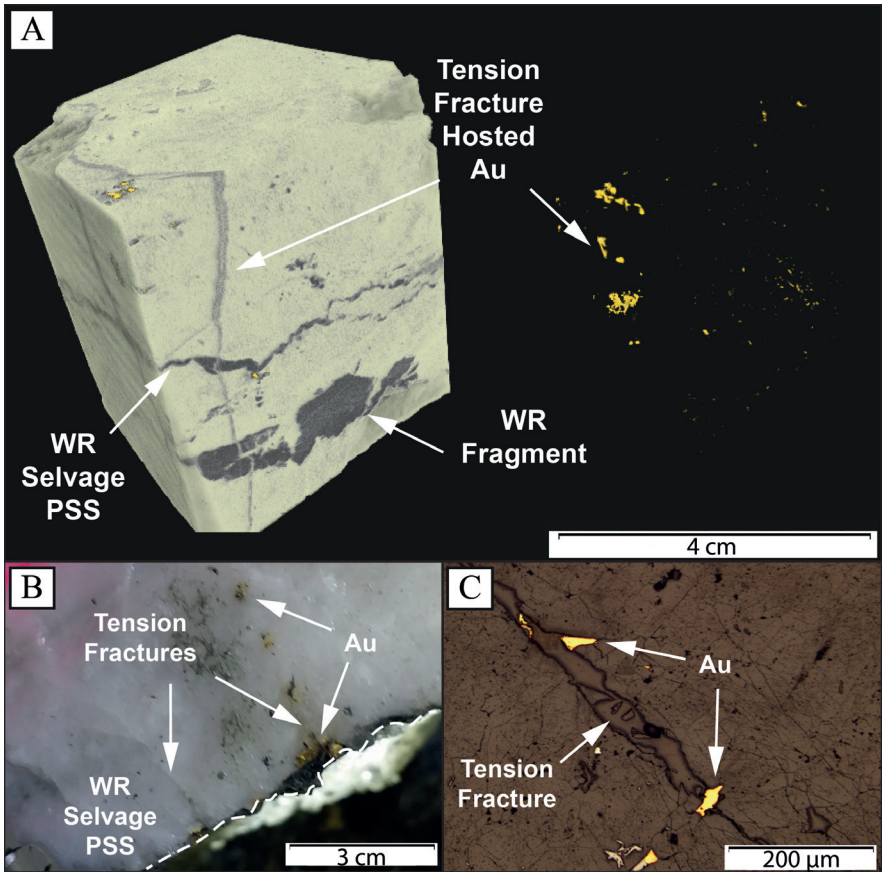

Figure 8: A) False-coloured 3D reconstruction from neutron computed tomography showing the three-dimensional distribution of Au. The highest concentration of Au occurring within the tension fracture perpendicular to PSS. B) Photograph of coarse-grained Au accumulated within tension fractures perpendicular to wall rock PSS. C) Photomicrograph of Au within termination points of a tension fracture.

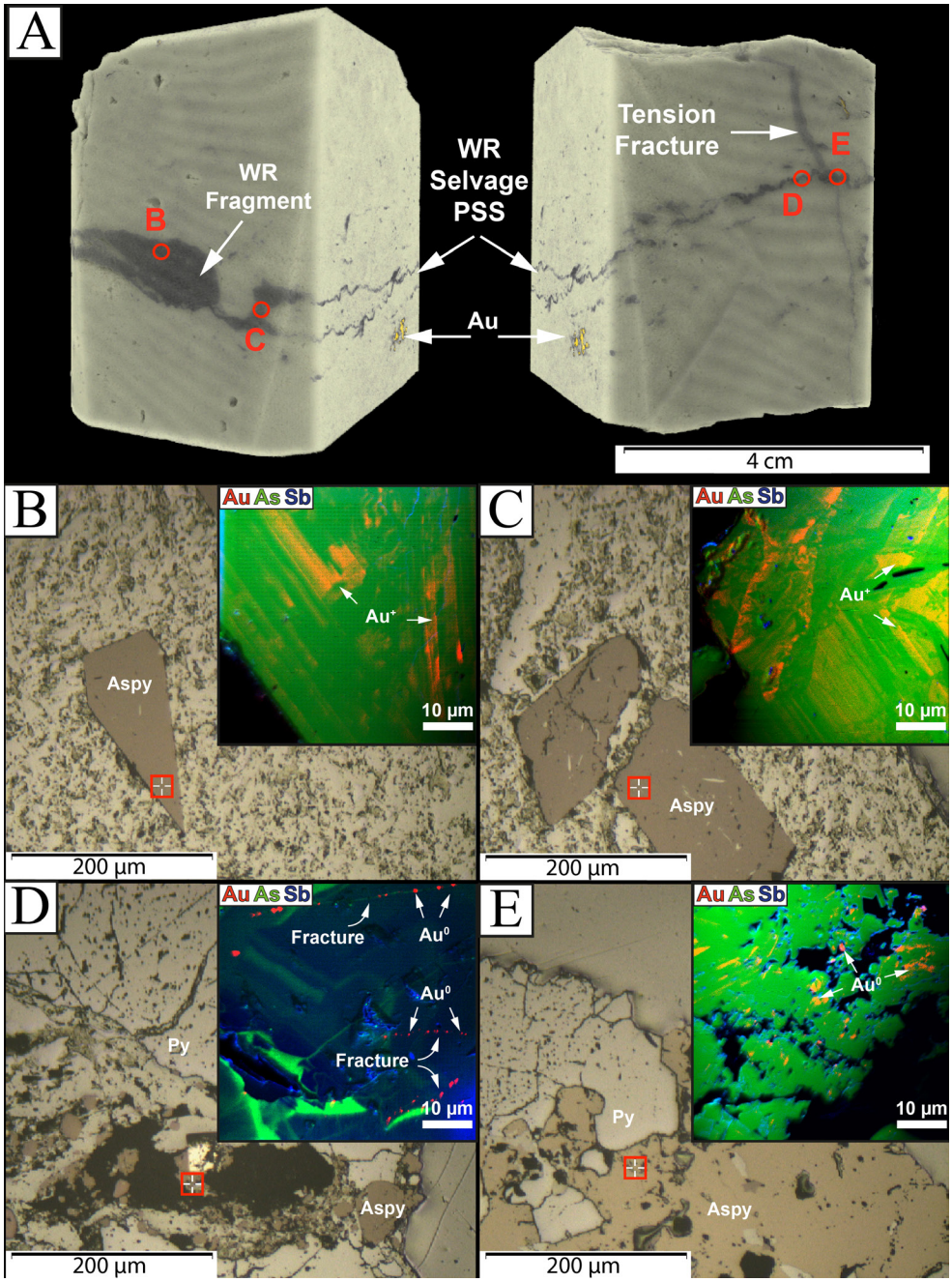

Figure 9: A) False-coloured 3D reconstruction from neutron computed tomography showing the sample areas selected for nanoSIMS analyses and labels corresponding to this figure. B) Photomicrograph of idiomorphic arsenopyrite crystal from area (B) in (A). Inlay is nanoSIMS elemental RGB map of the area highlighted by the red square. C) Photomicrograph of subhedral arsenopyrite crystals from area (C) in (A). Inlay is nanoSIMS elemental RGB map of the area highlighted be the red square. D) Photomicrograph of cataclastic arsenopyrite and pyrite within the pressure-dissolved wallrock selvage from area (D) in (A). Inlay is nanoSIMS elemental RGB map of a brecciated pyrite crystal within the area highlighted by the red square. E) Photomicrograph of variably cataclastic and sulfidized pressure-dissolved wallrock selvage from area (E) in (A). Inlay is nanoSIMS elemental RGB map of porous arsenopyrite within the area highlighted by the red square.

4. Discussion

4.1. Generation of Vein-Hosted Au Nanoparticles

Hydrothermal solutions may become supersaturated in Au via a number of mechanisms: (i) sudden changes in temperature, pH, or oxygen fugacity; (ii) boiling; or (iii) fluid mixing (or un-mixing), among others (Williams-Jones et al., 2009). It has been suggested that when extreme supersaturation occurs, Au may nucleate as colloidal particles (Saunders and Schoenly, 1995; Williams-Jones et al., 2009). In an orogenic system, maximum fluid pressures of Au-bearing solutions are close to lithostatic and then drop to, or below, hydrostatic pressures along the fault plane upon seismic failure (Sibson, 1975; Cox, 1991). At shallow levels in the crust, such a catastrophic drop in pressure can lead to fluid unmixing and ensuing Au supersaturation by partitioning of H_2S from the fluid into the vapour phase (Naden and Shepherd, 1989). Additionally, fluid interaction with carbonaceous rocks (e.g., turbidites) has been proposed to generate CH_4 and destabilise $Au(HS)_2^-$ by partitioning of H_2S into the CH_4-rich vapour phase (Naden and Shepherd, 1989). Based on fluid inclusion studies, it has been proposed that both mechanisms may have taken place for the sulphide-hosted Au mineralisation at Fosterville (Mernagh, 2000), and if so, these mechanisms may have influenced the generation of visible Au as well. During periods of supralithostatic fluid over pressure, Au-bearing fluids may initially percolate into, and interact with, the carbonaceous wall rock under high fluid pressures, before being drawn back into the fault zone during seismic depressurisation (Cox et al., 1995). We suggest that when both of these Au destabilising mechanisms are working in tandem, this is an ideal scenario for supersaturating Au in solution and generating Au nanoparticles in suspension.

4.2. Au Nanoparticle Transport and Aggregation

Gold nanoparticles may remain indefinitely in suspension without aggregating because each behaves as a negatively charged particle, repelling one another unless their total interaction potential or “aggregation barrier” is overcome (Polte, 2015). This barrier can be overcome by diffusion-limited aggregation (DLA), orthokinetic aggrega-

tion, Ostwald ripening or simple coalescence, allowing the growth of larger Au particles (Fig. 10) (Polte, 2015; Saunders and Burke, 2017). It is proposed that phase separation by rupture-induced depressurisation allows for Au nanoparticles to efficiently stick together upon collisions, rapidly forming metallic bonds by orthokinetic aggregation (where the energy of particle collisions is sufficient to overcome the aggregation barrier; cf. Saunders and Burke, 2017). Alternatively, negatively charged Au nanoparticles may adsorb onto minerals with positive surface charges (e.g., arsenopyrite) and/or physical defects such as areas with high roughness, porosity, or within fractures (Reich et al., 2006; Alonso et al., 2009; Fougerouse et al., 2016). It has been shown in mesothermal vein environments that silica becomes supersaturated along with Au and that colloidal silica accompanies the Au during vein formation (Herrington and Wilkinson, 1993). Following the annealing of a colloidal silica gel to form amoquartz crystals, the trapped Au colloids diffuse outwards and aggregate along grain boundaries and triple junctions, a commonly observed texture in orogenic Au veins (Herrington and Wilkinson, 1993).

4.3. Dissolution of Vein Material

Pressure-dissolution creep involves the dissolution of mineral aggregates under non-hydrostatic stress conditions. Pressure-dissolution is a major mechanism of ductile deformation of the upper crust, developing features such as dissolution cleavages and stylolites (Durney, 1972; Gratier et al., 2013). Although generally developed along grain boundaries at high differential stresses, experimental studies have shown that pressure-dissolution is largely governed by electrochemical potential differences between dissimilar crystals faces or minerals (Bons and den Brok, 2000; Greene et al., 2009; Kristiansen et al., 2011). These studies describe the pressure-dissolution phenomenon as a corrosion process, requiring the two surfaces to be electrochemically different for dissolution of one surface to occur. For example, the electrical potential between mica and quartz crystals due to overlapping electron double-layers provides an electrocatalytic reaction between the cathode mineral (mica) and the anode mineral (quartz), leading to dissolution of the quartz anode (Greene et al., 2009). The surfaces

do not have to be in contact, only in close proximity and connected by an ionic conductor, such as an electrolyte solution (i.e., hydrothermal fluid). This provides an explanation for the development of stylolitized wall-rock selvages commonly observed in Phanerozoic orogenic quartz veins, these wall rock selvages are typically mica- and/or graphite-rich turbidite material. The textural setting of Au at quartz crystal boundaries is also a favourable arrangement for pressure-dissolution. Randomly dispersed Au particles along quartz grain boundaries should affect quartz dissolution rates by providing two dissimilar surfaces of different surface potentials (quartz negative and Au positive) (Greene et al., 2009; Polte, 2015). This concept is supported by experimental research showing that Au acts as a strong catalyst during electrode reactions when in the form of nano- to micro-sized particles (Burke and Nugent, 1998). In this way, Au particles can become the focus of quartz dissolution, and thus fluid and element migration.

A relative mass balance $\Delta M/M_0$ can be calculated using the passive concentration of insoluble minerals due to dissolution in areas exposed to pressure-dissolution compared with relatively protected areas. This can be obtained by: $\Delta M/M_0 = (I_p/I_e) - 1$, where, I_p and I_e are the concentrations of insoluble minerals in the protected and exposed areas, respectively (Gratier et al., 2013). To understand the extent of pressure-dissolution of vein quartz, and passive Au grade increase caused by this local removal of quartz, equal volumes of sample F7B1 were compared with respect to their Au content- considered to be insoluble during pressure-dissolution (Fig. 7A). Assuming the F7B1 vein had an initially homogeneous Au-quartz ratio across the sample, the volume adjacent to the wall-rock PSS (I_e) was taken to be exposed to the effects of pressure-dissolution, whereas the volume away from the wall-rock PSS was taken to be protected (I_p). Gold volume was calculated using Drishti software ($I_{p\,Au}$ = 5.82496 μm^3 and $I_{e\,Au}$ = 21.0525 μm^3) and converted to total mass Au. Using the equation above, results show that there is a 72.331% relative enrichment of Au (or relative loss of quartz) in the area exposed to pressure-dissolution when compared to the protected vein mass.

4.4 **Nanoparticles to Nuggets**

Once vein material (quartz and carbonate) has been pressure-dissolved and their chemical components incorporated into a fluid phase, they may be reprecipitated in situ, diffuse into areas of relatively low concentration, localise into sites of low pressure to form new vein fill or pressure shadows, or escape from the local rock mass entirely (Gratier et al., 2013). Gold nanoparticles that become liberated during this process are likely to behave as a colloidal suspension within this grain boundary fluid if they remain sufficiently small. The maximum size of a particle to behave as a colloid is between 100 – 400 nm, depending on the viscosity, velocity and temperature of the solution it is suspended in (Alemán et al., 2007). The smallest Au particles hosted in quartz veins at Fosterville fall within this size range (Fig. 6), so it suggested that liberated Au nanoparticles may: (i) become concentrated at sites of vein dissolution and removal (e.g., along stylolitic wall-rock selvages where pressure-dissolution is enhanced) (Figs. 3, 4, 7); (ii) become entrained in the fluid phase and deposited into areas of positive charge (e.g., arsenopyrite surfaces), or high roughness, porosity, or within fractures (e.g., pre-existing stylolitic surfaces, porous reprecipitated secondary quartz, tension fractures, or brecciated sulphides) (Figs. 4, 7, 8, 9); or (iii) leave the localized vein mass entirely, perhaps contributing to Au-endowed flat-lying tension fractures found cross cutting shear veins, or accumulating in larger dilatational structures.

It has been shown in laboratory experiments that Au and Ag nanoparticles amalgamate by a process of self-assembly called diffusion-limited aggregation (DLA) (Weitz and Oliveria, 1984; Weitz and Huang, 1984; Zhou et al., 2013). This self-assembly reduces overall free energy by reducing the surface energy associated with non-bonded material and leads to distinct transitory structures, such as the fractal dendrites preserved in the epithermal Sleeper deposit, Nevada (Fig. 10) (Saunders and Shoenly, 1995). These temporary structures are precursors to the formation of metal crystals and textural evidence of their

existence is typically lost as atoms infill the spaces between dendrite branches during continued growth (Fig. 10) (Saunders and Burke, 2017). The DLA process has been proven significant in electrodeposition reactions, known as electric field-induced diffusion limited aggregation (e.g., Witten and Sander, 1981), whereby colloidal particles suspended in a fluid migrate under the effects of an electric field and deposit onto electrodes. Given that the electrochemical properties of pressure-dissolution is a corrosion process discussed above, Au nanoparticles are expected to grow at specific sites with ideal electrochemical potential along pressure solution seams; i.e., the cathodic surface, which is the mica-rich wall-rock selvage (Fig. 7).

Studies on colloid transport dynamics have been conducted to investigate favourable sites of nanoparticle accumulation in geological media (Alonso et al., 2009). These authors showed that during physical transport, the areas that accumulated the highest amount of Au nanoparticles were high-defect areas such as fractures and areas of high porosity. This experimental evidence is consistent with our observations that Au accumulations occur in: (i) rough stylolitic surfaces (Fig. 7), (ii) porosity of reprecipitated quartz margins parallel to PSS (Fig. 4), (iii) brecciated and porous sulphides (Fig. 9), and in micro-scale tension cracks (Fig. 8).

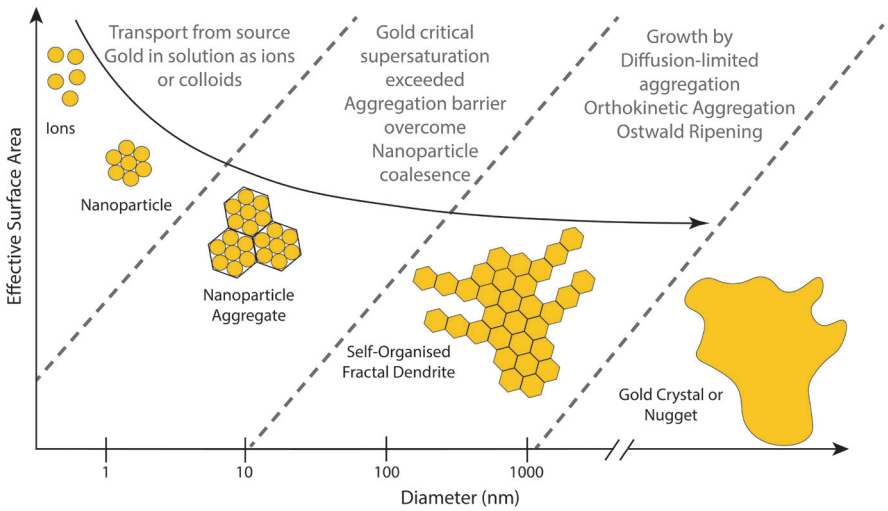

Figure 10:: Illustration of the progression from dissolved Au ions, to nanoparticles, to mesocrystals and self-organized fractal dendrites during growth. Associated mechanisms responsible for growth during each stage are indicated in grey. Modified from Saunders and Burke (2017).

4.5 Sulphide-hosted Au Nanoparticles

The widely observed setting of Au in arsenopyrite and As-rich (arsenian) pyrite consists of Au present as solid solution (Au^{+1}) in the crystal structure and/or nanoparticles (Au^0) < 250 nm in size (Reich et al., 2005; Cook et al. 2013). It has been established that the solubility of Au as solid solution in As-bearing sulphides is proportional to the concentration of As during mineral growth, defined by $C_{Au} = 0.02C_{As} + (4 \times 10^{-5})$, where C_{Au} and C_{As} represent the concentration of Au and As, respectively (Reich et al., 2005). Above this solubility limit, Au will precipitate as Au nanoparticles within the mineral phase. Additionally, crystal growth rate has been suggested to influence Au nanoparticles formation such that Au ions adsorbed onto the mineral surface may diffuse and bond with one another, leading to in-situ nanoparticle formation if crystal growth rates are sufficiently slow (Fougerouse et al., 2016). Au distribution in undeformed Fosterville arsenopyrite samples appears to be lattice bound and mimics crystal zoning (Fig. 9B, C), suggesting that the maximum Au solubility (~2 wt. %) was not met during initial crystallization and/or crystallization was too rapid for nanoparticle formation. However, arsenopyrites and pyrites that have become cataclastic during deformation contain nano- to micro-clusters of Au that are associated with fractures, irregular grain boundaries, and porosity (Fig. 9 D, E). These textural associations suggest that the Au clusters reflect a post depositional process as opposed to a primary co-precipitation of Au with the host phase.

4.6 Secondary Au in Sulphide-Hosted Ores

Previously, the concentration of Au in sulfarsenide minerals post crystallization has been attributed to: (i) exsolution from meta-stable mineral phases during cooling (e.g., Palenik et al, 2004); (ii) retrogressive replacement of a gold-bearing mineral with a non-gold-bearing mineral (Tomkins and Mavrogenes, 2001); (iii) melt formation and fractionation associated with high temperature metamorphism (e.g., Tomkins and Mavrogenes, 2002; Tomkins et al., 2004; 2006); (iv) hydrothermal infiltration, alteration, and remobilisation (e.g., Morey et al., 2008); (v) coupled dissolution-reprecipitation

reactions (e.g., Sung et al., 2009; Fugerouse et al., 2017; Dubosq et al. 2018); and (vi) formation of Au nanoparticles external to the system that are then transported in solution and precipitation on the surface of pre-existing sulphide minerals (e.g., Hough et al. 2011). Points (ii) and (iii) can be ruled out at Fosterville because the metamorphic grades were not high enough.(Buttard et al., 2011).

4.6.1 Au Nanoparticle Exsolution during cooling

Post-crystallization exsolution of Au from host minerals has been suggested for Au-rich, meta-stable sulfarsenides (Palenik et al., 2004; Deditius et al., 2011). Solubility calculations between 150-250 °C show that maximum Au solubility decreases as temperature decreases, so exsolution of lattice-bound Au may take place during cooling to form Au nanoparticles (Palenik et al., 2004; Reich et al., 2005). Such exsolved nanoparticles have been suggested to align themselves along the crystallographic planes of the host phase, whereas nanoparticles directly precipitated onto the mineral cluster along growth zones or as isolated inclusions (Deditius et al., 2011). Samples from Fosterville host native Au particles dominantly in fractures and irregular grain boundaries, although few solitary Au inclusions do exist (Figs. 9 & 11). This observation supports the interpretation that Au was precipitated onto the mineral surface, and not exsolved from the crystal lattice.

4.6.2 Hydrothermal Alteration & Chemical Remobilisation of Sulphide-Hosted Au

Cycles of hydrothermal infiltration during ore deposit evolution can act to alter pre-existing ore minerals and remobilize Au, among other chemical constituents (Morey et al., 2008; Cook et al., 2013). Visible Au concentrated around sulphide grain boundaries and fractures from the Eastern Goldfields, Western Australia, has been interpreted to be remobilized from earlier generations of sulphide-hosted ore (Morey et al., 2008). Such alteration was attributed to an increase in temperature (310° to 415°C) and an increase in sulfur fugacity of up to six orders of magnitude during peak meta-

morphism. These conditions lead to a depletion of invisible Au within overgrowth rims, which was scavenged by the hot, S-rich fluid, and redeposited at native Au within fractures and on grain boundaries. Although the cyclicity of variable composition fluids in orogenic systems is unequivocal (e.g., Peterson and Mavrogenes, 2014), there is no convincing relationship between Au distribution and chemical zonation/alteration in samples presented here.

4.6.3 Coupled Dissolution-Reprecipitation of Sulphide-Hosted Au Ore

Coupled dissolution-reprecipitation reactions have proven to be significant for the remobilisation and upgrading of sulphide-hosted Au ores in orogenic systems (Sung et al., 2009; Fougerouse et al., 2016; Dubosq et al. 2018). These reactions are controlled by the relative solubilities of the reactant and product minerals, and requires full dissolution of the parent mineral coupled with precipitation of the daughter mineral at the nanometre scale (Putnis, 2002). The product mineral typically exhibits high porosity, and preservation of the original crystal shape and crystallographic orientation (Putnis, 2009). At Sunrise Dam, Eastern Goldfields, Western Australia, there is textural evidence consistent with replacement of arsenian pyrite and remobilized gold was precipitated as native inclusions oriented parallel to crystal faces, or in fractures (Sung et al., 2009). Deformed arsenopyrites from Obuasi, Ghana, display cross-cutting of Au-As rich domains with Au-poor, more stoichiometric compositions, inferring the release of Au from the host crystal (Fougerouse et al., 2016). Furthermore, psuedomorphic replacement of Au-rich arsenopyrite with nickeliferous arsenopyrite allowed for the remobiliziation of lattice-bound Au to precipitate as native Au at Obuasi (Fougerouse et al., 2016). In both of these examples, textural evidence supporting dissolution-reprecipitation were observed, but for Fosterville sulphides this does not appear to be the case. No obvious mineral replacement textures are evident in either samples containing lattice-bound Au or native Au (Fig. 9). This suggests that dissolution-reprecipitation is not likely to be a dominant factor for Au redistribution in Fosterville sulphides.

There is, however, abundant porosity in highly-deformed, native Au-bearing ar-

senopyrites and a distinct lack of Au-rich chemical zoning when compared to undeformed arsenopyrite (Fig. 9). It has been shown that native Au deposition on cracks and grain boundaries of arsenopyrite can be explained by a partial, incomplete, dissolution of arsenopyrite that would provide a local redox trap for Au (Pokrovski et al., 2002). Gold distributions in arsenopyrite from Oberon, north-central Australia, was attributed to this mechanism, whereby Au release was facilitated by fluid-crystal reactions in brecciated sulphides during deformation (Cook et al., 2013). Those textures were similar to those presented here, showing Au enrichment within nano- to micro-sized pore spaces and along brittle fractures in the host crystal. Partial dissolution, as well as the selective reduction and adsorption of Au onto the surface of deformed arsenopyrite and arsenian pyrite can be explained by its semiconducting and surface potential properties (see Möller and Kersten, 1994; Maddox et al., 1998; Laird et al., 2015).

4.7 Electrochemical Potential & Au Nanoparticle Formation

The semiconducting properties of both arsenopyrite and pyrite are governed by As content (i.e., change from n-type to p-type conductance with an increase in As concentration), where n-type conductors are considered to act as anodes (e^- donors) and p-type conductors are considered to act as cathodes (e^- acceptors) in a linked system (Möller and Kersten, 1994). The adsorption of Au has been shown to preferentially occur on As-rich cathodic (p-type conductivity) domains of these sulphide minerals in H_2S-saturated solutions (Möller and Kersten, 1994; Maddox et al., 1998; Laird et al., 2015, 2018). This is facilitated by the donation of electrons from the cathodic surface along the sulphide-solution interface, leading to reduction of Au-bearing ligands in the fluid phase and dissolution of the anodic sulphide species. This mechanism has been shown to be significant during both syn- and post-mineral growth, if auriferous fluids interact at n-p junctions where electron transfer occurs (Möller and Kersten, 1994). Given that the zonation of As content in both arsenopyrite and pyrite is pervasive, fracturing of these crystals creates numerous n-p junctions accessible to infiltrating fluids (Fig. 11). Electron flow can also be established away from n-p junctions, where

n-type and p-type sulfarsenides are hosted in an electron-conducting matrix, such as graphitic shear bands (Xavier and Foster, 1991). Furthermore, colloidal Au particles can also be adsorbed onto minerals with positive surface charge (p-type conductors), such as arsenian pyrite and arsenopyrite, by electrostatic attraction (William-Jones et al., 2009; Buttard et al., 2011). Both of these processes are amplified in areas of high field strength, such as corners, irregular fractures and areas of high porosity (Möller and Kersten, 1994; Alonso et al., 2009). Therefore, sulfidized carbonaceous wall-rock selvages that have undergone pressure-dissolution, and coincident cataclasis of sulphide

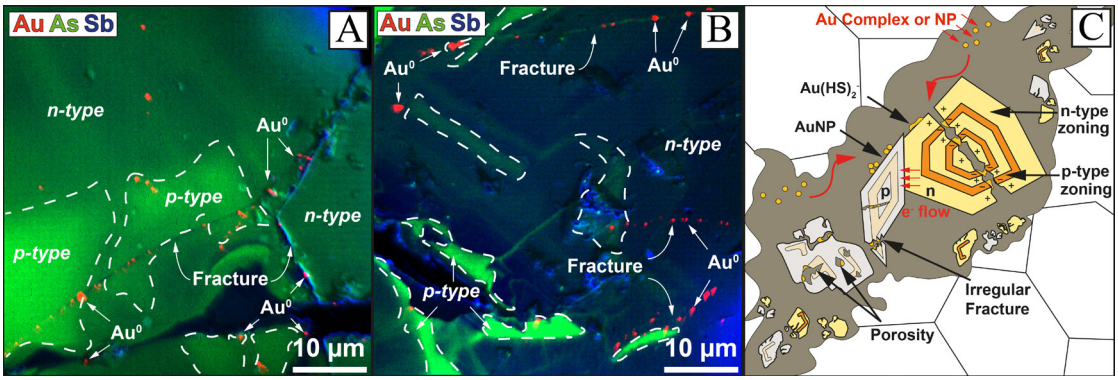

Figure 11: A) NanoSIMS elemental RGB map of arsenopyrite from pressure-dissolved wallrock selvage. Zones rich in As that act as p-type conductors are outlined by dashed lines. B) NanoSIMS elemental RGB map of pyrite from pressure-dissolved wallrock selvage. Zones rich in As that act as p-type conductors are outlined by dashed lines. C) Schematic of the Möller model for secondary electrochemical reduction of Au onto p-type mineral surfaces caused by micro-galvanic reactions driven by n-p junctions. Schematic has been modified to suite the structural settings and sample textures that are present in this study.

crystals within, are an ideal setting for the concentration of Au from either auriferous ligands in solution or Au nanoparticle suspensions.

Many pyrite and arsenopyrite crystals at Fosterville show signs of dissolution in the way of embayed/corroded margins and porosity (Figs. 9 & 11). The electropotential difference between two sulphide mineral electrodes is the driving force for galvanic corrosion of the anode mineral, which dissolves into the solution phase. It is possible that dissolution of sulphide ore minerals subjected to this electropotential – by being in close proximity to one another or electrically connected through graphitic PSS – provided a means to remobilize Au from their crystal structure to be redeposited as second-

ary Au on nearby grain margins or fractures. The resultant corroded texture provides has an increased effective porosity enhancing fluid-mineral interaction in areas of high field strength that have an affinity for the adsorption of Au-complexes and Au nanoparticles (Möller and Kersten, 1994). Fosterville sulphides host abundant Au clusters and nanoparticles along these grain margin embayments and within pore spaces (Fig. 9E). The Au in fractures in As-zoned arsenopyrite and pyrite (e.g., Fig. 11) are examples where brecciation and fracturing increased permeability for fluid-crystal interactions and exposed numerous n-p junctions for sequestering Au. Gold may deposit from solution on cathodic surfaces by $Au^{+} + e^{-} \leftrightarrow Au^{0}$ or, to a lesser extent, on anodic surfaces by $Au(HS)_2^{-} \leftrightarrow Au^{0} + 2S + 2H^{+} + 3e^{-}$ (Möller and Kersten, 1994). Any colloidal Au particles would also be preferentially adsorbed as Au nanoparticles onto minerals surfaces acting as cathodes, or on irregular fracture surfaces (Alonso, et al. 2009; Buttard et al., 2011). This is evident in the Fosterville sulphides where there are abundant Au nanoparticles and micro clusters associated with fracturing across As-rich areas.

The diversity of textural settings of remobilized Au associated with variable amounts of stylolite development at Fosterville emphasises the importance of the aseismic period and the fate of Au during the 'quiet times' of orogenic ore genesis. Auriferous ore sulphides in pressure-dissolved wall-rock selvages exclusively host Au as nano- to micro-metre sized clusters within features associated with corrosion and brittle failure. Sulphide minerals from wall-rock selvages that have not been subjected to pressure-dissolution contain Au bound in the crystal structure and no such clusters. It is possible that remobilized Au was derived locally from galvanic dissolution of Au-rich sulphides and redeposited as native Au within advantageous sites for adsorption, or that Au nanoparticles were derived externally from inter-grain boundary fluids liberated from the host vein that percolated along stylolitic surfaces. It is likely that both options are significant during deposit development because both pathways of fluid migration are observed to have been active.

5. The Aseismic Refinement Model

Gold mineralization in orogenic systems involves kilometerscale Au transport and precipitation during seismic failure. We suggest that, once precipitated, mineralization can be significantly locally enriched through a combination of pressure solution removal of quartz and remobilization-related addition of Au in specific sites during aseimic periods, emphasizing that the entire seismic cycle is important in lode formation. A suggested seismic to aseismic cycle of events within the Fosterville deposit (Fig. 12) is envisaged as follows:

1. Upon fault failure, critical supersaturation of Au due to the destabilization of Au-bearing (H2S)– complexes by partitioning of (H2S)– into the vapor phase during fluid unmixing leads to rapid formation of Au nanoparticles (Fig. 12A). These Au nanoparticles efficiently stick together upon particle collisions by orthokinetic aggregation and are deposited within quartz-carbonate veins along crystal boundaries. Rapid fluid migration fractures off wall-rockhosted auriferous sulfide mineralization to be preserved as a selvage in the quartz carbonate vein (Fig. 12B; cf. Robert and Poulsen, 2001), making it available as a pressure dissolution plane with associated deformation and breakdown of sulfides rich in Au.

2. During the interseismic period at lower fluid pressure, pressure dissolution and localized removal of quartz and carbonate vein material proceeds, particularly at wall-rock selvages and mineral inclusions (including Au inclusions), allowing for the liberation of trapped Au nanoparticles into grain boundary fluids. Once liberated, the Au nanoparticles may behave as colloids and migrate to allow growth (Fig. 12C) by DLA along wall-rock selvage pressure solution seams (Fig. 7), adsorption onto p-type sulfides hosted within wall-rock selvage pressure solution seams (Fig. 10), or accumulation on defect areas of high surface roughness, such as tension fractures and brecciated sulfides (Figs. 8, 9). Tension fractures developed perpendicular to pressure solution seams within veins are ideal for entrainment of nanoparticulate Au, because they provide local areas of dilation, allowing migration of Au into microfracture networks

within quartz veins. Similarly, brecciation and fracturing of As-zoned sulfide minerals increase permeability within the pressure solution seams and expose numerous n-p junctions and high field strength features for sequestering Au onto sulfide surfaces. Given that the wall-rock selvages are graphitic, it is likely that the electrical connectivity along these features is extensive and can influence Au nanoparticle attraction at some distance from n-p sulfide couplings, as well as facilitate galvanic dissolution of anodic sulfide ore to liberate lattice-bound Au for remobilization.

3. When fluid pressures begin to build again (Fig. 12), and if differential stress remain low, tension fractures may manifest themselves on a mesoscale as subhorizontal hydraulic extension veins. This progression is evidenced by the development of Au-bearing extension veins, which can be found crosscutting shear veins in orogenic systems. Fluid overpressure in the vein system during late aseismic periods allows for fluid-rock interaction by percolation into adjacent wall rocks, allowing for development or replacement of lattice-bound Au mineralization in sulfides, depending on fluid chemistry. At this stage, it is possible that Au may be liberated from replaced sulfides during the buildup to the next major mineralization event, when the fluids can be drawn into the vein. Once the fault is hydrothermally selfsealed, and critical fluid pressures are achieved, the system may fail again, initiating the next cycle. This refinement process tends to focus Au into quartz veins that go through periods of mass gain and loss, leading to higher Au/quartz ratios than might otherwise be expected. In this model, the greater the duration of tectonic activity, the greater the capacity for mineralization, and subsequent tectonic events can also lead to enrichment through similar mechanisms. This process will be most effective where stress is localized onto discrete faults, rather than in faults that show large damage zones or cataclasis that can accommodate interseismic strain through grain rotation or sliding. Given that orogenic systems predominantly reside in the interseismic regime over the lifetime of their formation and that fault/ vein systems commonly have several thousand cycles of shear failure, it is likely that aseismic processes are significant for the development high-grade Au lodes in thesesettings.

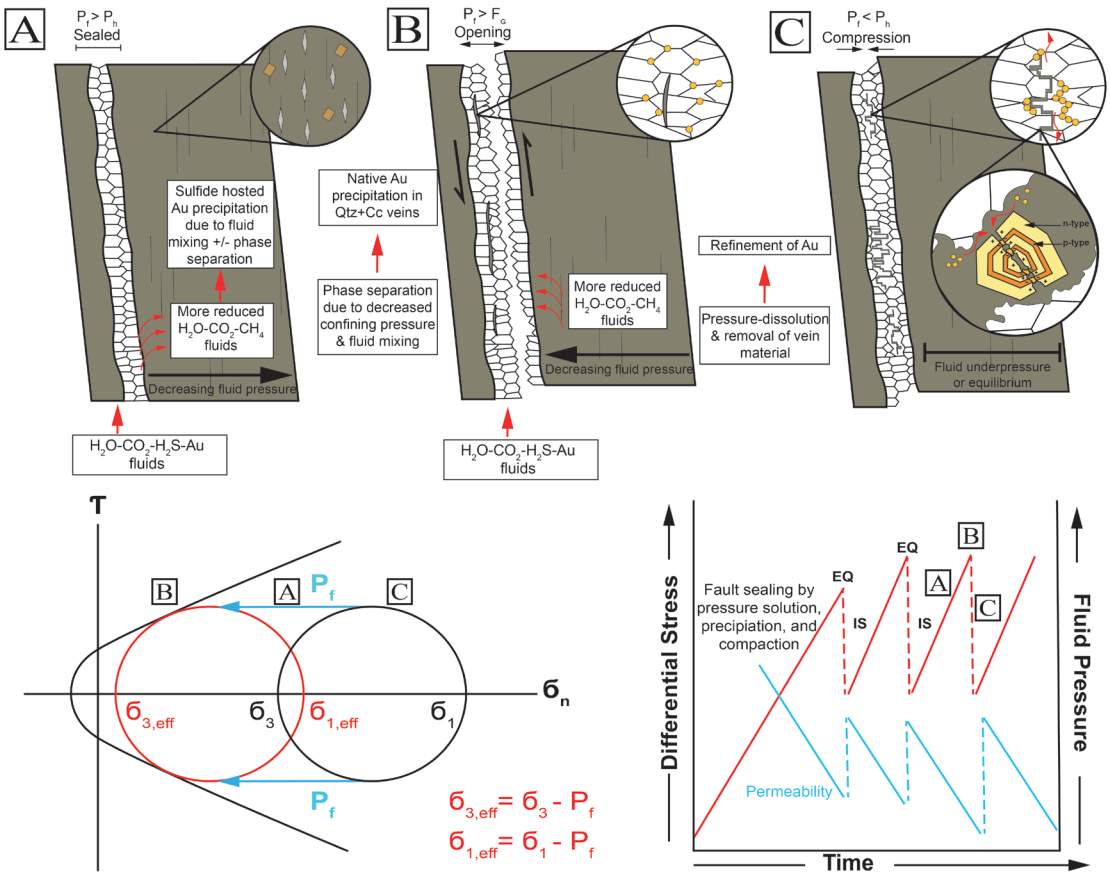

Figure 12: A schematic model for Au mineralisation and refinement at Fosterville during seismic and aseismic intervals. A) During fluid overpressure, H2O-CO2-H2S-Au composition fluids flow out of the vein and interact with host rocks. During this time, fluids react with reduced fluids/carbonaceous material leading to fluid unmixing and refractory Au mineralisation. B) When fluid pressure becomes critical and fault failure occurs, some fluid is drawn in from the surrounding host rock, accompanying the new fluid flux from below, leading to native Au deposition from depressurisation and fluid unmixing. C) During fluid the under pressure phase that follows seismic failure, the vein material is compressed and undergoes pressure-dissolution, removing gangue material (qtz+cc) and allowing for self-organisation and growth of nanoparticulate Au along PSS and corroded/ brittle deformed sulphide minerals.

6. Conclusion

Textures in high-grade vein-hosted Au ore from the Fosterville deposit are interpreted here to be best explained by the deposition and growth of nano-particulate Au through the combination of pressure-dissolution and self-assembly. At Fosterville, it is likely that depressurization and fluid unmixing during fault failure led to critical supersaturation and deposition of abundant Au nanoparticles amongst quartz along fault surfaces. Subsequent pressure-dissolution of quartz-carbonate during inter-seismic intervals allowed for removal of some quartz and carbonate from the host vein and the liberation of Au nanoparticles within inter-grain boundary fluids. Gold nanoparticle growth occurs along pressure-solution seams (e.g., stylolitic surfaces) or at sites of high surface roughness, such as tension fracture networks and brecciated sulphide surfaces. Auriferous sulphide minerals from wall-rock selvages that have not been subjected to pressure-dissolution contain Au bound in the crystal structure. However, those associated with pressure-dissolved wall-rock selvages exclusively host Au as nano- to micro-metre sized clusters within features associated with corrosion and brittle failure. It is proposed that: (i) remobilisation of Au occurred by galvanic dissolution of Au-rich sulphides and redeposition of native Au within advantageous sites for adsorption, and/or (ii) that Au nanoparticles were liberated from the host vein by inter-grain boundary fluids that percolated along stylolitic surfaces. In this way it is likely that vein-hosted native Au and sulphide-hosted Au ores may become coupled during deposit evolution. By considering that nanoparticulate Au suspensions may form at several stages in a seismic-interseismic cycle, each promoting accumulation of gold in quartz veins, and that quartz and carbonates may be episodically removed from vein, a new model for generating high gold/quartz lodes has been proposed for orogenic settings. This refinement model emphasises the importance of aseismic intervals in the deposit's formation history and may prove to be crucial in the genesis of orogenic-type Au ore.

Acknowledgments

We wish to thank Braden Verity, Simon Hitchman, Nathan Phillips, Harry Atton, and the geological team at the Fosterville Gold Mine for their assistance, enthusiasm, and advice. We would also like to thank Rob Duncan and the Geological Survey of Victoria for their partnership in this endeavour. Paul Bons and Nicholas Hunter are thanked for their exhilarating discussions regarding topic material. Part of this research was undertaken using the TEM and FIB-SEM at the John de Laeter Centre, Curtin University, and authors would like to thank Denis Fougerouse for their assistance and interest. Matthew Kilburn is thanked for his assistance, as well as persistence, with the NanoSIMS at the Centre for Microscopy, Characterisation and Analysis at UWA. Nick Wilson is thanked for his assistance collecting CL and EPMA data at the Commonwealth Scientific and Industrial Research Organisation Microbeam Laboratory, Clayton. Finally, we would like to thank the constructive comments of the Economic Geology reviewers. This project was funded by the ARC Linkage grant (LP150100717) and supported by Australian Centre for Neutron Scattering project 5708.

References

Alemán, J., Chadwick, A. V., He, J., Hess, M., Horie, K., Jones, R. G., Kratochvíl, P., Meisel, I., Mita, I., and Moad, G., 2007, Definitions of terms relating to the structure and processing of sols, gels, networks, and inorganic-organic hybrid materials (IUPAC Recommendations 2007): Pure and Applied Chemistry, v. 79, p. 1801-1829.

Alonso, U., Missana, T., Patelli, A., Ceccato, D., Albarran, N., Garcia-Gutierrez, M., Lopez-Torrubia, T., and Rigato, V., 2009, Quantification of Au nanoparticles retention on a heterogeneous rock surface: Colloids and Surfaces A: Physicochemical and Engineering Aspects, v. 347, p. 230-238.

Bons, P. D., and den Brok, B., 2000, Crystallographic preferred orientation development by dissolution–precipitation creep: Journal of Structural Geology, v. 22, p. 1713-1722.

Burke, L., and Nugent, P., 1998, The electrochemistry of gold: II the electrocatalytic behaviour of the metal in aqueous media: Gold bulletin, v. 31, p. 39-50.

Buttard, D., Oelher, F., and David, T., 2011, Gold colloidal nanoparticle electrodeposition on a silicon surface in a uniform electric field: Nanoscale research letters, v. 6, p. 580.

Cook, N. J., Ciobanu, C. L., Meria, D., Silcock, D., and Wade, B., 2013, Arsenopyrite-pyrite association in an orogenic gold ore: Tracing mineralisation history from textures and trace elements: Economic Geology, v. 108, p. 1273-1283.

Cooke, D. R., and Simmons, S. F., 2000, Characteristics and Genesis of Epithermal Gold Deposits, *in* Hagemann, S. G., and Brown, P. E., eds., Gold in 2000, Society of Economic Geologists.

Cox, S., Wall, V., Etheridge, M., and Potter, T., 1991, Deformational and metamorphic processes in the formation of mesothermal vein-hosted gold deposits—examples from the Lachlan Fold Belt in central Victoria, Australia: Ore geology reviews, v. 6, p. 391-423.

Cox, S. F., 1995, Faulting processes at high fluid pressures: An example of fault valve behavior from the Wattle Gully Fault, Victoria, Australia: Journal of Geophysical Research: Solid Earth, v. 100, p. 12841-12859.

Deditius, A. P., Utsunomiya, S., Reich, M., Kesler, S. E., Ewing, R. C., Hough, R., and Walshe, J., 2011, Trace metal nanoparticles in pyrite: Ore Geology Reviews, v. 42, p. 32-46.

Dierick, M., Masschaele, B., and Van Hoorebeke, L., 2004, Octopus, a fast and user-friendly tomographic reconstruction package developed in LabView®: Measurement Science and Technology, v. 15, p. 1366.

Dubosq, R., Lawley, C.J.M., Rogowitz, A., Schneider, D.A., & Jackson, S. (2018), Pyrite deformation and connections to gold mobility: Insight from micro-structural analysis and trace element mapping. Lithos, 310-311, 86–104. doi: 10.1016/j.lithos.2018.03.024

Durney, D., 1972, Solution-transfer, an important geological deformation mechanism: Nature, v. 235, p. 315.

Fougerouse, D., Micklethwaite, S., Tomkins, A. G., Mei, Y., Kilburn, M., Guagliardo, P., Fisher, L. A., Halfpenny, A., Gee, M., and Paterson, D., 2016a, Gold remobilisation and formation of high grade ore shoots driven by dissolution-reprecipitation replacement and Ni substitution into auriferous arsenopyrite: Geochimica et Cosmochimica Acta, v. 178, p. 143-159.

Fougerouse, D., Reddy, S. M., Saxey, D. W., Rickard, W. D., Van Riessen, A., and Micklethwaite, S., 2016b, Nanoscale gold clusters in arsenopyrite controlled by growth rate not concentration: Evidence from atom probe microscopy: American Mineralogist, v. 101, p. 1916-1919.

Goldfarb, R., Groves, D., and Gardoll, S., 2001, Orogenic gold and geologic time: a global synthesis: Ore geology reviews, v. 18, p. 1-75.

Gratier, J.-P., Dysthe, D. K., and Renard, F., 2013, The role of pressure solution creep in the ductility of the Earth's upper crust, Advances in Geophysics, 54, Elsevier, p. 47-179.

Gray, D., and Foster, D., 2004, Tectonic evolution of the Lachlan Orogen, southeast Australia: historical review, data synthesis and modern perspectives: Australian Journal of Earth Sciences, v. 51, p. 773-817.

Gray, D. R., and Foster, D. A., 1998, Character and kinematics of faults within the turbidite-dominated Lachlan Orogen: implications for tectonic evolution of eastern Australia: Journal of Structural Geology, v. 20, p. 1691-1720.

Greene, G. W., Kristiansen, K., Meyer, E. E., Boles, J. R., and Israelachvili, J. N., 2009, Role of electrochemical reactions in pressure solution: Geochimica et Cosmochimica Acta, v. 73, p. 2862-2874.

Groves, D., 1993, The crustal continuum model for late-Archaean lode-gold deposits of the Yilgarn Block, Western Australia: Mineralium deposita, v. 28, p. 366-374.

Groves, D. I., Goldfarb, R. J., Gebre-Mariam, M., Hagemann, S., and Robert, F., 1998, Orogenic gold deposits: a proposed classification in the context of their crustal distribution and relationship to other gold deposit types: Ore geology reviews, v. 13, p. 7-27.

Hannington, M., Harðardóttir, V., Garbe-Schönberg, D., and Brown, K. L., 2016, Gold enrichment in active geothermal systems by accumulating colloidal suspensions: Nature Geoscience, v. 9, p. 299.

Herrington, R., and Wilkinson, J., 1993, Colloidal gold and silica in mesothermal vein systems: Geology, v. 21, p. 539-542.

Hitchman, S. P., Phillips, N. J., and Greenberger, O. J., 2018, Fosterville Gold Deposit: Australian Ore Deposits (Sixth Edition), v. Monograph Number 32.

Hough, R., and Reich, M., 2011, Noble metal nanoparticles in ore systems: Ore Geology Reviews, v. 42, p. 55-61.

Kristiansen, K., Valtiner, M., Greene, G. W., Boles, J. R., and Israelachvili, J. N., 2011, Pressure solution–The importance of the electrochemical surface potentials: Geochimica et Cosmochimica Acta, v. 75, p. 6882-6892.

Laird, J. S., MacRae, C. M., Halfpenny, A., Large, R., and Ryan, C. G., 2015, Microelectronic junctions in arsenian pyrite due to impurity and mixed sulphide heterogeneity: American Mineralogist, v. 100, p. 26-34.

Leader, L. D., Robinson, J. A., and Wilson, C. J., 2012, Numerical modelling of fluid infiltration constrained by fault and bedding relationships in the Fosterville goldfield, Victoria, Australia: Ore Geology Reviews, v. 48, p. 384-402.

Maddox, L. M., Bancroft, G. M., Scaini, M., and Lorimer, J., 1998, Invisible gold: Comparison of Au deposition on pyrite and arsenopyrite: American Mineralogist, v. 83, p. 1240-1245.

Mernagh, T. P., 2001, A fluid inclusion study of the Fosterville mine: A turbidite-hosted gold field in the western Lachlan fold belt, Victoria, Australia: Chemical Geology, v. 173, p. 91-106.

Möller, P., and Kersten, G., 1994, Electrochemical accumulation of visible gold on pyrite and arsenopyrite surfaces: Mineralium Deposita, v. 29, p. 404-413.

Moore, D., 2007, Classifying gold-bearing deposits in central and western Victoria: Geoscience Victoria Gold Undercover Report, v. 1, p. 1-32.

Morey, A. A., Tomkins, A. G., Bierlein, F. P., Weinberg, R. F., and Davidson, G. J., 2008, Bimodal distribution of gold in pyrite and arsenopyrite: examples from the Archean Boorara and Bardoc shear systems, Yilgarn Craton, Western Australia: Economic Geology, v. 103, p. 599-614.

Naden, J., and Shepherd, T. J., 1989, Role of methane and carbon dioxide in gold deposition: Nature, v. 342, p. 793.

Palenik, C. S., Utsunomiya, S., Reich, M., Kesler, S. E., Wang, L., and Ewing, R. C., 2004, "Invisible" gold revealed: direct imaging of gold nanoparticles in a Carlin-type deposit: American Mineralogist, v. 89, p. 1359-1366.

Peterson, E. C., and Mavrogenes, J. A., 2014, Linking high-grade gold mineralisation to earthquake-induced fault-valve processes in the Porgera gold deposit, Papua New Guinea: Geology, v. 42, p. 383-386.

Phillips GN, Powell R., 2011, Origin of Witwatersrand gold: a metamorphic devolatilisation – hydrothermal replacement model. Appl Earth Sci. 120:112–129.

Phillips, G.N., Australian and global setting for gold in 2013, in Proceedings World Gold 2013, Brisbane, Australia, 26–29 September, 2013: The Australian Institute of Mining and Metallurgy, p. 15–21.

Phillips, G. N., and Powell, R., 2015, A practical classification of gold deposits, with a theoretical basis: Ore Geology Reviews, v. 65, p. 568-573.

Pokrovski, G. S., Borisova, A. Y., and Bychkov, A. Y., 2013, Speciation and transport of metals and metalloids in geological vapors: Reviews in Mineralogy and Geochemistry, v. 76, p. 165-218.

Pokrovski, G. S., Kara, S., and Roux, J., 2002, Stability and solubility of arsenopyrite, FeAsS, in crustal fluids: Geochimica et Cosmochimica Acta, v. 66, p. 2361-2378.

Polte, J., 2015, Fundamental growth principles of colloidal metal nanoparticles–a new perspective: CrystEngComm, v. 17, p. 6809-6830.

Putnis, A., 2002, Mineral replacement reactions: from macroscopic observations to microscopic mechanisms: Mineralogical Magazine, v. 66, p. 689-708.

Putnis, A., 2009, Mineral replacement reactions: Reviews in mineralogy and geochemistry, v. 70, p. 87-124.

Reich, M., Kesler, S. E., Utsunomiya, S., Palenik, C. S., Chryssoulis, S. L., and Ewing, R. C., 2005, Solubility of gold in arsenian pyrite: Geochimica et Cosmochimica Acta, v. 69, p. 2781-2796.

Reich, M., Utsunomiya, S., Kesler, S. E., Wang, L., Ewing, R. C., and Becker, U., 2006, Thermal behavior of metal nanoparticles in geologic materials: Geology, v. 34, p. 1033-1036.

Robert, F., Boullier, A. M., and Firdaous, K., 1995, Gold-quartz veins in metamorphic terranes and their bearing on the role of fluids in faulting: Journal of Geophysical Research: Solid Earth, v. 100, p. 12861-12879.

Robert, F., and Poulsen, K., 2001, Vein formation and deformation in greenstone gold deposits: Reviews in Economic Geology, v. 14, p. 111-155.

Roberts, C., Jackson, T., Allwood, K., Shawcross, M., Story, J., Barbetti, L., Tielen, R., Boucher, R., and Norris, N., 2003, Fosterville—rise of the Phoenix. The emerging goldfield at Fosterville: The New Generation Gold Conference Abstracts, 2003.

Saunders, J., and Burke, M., 2017, Formation and aggregation of gold (electrum) nanoparticles in epithermal ores: Minerals, v. 7, p. 163.

Saunders, J., and Schoenly, P., 1995, Boiling, colloid nucleation and aggregation, and the genesis of bonanza Au-Ag ores of the Sleeper deposit, Nevada: Mineralium Deposita, v. 30, p. 199-210.

Sibson, R., Moore, J. M. M., and Rankin, A., 1975, Seismic pumping—a hydrothermal fluid transport mechanism: Journal of the Geological Society, v. 131, p. 653-659.

Sibson, R. H., Robert, F., and Poulsen, K. H., 1988, High-angle reverse faults, fluid-pressure cycling, and mesothermal gold-quartz deposits: Geology, v. 16, p. 551-555.

Sung, Y.-H., Brugger, J., Ciobanu, C., Pring, A., Skinner, W., and Nugus, M., 2009, Invisible gold in arsenian pyrite and arsenopyrite from a multistage Archaean gold deposit: Sunrise Dam, Eastern Goldfields Province, Western Australia: Mineralium Deposita, v. 44, p. 765.

Tomkins, A. G., 2013, A biogeochemical influence on the secular distribution of orogenic gold: Economic Geology, v. 108, p. 193-197.

Tomkins, A. G., and Grundy, C., 2009, Upper temperature limits of orogenic gold deposit formation: Constraints from the granulite-hosted Griffin's Find deposit, Yilgarn craton: Economic Geology, v. 104, p. 669-685.

VandenBerg, A., 2000, The Tasman Fold Belt system in Victoria: geology and mineralisation of Proterozoic to Carboniferous rocks, Geological Survey of Victoria.

Weitz, D., and Huang, J., 1984, Self–similar structures and the kinetics of aggregation of gold colloids, Kinetics of aggregation and gelation, Elsevier, p. 19-28.

Weitz, D., and Oliveria, M., 1984, Fractal structures formed by kinetic aggregation of aqueous gold colloids: Physical Review Letters, v. 52, p. 1433.

Williams-Jones, A. E., Bowell, R. J., and Migdisov, A. A., 2009, Gold in solution: Elements, v. 5, p. 281-287.

Willman, C., Korsch, R., Moore, D., Cayley, R., Lisitsin, V., Rawling, T., Morand, V., and O'Shea, P., 2010, Crustal-scale fluid pathways and source rocks in the Victorian gold province, Australia: Insights from deep seismic reflection profiles: Economic Geology, v. 105, p. 895-915.

Wilson, C. J., Schaubs, P. M., and Leader, L. D., 2013, Mineral precipitation in the quartz reefs of the Bendigo gold deposit, Victoria, Australia: Economic Geology, v. 108, p. 259-278.

Witten Jr, T., and Sander, L. M., 1981, Diffusion-limited aggregation, a kinetic critical phenomenon: Physical review letters, v. 47, p. 1400.

Xavier, R. P., and Foster, R. P., 1991, The role of carbonaceous shear bands in fluid-flow and gold-precipitation in the Fazenda Maria Preta mine, Bahia, northeast Brazil: Brazil Gold v. 91, p. 269-277.

Zhou, Q., Wang, B., Wang, P., Dellago, C., Wang, Y., and Fang, Y., 2013, Nanoparticle-based crystal growth via multistep self-assembly: CrystEngComm, v. 15, p. 5114-5118.

Chapter 4

The first analysis of a telescoped orogenic gold system:

Insights from the Fosterville deposit.

Christopher R. Voisey[1], Andrew G. Tomkins[1], Yanlu Xing[1]

[1]*School of Earth, Atmosphere & Environment, Monash University, Clayton, VIC 3800, Australia*

"Do you ever actually *know* if you're right?"
-Words of a diffident man

Abstract

The Fosterville Au deposit is hosted in the Bendigo Zone within the western Lachlan Orogen, south east Australia, and contains three distinct mineralisation styles: (i) refractory Au in fine-grained arsenopyrite and arsenian pyrite disseminated throughout metasedimentary rocks near brittle faults; (ii) visible Au hosted in fault-controlled quartz-carbonate veins associated with stibnite mineralisation; and (iii) vein-hosted native Au with little or no associated stibnite. Refractory Au mineralisation is found throughout the deposit, whereas visible Au ± stibnite occurs deeper in the system (>800 m depth from surface). Thus, Fosterville provides a unique opportunity to study a telescoped orogenic Au system that changes mineralisation style as a function of depth. Microscopy, neutron tomography, nanoscale secondary ion mass spectrometry and field observations have been conducted to investigate mineralogical and structural controls on the various styles of Au mineralisation. These observations are used as the foundation for equilibrium geochemical modelling using HCh software. Results are considered in the context of an evolving mineral system over the history of the deposit and relative timing of mineralisation is inferred. Two alternatives for the genesis of such a system include: (1) metal deposition was controlled by ongoing physiochemical changes at a very shallow level in the crust in one evolving mineralisation stage, or (2) two or three deposits formed in the same location, with each different style of mineralisation representing a separate period of fluid infiltration, each potentially tens of millions of years apart. Based on our results, we suggest that the latter is more likely. Therefore, we suggest that Fosterville is the first example to be recognized of a telescoped orogenic Au system, where relatively high-temperature mineralisation and alteration assemblages were overprinted vertically by later, lower temperature assemblages.

Chapter 4

1. Introduction

Telescoped ore deposits are those in which early, usually deeper, high-temperature mineralisation and alteration are over-printed vertically by later, usually shallower and lower temperature mineralisation events and their characteristics. This term is commonly used to describe the juxtaposition of epithermal-type mineralisation over porphyry-style deposits (Sillitoe, 1994). In those, syn-hydrothermal degradation of the paleosurface may have occurred by rapid erosion or volcanic edifice collapse, leading to decompression of the ore system and subsequent overprinting. Alternatively, uplift facilitated by faulting may bring earlier, deeper sections of a deposit to shallower depths to be overprinted and/or upgraded by late-stage epithermal mineralisation (e.g., Porter, 2016). There has been little consideration of whether telescoped orogenic ore systems exist, although their mineralogy does vary between deposits with depth of emplacement (Groves et al. 1998). This may be due to the typically large distances separating the distinct mineralisation styles/deposits across a given district, so they are considered individually. Or, if vertical zonation was local it may have been lost to erosion or re-working, or simply not seen due to insufficient depth-extent of mining.

Since orogenic deposits are thought to form over a crustal depth range of 10 km or more (Groves et al., 1998), many mineralized systems extend well beyond the depth limits of current mining technology; we currently have no idea whether some deposits extend well beyond 3 km depth extent. Since orogenic Au deposits form in second or third order structural traps associated with crustal scale faults, it should be expected that some structural systems were active for very long periods, and/or were reactivated multiple times as regions evolved tectonically. Thus intuitively, there is reason to expect that some orogenic deposits experienced multiple stages of mineralisation at differing P-T-X conditions.

Gold has a bimodal distribution in orogenic systems, occurring in some deposits primarily within or attached to sulphides (including refractory Au) and in others

occurring mainly as visible gold in quartz-carbonate veins. Additionally, Phanerozoic metasedimentary rock-hosted deposits sometimes have a Au-Sb association (e.g., Hagemann & Lüders 2003). This variety is commonly seen within individual mineralized belts. For example, the Victorian Goldfields in Australia has many deposits where Au is contained in quartz veins, and a small number where the other examples exist. In this same region, the Fosterville deposit hosts all three Au mineralisation styles, each occurring at distinct depth extents. This occurs despite a low variance in host rock geochemistry; they are an unremarkable package of turbidites. This deposit thus provides an ideal setting for investigating how geochemical and structural controls on metal accumulation varied with depth in a single deposit.

In this study, we investigate whether the Fosterville system reflects: (1) a single fluid infiltration period with mineralogical variation controlled by ongoing changes in pressure, temperature and/or fluid composition with decreasing depth, (2) two or more fluid infiltration periods with mineralogical variation controlled by external changes in infiltrating fluid chemistry over time, or (3) both. Our findings have implications for the broader understanding of orogenic gold systems globally.

2. Regional Geology

Eastern Australia is composed of a series of geologic terranes, known as the Tasmanides, that were accreted to the Pacific margin of Gondwana during the Paleozoic (VandenBerg et al., 2000; Willman et al., 2010; Phillips et al., 2012). The terranes that make up the Tasman Fold Belt System include the Delamerian, Lachlan, and New England Orogens (Fig.1). The Lachlan Orogen is the remnant of a Paleozoic subduction-accretionary system consisting of various oceanic tholeiites, turbiditic sandstone and mudstone sequences, as well as arc-related volcanics (VandenBerg et al., 2000; Cayley et al., 2002 ; Gray & Foster, 2004). It is also believed that in the lower crust this orogenic belt contains fragments of Neoproterozoic continental crust that have been underthrusted into the system from the Selwyn Block during late-stage collisional tectonics (Willman et al., 2010; and references therein). The Lachlan Orogen itself

has been divided into western, central, and eastern sub-provinces, where the western sub-province is host to the vast majority of the orogenic Au-style mineralisation in Victoria (Phillips et al., 2012).

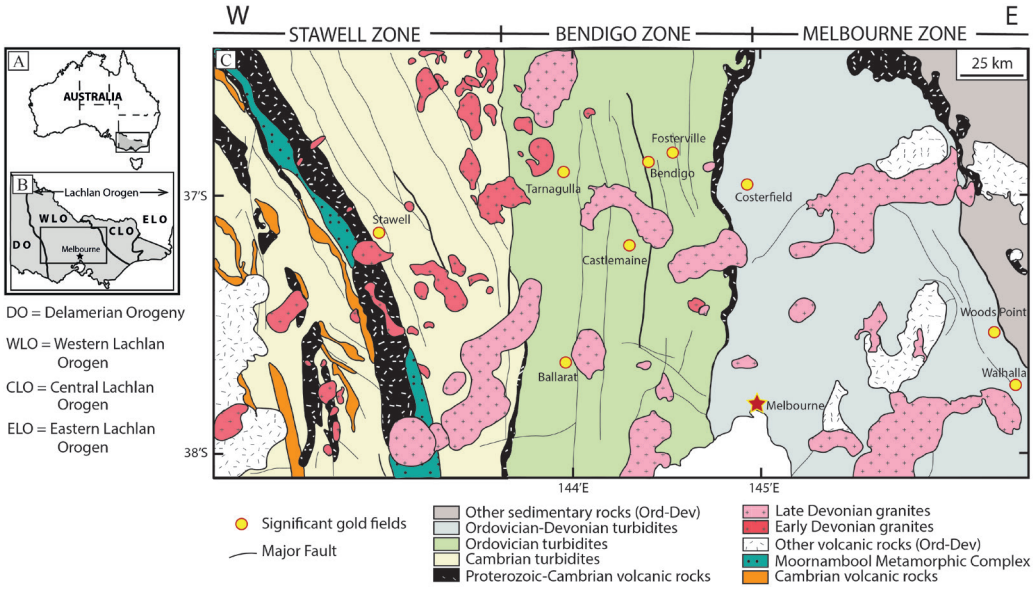

Figure 1:A) Schematic of Australia with the state of Victoria highlighted in grey. Position of B is indicated. B) Inset map of Victoria and part of New South Wales showing the locations of the Lachlan Orogen and the Delamerian Orogen modified from Willman et al. (2010). Position of C is indicated. C) Simplified geological map of central Victoria modified from Phillips et al. (2012). Infilled circles show major goldfields

2.1 The Western Lachlan Orogen

The Western Lachlan Orogen is defined by ~12 km thick, Cambrian to Silurian turbidite sequences, that overlie a ~25km thick Cambrian basement of oceanic mafic volcanics (VandenBerg et al., 2000; Gray & Foster, 2003). This sub-province is also host to post-tectonic granitic plutons and their associated lithologies that intruded throughout the Devonian (Paterson et al., 1990; Tobisch & Paterson, 1990). The sedimentary and volcanic rocks have undergone sub-greenschist to amphibolite facies metamorphism and were strongly deformed into dominantly north-south trending chevron folds that are bounded between thick-skinned thrust systems (VandenBerg et al., 2000). The Western Lachlan Fold Belt is further sub-divided into three major lithological/structural zones, the Stawell, Bendigo, and Melbourne Zones, which are

separated by north-south striking, high angle reverse faults (Fig. 1) (VandenBerg et al., 2000; Gray & Foster, 2003; Cayley et al., 2011). Phillips et al. (2003) estimated that ~80% of historic Au production from Victoria was derived from the Bendigo Zone. This region (Fig. 1) is host to gigantic structurally localized orogenic gold systems such as Bendigo (~15 km long by 8 km wide by >1.5 km deep), Ballarat East (~14 km long by 0.5 km wide by 0.5 km deep), Ballarat West (~7 km long by 1 km wide by ~1 km deep) and Castlemaine (~11.4 km long by 5.7 km wide by >1 km deep) (cf. Phillips & Hughes, 1996; Fairmaid et al., 2011; Willman, 2007), as well as the currently mined Fosterville deposit, which is currently the largest Au producer in the state of Victoria.

2.2 The Bendigo Zone

The Bendigo Zone is bound by two steeply dipping reverse faults, the Avoca Fault to the west and the Mt William Fault, belonging to the Heathcote Fault Zone, to the east (Fig. 1) (Willman et al., 2010; Cayley et al., 2011). This zone contains a basement composed of Cambrian mafic volcanics/volcaniclastic rocks that are overlain by thick sequences of Ordovician turbiditic sandstones and mudstone belonging to the Castlemaine Group (VandenBerg et al., 2000). Late Silurian to early Devonian granitic intrusions are located in the northwest of the Bendigo Zone, and middle to late Devonian granites can be found throughout (Chappell & White, 1992). The volcanic and sedimentary sequences have been deformed into upright, gently-plunging, north–south trending folds in response to east–west shortening (D_2) during the Late Ordovician (455–440 Ma) and Middle Devonian (380 Ma) (VandenBerg et al., 2000; Willman, 2010). It is believed that the Bendigo Zone originated as oceanic or ocean back-arc succession and belongs to an east-vergent, fold and thrust belt system (Gray et al., 1988; Gray et al., 2003; Cayley et al., 2011; Moresi et al., 2014). Gold mineralisation in this zone most commonly occurs as coarse particles hosted in laminated quartz veins related to chevron-style folding of turbidites (e.g., saddle reefs) or small-scale fault-controlled dilation structures (Cox, 1995; Wilson et al., 2013). However,

the eastern Bendigo Zone hosts 'pyrite-arsenopyrite-stibnite' style Au mineralisation, where elevated amounts of Sb occur along with Au and As. Fosterville is an example of this deposit type, with Au-rich pyrite and arsenopyrite grains that are finely disseminated within the host rock and stibnite-bearing, quartz-carbonate stockwork veins are at depth (Leader et al, 2010; Phillips et al., 2013).

2.3 Timing of Mineralisation

The timing of gold mineralisation in central Victoria has been constrained using $^{40}Ar/^{39}Ar$, U-Pb, and Re-Os isotopic methods, as well as traditional cross-cutting and field relationships. Gold is generally believed to have been introduced in three main events, at ca 450-435 Ma, 420-400 Ma, and ca 380-370 Ma (Fig. 2) (e.g., VandenBerg et al., 2000; Arne et al., 2001; Bierlein et al., 2001; Phillips et al., 2003).

The first Au mineralisation episode is broadly constrained to have occurred between 450-435 Ma, with most notable activity at 440 Ma (VandenBerg et al., 2000; Bierlein et al., 2001; Phillips et al., 2003). This episode comprises 'pyrite-arsenopyrite' assemblages and is the most common throughout Victoria. This is believed to be the most significant Au mineralisation event in the Bendigo Zone and occurred during stages of crustal shortening and heating related to the Benambran Orogeny (D_2). Regional scale metamorphism and deformation produced hydrothermal ore-bearing fluids from a large crustal reservoir and concentrated them within host structures (Vandenberg et al., 2000; Bierlein et al., 2001; Phillips 2012).

The second mineralisation event, although considered to be minor, occurred between 420-400 Ma and is also of the 'pyrite-arsenopyrite' classification. This episode is thought to be related to the onset of magmatism during the waning stages of the Benambram Orogeny, in which extensive melting of structurally thickened crust lead to widespread plutonism (Vandenberg et al., 2000, Bierlein et al., 2001).

The third and final Au episode occurred between 380-370 Ma and deposits of this age are related to the Tabberabberan deformation and post-tectonic plutonism (Van-

denBerg et al., 2000; Bierlein et al., 2001). Mineralisation of this type is distinctively antimony-rich, considered to be 'pyrite-arsenopyrite-stibnite' type assemblages, and can be found throughout the Melbourne Zone and the eastern parts of the eastern Bendigo Zone. In this major Au mineralisation event, it is debated whether metamorphic devolatilization or partial melting by crustal by anatexis is the driver for production of the hydrothermal fluid that mobilized Au (Willman et al., 2010; Phillips et al., 2012).

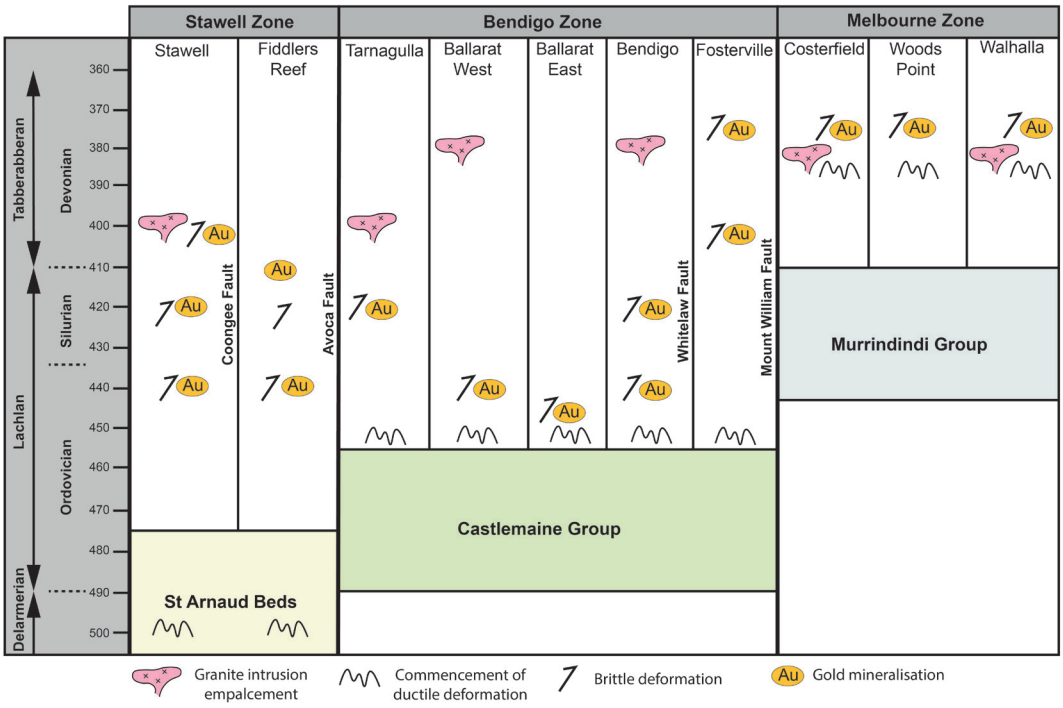

Figure 2: Schematic time-space summary of stratigraphy, deformation, magmatism, and mineralisation for significant Victorian Au deposits, south east Australia. The late stage (~380 Ma) mineralisation for Fosterville is interpreted in this manuscript.

3. Deposit Geology and Mineralisation

3.1 Ore Deposit Features

The Fosterville Gold Mine is hosted in lower Ordovician turbidite sequences belonging to the Castlemaine group, which are comprised of interbedded sandstone, siltstone and shale layers, many of which are weakly to strongly carbonaceous. Late Silurian to mid-Devonian aged quartz-feldspar porphyry dykes intrude the stratigraphic sequences along anticlinal axial surfaces in the north-eastern portion of the mine

lease. These dykes are up to 10m in width and are altered by white mica with variable arsenopyrite-pyrite and stibnite mineralisation. Middle Jurassic aged lamprophyre dykes also intrude along the Fosterville fault, are unmineralized with respect to Au or stibnite, and are similar to those found throughout the Bendigo Zone. The sedimentary sequences at Fosterville have undergone sub-greenschist facies metamorphism and are folded into upright chevron folds with wavelengths up to 350 m and parasitic fold wavelengths of roughly 50 m (Hitchman et al., 2018). These folds doubly plunge to the north and south at angles of up to 30º and have axial planar cleavage (S_2) that is best developed in the hinge zone of the folds. The cleavage is a well-defined axial planar spaced cleavage with penetrative planes spaced up to 1 cm apart in siltstones and less than 0.5 cm apart in mudstones (Leader, et al. 2010). Orientation of the north-south trending S_2 cleavage implies that folding was a result of east-west directed shortening.

To the west of the Fosterville anticline and east of the syncline, the dominant structures are steep west-dipping bedding-parallel quartz-carbonate veins (Fig. 3). These faults occur mostly in mudstone or at mudstone-sandstone contacts and are carbonaceous and white mica altered. To the east of the anticline, the faulting becomes moderately dipping and discordant, with either hangingwall or footwall bedding being oblique to the fault angle. These splay faults were interpreted to have been developed during the late stages of D_2 deformation when F_2 folds become so tight that they locked up, leading to the propagation of bedding-parallel veins across fold hinges when further reverse movement occurred (Leader et al., 2010). Many of these faults are associated with dilational brecciated zones and link eastward from the anticlinal to the synclinal structures (Fig. 3). In these zones, wall rock alteration is dominated by white mica and has a similar spatial distribution to that of the sulphide ore, with zones around bedding-parallel faults being poorly mineralized relative to those with more discordant, high bedding-fault angles. Faults with larger reverse offsets have more extensive zones of disseminated sulphide mineralisation and are thus believed to be associated with enhanced wall rock fracturing and permeability (Hitchman et al.,

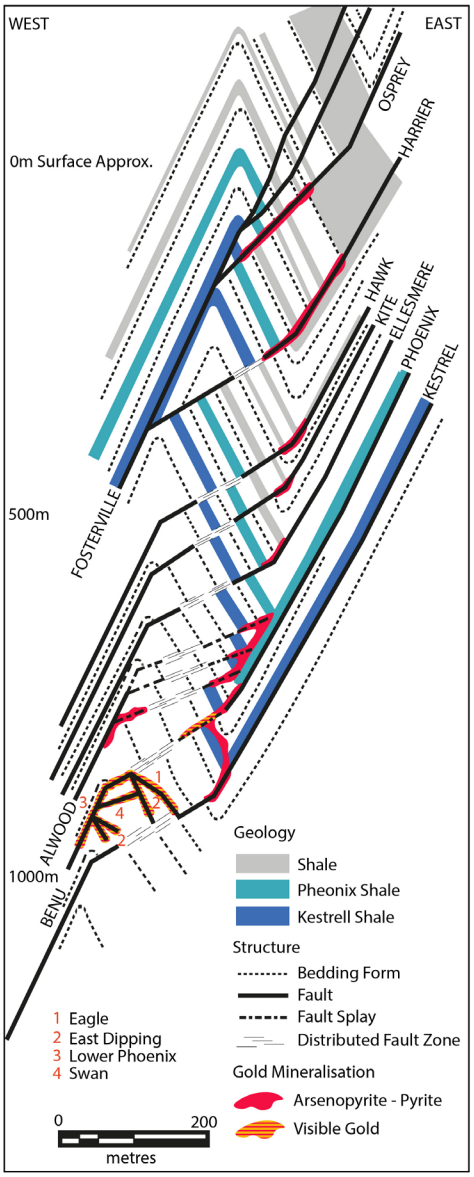

Figure 3:: Schematic cross section of the Fosterville gold deposit, Victoria, Australia, adapted from Hitchman et al., (2018). Proportion of gold-bearing arsenopyrite increases towards mineralised quartz veins and along bedding discordant fault intersections. Visible vein-hosted gold grades are highest on west-dipping high-order linkage faults (faults labelled with numbers) at and below the Eagle Zone -e.g., Swan (4).

2018).

3.2 Mineralisation Styles

Disseminated sulphide-hosted ore is the dominant Au mineralisation phase at Fosterville, with average grades of 5-10 g/t Au and individual assays of up to 60 g/t Au (Hitchman et al., 2018). This mineralisation is structurally controlled by discordant bedding-fault relationships, such that mineralisation is best developed where the most porous rock is oriented perpendicular to the fault plane and poorly where low porosity rock parallels the fault. From the surface to ~600 m depth the Phoenix fault is the dominant control on Au mineralisation. Below ~600 m depth, sulphide-hosted Au mineralisation weakens proximal to the Phoenix fault and is instead pervasively developed along the Lower Phoenix anticline adjacent to the Benu fault (Fig. 3). Disseminated sulphides containing refractory gold occur as selvages to quartz-carbonate veins, commonly dispersed ~0.5 m into the wall rock, but may persist to considerable distances from the fault planes (Fig. 3) (Leader et al., 2010). These refractory ore shoots are typically 4-15 m wide, 50-150 m in dip extent and 300 – 2500 m in length down – plunge (Hitchman et al., 2018). Arsenopyrite contains 100-1000 ppm

Au, whereas pyrite contains 10-100 ppm (Roberts et al., 2003).

Stibnite mineralisation occurs mostly below ~800 m depth, primarily within quartz veins along bedding-discordant faults (Fig. 4). West-dipping faults such as the Lower Phoenix and Lower Phoenix Footwall faults, as well as the east-dipping Eagle fault are host to most of the stibnite at Fosterville. This mineralisation can replace and infill earlier quartz-carbonate veins (e.g., stibnite-quartz matrix supporting quartz-carbonate breccia fragments), is commonly vuggy, and can occur as massive stibnite-quartz breccias up to 0.5 m wide along fault margins. Areas with stibnite mineralisation may contain disseminated visible Au (<3 mm), although the grade is highly variable.

High-grade visible Au is found in the Eagle zone below ~800 m from the surface (Fig. 4). The Eagle zone is associated with shallow east-dipping faults east of the main anticline. Here, the visible Au mineralisation is hosted in quartz veins and variably overprints wall rock-hosted sulphide mineralisation. The Eagle zone is approximately 0.5-6 m wide, 50-80 m in dip extent and plunges to lengths of 700 m (Hitchmann et al., 2018). Average grades are ~15 g/t Au with individual assays as high as 3% Au. Gold occurs as disseminated grains with sizes <2 mm and are loosely arranged in an orientation parallel to their host veins and/or stylolitic seams of wall rock. In the Ea-

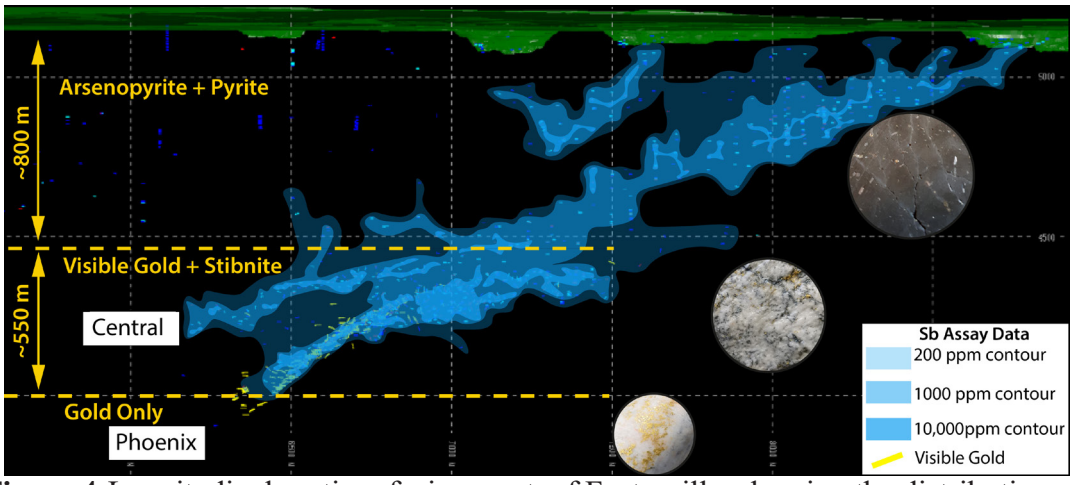

Figure 4: Longitudinal section, facing west, of Fosterville, showing the distribution of mineralisation styles. Inset photos are of hand sample specimens of the various ore styles; top being arsenopyrite- & pyrite- hosted Au, middle is Au-Sb vein-hosted ore, bottom is Au-only vein-hosted ore. All Sb contours are based on Fosterville assay data, yellow dashes are visible Au occurrences.

gle zone, visible Au contributes ~40% of the total contained Au, with the remainder as refractory gold, and visible Au in this zone contributes 10% of total mineral resources at Fosterville overall (Hitchman et al., 2018).

4. Methods

A suite of samples was prepared as 30µm thick polished thin sections for optical and scanning electron microscopy (SEM). SEM imaging was conducted at the Monash Centre of Electron Microscopy using a JOEL 7001 FEG-SEM to confirm mineralogy and to examine paragenetic mineral relationships in vein-hosted and refractory ore samples. Images were taken using a backscattered electron (BSE) detector using an acceleration voltage of 15.0 kV at a working distance of 9.1 mm and a probe current of 1.5 nA.

To inspect quartz growth generations in vein-hosted Au and Au-Sb samples, cathodoluminescence (CL) and element mapping were conducted at the Commonwealth Scientific and Industrial Research Organisation Microbeam Laboratory, Clayton. These maps were collected using a JOEL 8500F electron probe microanalyser (EPMA) at an acceleration voltage of 25 kV and a probe current of 40 nA. Element and CL maps were gathered concurrently using 10 µm step sizes and 30 ms dwell time per pixel.

Neutron tomography was conducted on a vein-hosted Au-Sb sample at the Australian Centre for Neutron Scattering to map the 3D distribution of Au and stibnite. Using the DINGO instrument (Garbe, 2015), the high spatial resolution configuration (with the ratio of collimator-detector length to inlet collimator diameter equal to 1000) generating a voxel size of 27 µm. Projections were obtained by rotating the sample around its vertical axis for 1339 angles equiangularly spaced from 0° to 360° during measuring. At each step the samples were exposed to the neutron beam for a period of 60s. The portion of the beam transmitted through the sample was converted into visible light using a 50µm thick 6LiF/ZnS scintillator, which is then guided via a mirror to an Andor

DW434 CCD camera with 1024 x 1024 pixels. The data sets were reconstructed with the Octopus package (Dierick et al. 2004), and ANU Vizlab's Drishti software was used for visualization, analysis, and full three-dimensional image reconstruction.

High-resolution elemental mapping of wall rock-hosted auriferous pyrite and arsenopyrite samples was carried out using the Cameca NanoSIMS 50L at the Centre for Microscopy, Characterization and Analysis (CMCA) at The University of Western Australia. The crystals of interest were removed from hand sample specimens using a handheld rotary tool and then prepared as a one-inch polished resin mount and carbon coated (~15 nm thickness). NanoSIMS measurements were performed with a Cs^+ primary beam, using a spot size of approximately 100 nm, impact energy of 16 keV, and a beam current of 10 pA. The instrument was operated in multicollector mode, allowing for detection of seven ion species in tandem (^{34}S, $^{54}Fe^{32}S$, $^{60}Ni^{32}S$, $^{75}As^{32}S$, ^{123}Sb, ^{130}Te and ^{197}Au). Secondary ion images were obtained by rastering the primary ion beam across areas measuring 50 x 50 µm, at a resolution of 512 x 512 pixels (each pixel measuring approximately 97 nm), with dwell time of 40 ms per pixel. The sample surface was presputtered with the primary ion beam (using 250 pA beam current) to 1.5 x 10^{17} ions/cm^2 in order to remove surface contamination and implant Cs^+ ions into the samples to reach a steady-state of ion emission. In all experiments an electron flood gun was used to minimize sample charging effects.

Equilibrium geochemical modelling was conducted using the HCh software package. This package was developed for modelling fluid-rock systems at moderate to high temperatures (up to 1000 °C) and moderate pressures (<500 MPa) using a thermodynamic database (Unitherm). The system modelled here was Al-As-Au-Sb-Fe-Mg-S-Cl-Si-K-Na-Ca-C-H-O to best represent the bulk rock compositions found in the Victorian gold fields and deposit ore mineralogy. This model assumes a turbidite source rock with the average composition of that reported by Bierlein et al. 2001 for Victorian 'background' slates (Table 1). A model using basaltic source rocks was also tested but could not produce a mineral system similar to Fosterville. In the model, H_2O doped with Au, Sb and As is reacted with the turbiditic source rock at the

base of the modelled rock column. These doped elements do not reach saturation in the fluid but allow for precipitation of their related phases later as the model evolves. Once equilibrated at greenschist-amphibolite boundary conditions, the fluid derived from the source rock is then migrated through a rock column with the same turbiditic composition – excepting the Au content, which is set to the average shale value of 3 ppb (Mason, 1985) – at a 50:1 fluid:rock ratio through a modern geothermal gradient of 30 °C per km. The entire modeled rock column is constructed of 134 'reaction cells', whereby the fluid equilibrates with the rock in each cell before passing through to the next. Thus, each reaction cell in the model is set to decrease in temperature by 3 °C and pressure by 33 bar per step. This process is repeated for 20 waves to best represent the fault valving nature of orogenic deposits, where large volumes of fluid are repeatedly flushed through relatively narrow interconnected fault/vein networks. At the beginning of each new wave, the initial Au-doped fluid is equilibrated with the turbidite host rock and then reacted with cells of the previously altered rocks from the preceding wave. In this way, the model is intended to examine the affects that progressive wall rock alteration and metal precipitation play on the outcome of deposit

Table 1 Mineralogical and chemical compositions used in HCh equilibrium modelling. Column rock and source rock compositions are based on XRD data from Victorian turbidites (Beirlein, 2001).

Composition	Source Rock	Fluid	Column Rock
Muscovite (wt. %)	29.86		29.86
Quartz (wt. %)	29.72		29.72
Chlorite (wt. %)	7.78		7.78
Illite (wt. %)	7.3		7.3
Ferrodolomite (wt. %)	6.64		6.64
Siderite (wt. %)	6.4		6.4
Albite (wt. %)	5.42		5.42
Pyrite (wt. %)	3.1		3.1
Kaolin (wt. %)	2.32		2.32
Calcite (wt. %)	0.4		0.4
Arsenopyrite (wt. %)	0.3		0.3
Graphite (wt. %)	0.1		0.1
Stibnite (wt. %)	0.0005		0.0005
Au (ppb)	7		3
H2O (wt. %)		99	
Sb(OH)3 (wt. %)		0.09	
As(OH)3 (wt. %)		0.04	
Au(HS) (ppb)		100	

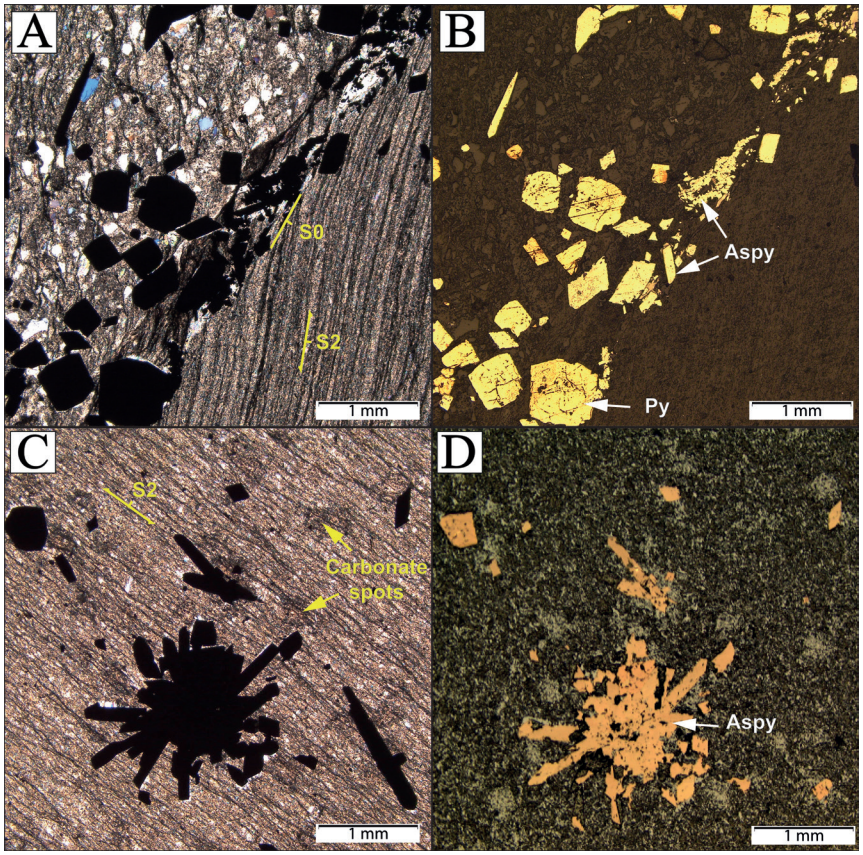

Figure 5: 'Shallow' refractory ore from <800 m depth above the Phoenix zone of Fosterville A) Polarized light photomicrograph of refractory ore, which has relict bedding defined by fine-grained muddy layers and coarser-grained sandy layers (S0). B) Reflected light photomicrograph of (A) showing pyrite and arsenopyrite. C) Polarized light photomicrograph showing S2 foliation and extensive carbonate spotting. D) Reflected light photomicrograph of (C) showing radial arsenopyrite.

formation.

5. Results

5.1 Vein and Ore Textures

Refractory Au ore mineralisation is found throughout the entire Fosterville at all structural levels. Arsenopyrite occurs as fine-grained (0.05-6 mm) acicular needles that in some samples are aligned with the north-south trending S_2 cleavage, and in others have no preferred orientation. In some samples, particularly in shallow levels of the deposit, arsenopyrite crystals exhibit a radial complex twinning pattern (Fig. 5). Arsenopyrite crystals have small pressure shadows that host variable amounts of stibnite. Auriferous arsenian pyrite crystals are pyritohedrons of 0.1-2 mm in size and

commonly have significantly larger pressure shadows that intermittently host stibnite (Fig. 6). At deeper levels in the deposit associated with Au-Stb mineralisation (i.e., ~ 800 m depth), pressure shadows/fringes on both arsenopyrite and pyrite host considerable amounts of aurostibite and white mica, as well as stibnite (Figs. 6 & 7). Additionally, at this depth, wall rocks are much more sericite altered and sericite-rich veinlets

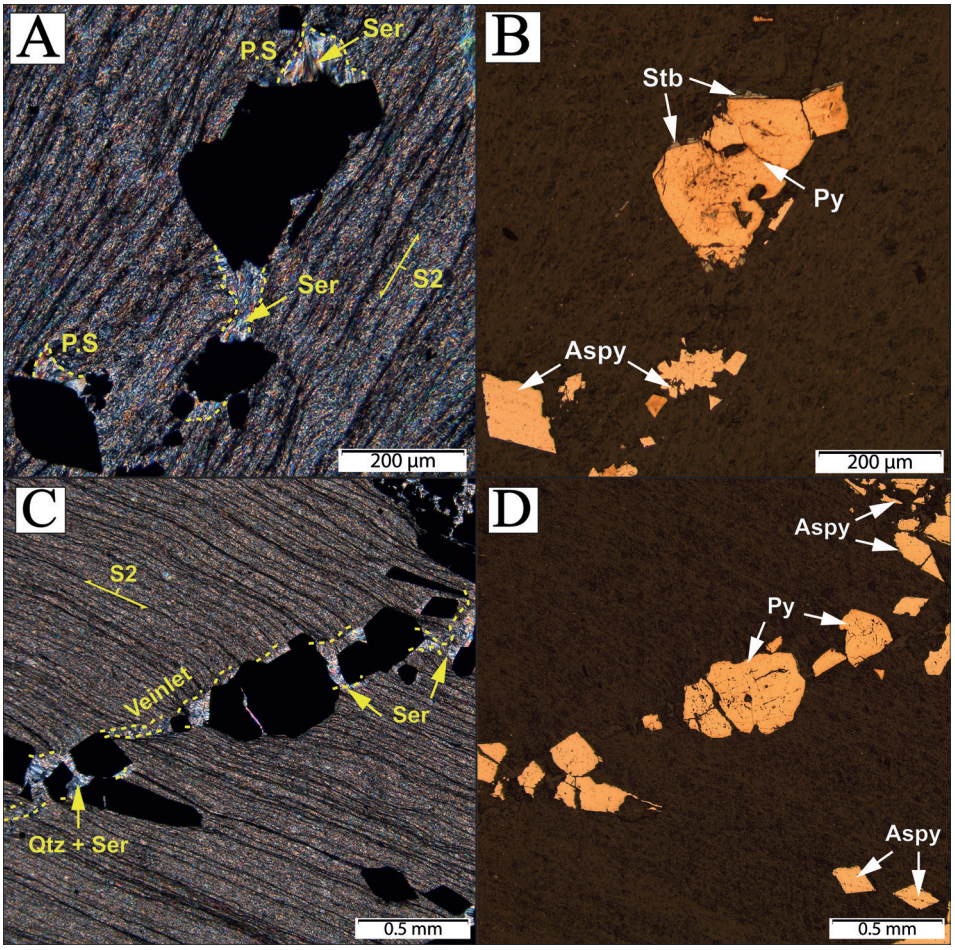

Figure 6:'Deep' refractory ore from ~800 m depth in the Phoenix zone of Fosterville. A) Polarized light photomicrograph of refractory ore that has sericite-filled pressure shadows (P.S) and wall rock is extensively white-mica altered. B) Reflected light photomicrograph of (A) showing pyrite and arsenopyrite with minor stibnite on grain boundaries of pyrite correlating with the sericite-rich pressure shadows. C) Polarized light photomicrograph of refractory ore cross-cut and fractured by a sericite-rich quartz veinlet. D) Reflected light photomicrograph of (C) showing arsenopyrite aligned with S2 wall rock fabrics (bottom right) as well as vein-fractured sulphides.

can be found cross-cutting refractory ore mineralisation in wall rocks adjacent to faults (Fig. 6).

NanoSIMS results reveal the element distributions and textural settings of au-

riferous arsenopyrite and pyrite from wall rock adjacent to Au-Sb mineralisation in the Phoenix zone. Although a suite of seven ion species were analysed (^{34}S, $^{54}Fe^{32}S$, $^{60}Ni^{32}S$, $^{75}As^{32}S$, ^{123}Sb, ^{130}Te and ^{197}Au), only those with considerable concentrations and/or a relationship with Au & Sb content are displayed. In most cases for arsenopyrite, there is no detectable compositional zoning with respect to Fe, S, or As, and Au appears to be lattice bound, as it mimics crystal zoning (Fig. 8). Pyrite shows compositional zoning with respect to As concentration and Au-bearing fractures that crosscut the crystal are Sb-rich. Gold within the pyrite grain shown in Figure 8 is clearly frac-

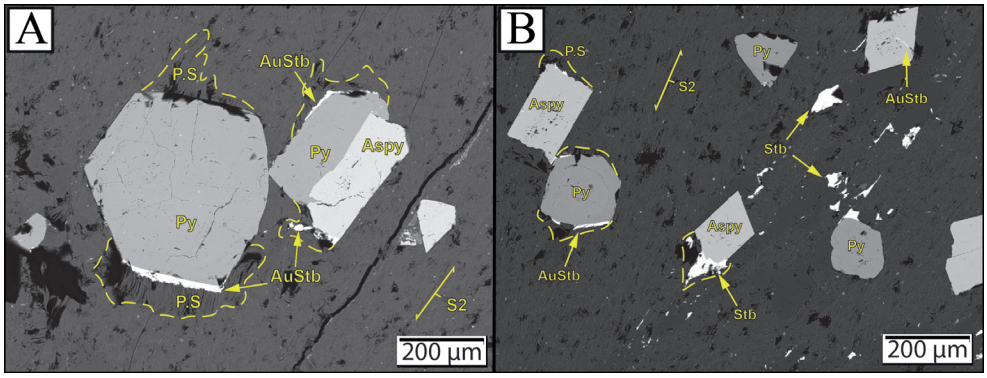

Figure 7: Auriferous sulphide mineralisation from the Fosterville gold mine. (A) BSE image of refractory sulphide ore from ~800m depth in Fosterville. Subhedral pyrite and intergrown pyrite/arsenopyrite porphyroblasts roughly aligned with S2 fabric, showing D2-3-related pressure shadows (P.S) hosting aurostibite (AuStb). (B) Arsenopyrite and pyrite porphyroblasts with stibnite and aurostibite contained in pressure shadows (P.S) as well as mineral fractures and associated foliation. Minor amounts of anhedral stibnite also occur aligned within S2 wall rock fabrics.

ture-hosted and occurs as nanometer- to micrometer-sized clusters. Stibnite mineralisation in all cases is contained in fractures, in-filled porosity, and pressure shadows, with no obvious crystal-bound Sb (Figs. 7 & 8).

Underground exposures show that Sb mineralisation commonly occurs on the margins of splay faults below the Phoenix level (Fig. 9). This mineralisation phase exists as stibnite-quartz breccias, massive stibnite veins sporadically intergrown with visible Au (< 3 mm), or within variably sized vugs (1-5 cm) (Fig. 9). Stibnite textures in fault veins can be massive, acicular, or dendritic. Microscopy and 3D neutron tomography show an intimate relationship between Au and stibnite (Fig. 10). Some of the highest-grade Au samples from Fosterville (upwards of 1% Au) consist of miner-

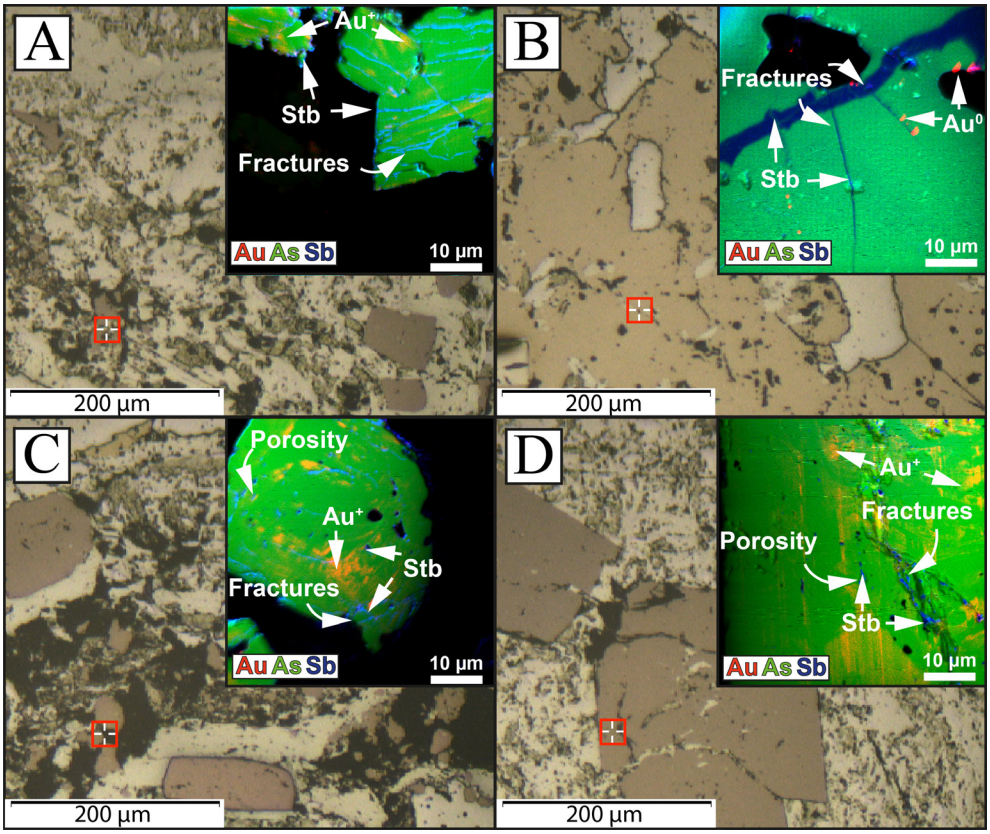

Figure 8: Auriferous sulphide mineralisation from the Fosterville gold mine. A) Photomicrograph of arsenopyrite crystals in a mineralized wall rock selvage hosted within a quartz vein. Inlay is nanoSIMS elemental RGB map of the area highlighted by the red square. High Sb values equate to stibnite in cross-cutting fractures. B) Photomicrograph of a pyrite crystal in a mineralized wall rock selvage hosted within a quartz vein. Inlay is nanoSIMS elemental RGB map of the area highlighted by the red square. High Sb values equate to stibnite filled, with Au occurring as nanometer- to micrometer-scale clusters on separate fractures. C & D) Photomicrographs of arsenopyrite crystals in a mineralized wall rock selvage hosted within the quartz vein. Inlays are nanoSIMS elemental RGB maps of the areas highlighted by the red squares. Bands of orange indicate zones of lattice-bound gold enrichment, and transgressive areas in the same colour indicate gold on fractures. Elevated Sb indicates stibnite within microscale pores and fractures

alisation of this type. When Au and stibnite are intergrown in vuggy vein cavities, it appears that Au has grown onto stibnite crystals (Fig. 10B). CL images of vein-hosted Au-Sb show that quartz has not been recrystallized or damaged post-crystallization and crystal zoning is preserved (Fig. 9). Quartz-stibnite veins emplaced along the Fosterville and Phoenix faults truncate the S_2 cleavage, and wall rock fragments within the veins contain well-developed S_2 cleavage as well as arsenopyrite-pyrite mineralisation.

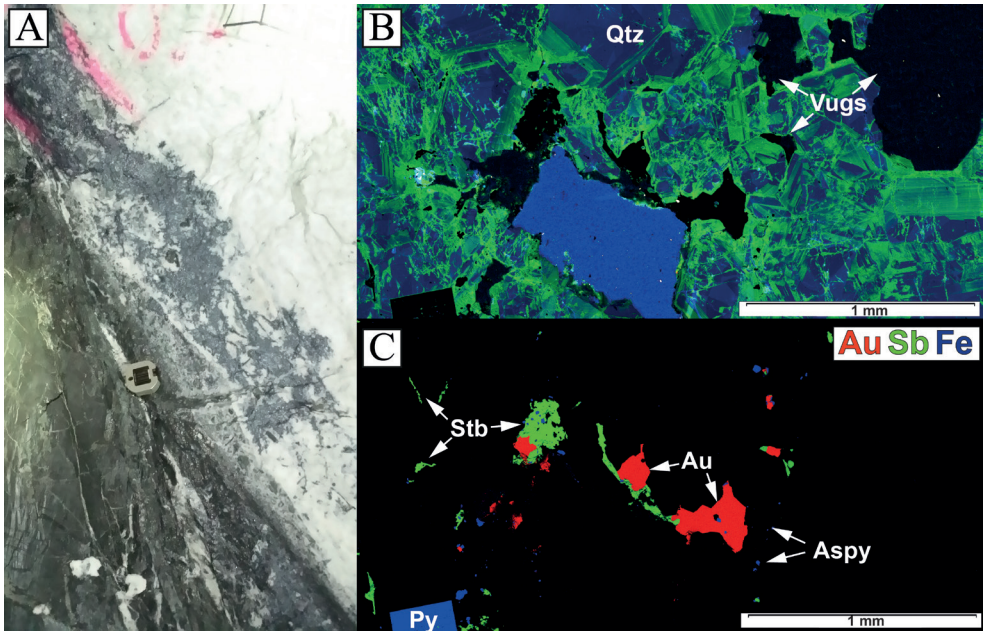

Figure 9: Au-Stibnite (Stb) mineralisation from the Fosterville gold mine. A) Underground exposure of massive stibnite-quartz breccia from the Swan fault at Fosterville, compass for scale. B) Cathodoluminescence map of Au-Sb mineralized quartz vein showing preserved crystal growth zones and cavities. C) Element map of (B) highlighting Au-Sb mineralisation with minor pyrite and arsenopyrite.

High-grade visible Au occurs below ~800 m from the surface in shallow east-dipping splay faults east of the main anticline (Figs. 4 & 5). Here, visible Au mineralisation is hosted in quartz-carbonate veins, associated with sericite alteration, and overprints the wall rock-hosted sulphide mineralisation. Gold grains are usually < 3mm in size, rounded to sub-rounded and disseminated in quartz veins and along quartz grain boundaries (Fig 11). Gold grains are concentrated along planes parallel to vein-incorporated wall rock selvages, giving rise to a “dusty Au” seam texture (Voisey et al., 2020). It is also common that Au grains are abundant in and along pressure-dissolved (stylolitized) wall-rock selvages. Microfracture networks within quartz veins also host considerable Au mineralisation.

5.2 Thermodynamic Modelling of the Fosterville System

The HCh modelling is successful at reproducing the Fosterville ore mineral associations (Fig. 11). At the top of Fig. 12 it can be seen that Au and stibnite are stable during early fluid influx waves at depths between 1.8 and ~5.43 km and temperatures between 150 and ~231 ºC. During subsequent fluid influx events this co-stability

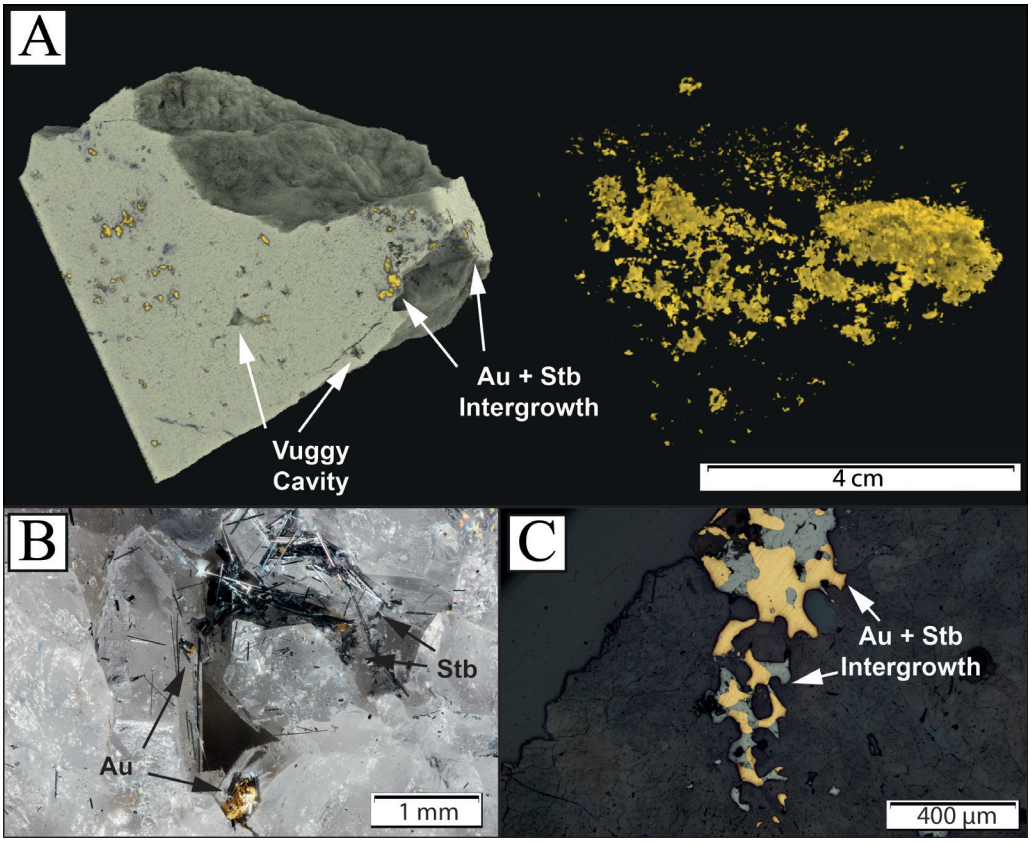

Figure 10: Au-Stibnite (Stb) mineralisation from the Fosterville gold mine. A) Neutron tomographic reconstruction of vein-hosted Au-Sb ore showing Au distribution relative to cavities. B) Photograph of vugh-hosted Au-Sb ore within a quartz-carbonate vein, with Au occurring on stibnite crystals. C) Reflected light photomicrograph of intergrown Au-stibnite mineralisation in a quartz-carbonate vein.

becomes confined to 1.8 and ~4.8 km and temperatures between 150 and 213 ºC, but the concentration (i.e., grade) of both minerals increases. Arsenopyrite and pyrite are stable in appreciable concentrations throughout this entire interval and increase in concentration during progressive fluid rock reactions. This depth range is in fair agreement with fluid inclusion studies that estimate the formation of auriferous arsenopyrite at Fosterville to have occurred between 2.6 to 5.7 km depth and temperatures of 180 to 270 ºC (Mernagh, 2001). Muscovite (sericite) is stable throughout the entire model, but notably increases in concentration as temperature decreases to 372ºC and pressure to 3.02 kbar in the early fluid influx events (n = 5), which corresponds to a drop in fluid pH from 6.5 to 5.5. Carbonates (both calcite and siderite) are stable in this same depth range, and can be considered equivalent to the calcite-ankerite spotting at Fosterville. Figure 12 highlights the dominant controls on fluid pH and shows

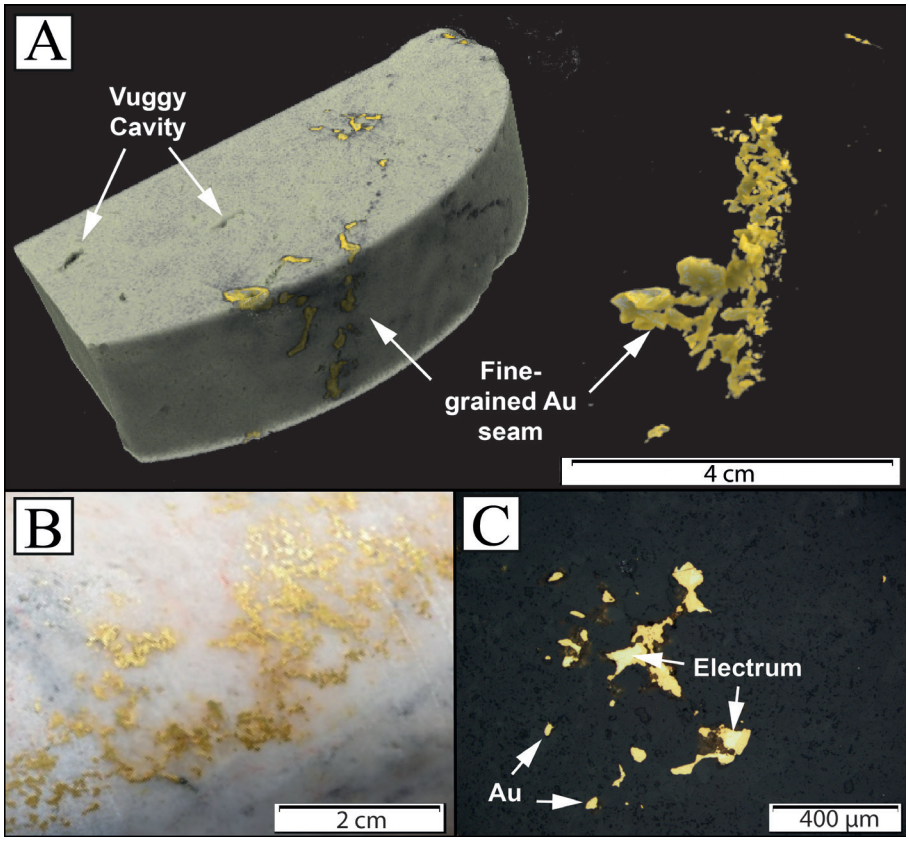

Figure 11: Au-only mineralisation from the Fosterville gold mine. A) Neutron tomographic reconstruction of vein-hosted Au-only ore showing Au distribution and minor cavities. Gold in this sample is distributed roughly parallel to the vein margin and pressure-dissolved wall rock selvages. B) Photograph of disseminated Au within a quartz vein with no obvious preferred orientation. C) Reflected light photomicrograph of finely disseminated Au ore with whiter areas minor areas of high Ag content (i.e., electrum).

that the breakdown of orthoclase corresponds with increase in sericite concentration. This corresponds to the sericite alteration found at Fosterville, especially at deeper levels in the system near the Phoenix zone. During progressive fluid-rock reactions (waves), the increase in concentration of sericite and associated pH drop migrates further up the rock column, as do Au and stibnite concentrations. This migration is accompanied by the onset of kaolin formation, albeit in minor concentrations, which is consistent with observations at Fosterville from Bierlein et al. (1998). After 20 waves of fluid-rock reaction, Au and stibnite remain stable and only grow in concentration in the rock. The final result shows a discrete zone of Au-stibnite co-stability at shallow depth, a narrow window of 'Au-only' stability below that zone, and arsenopyrite + pyrite stability throughout both of these zones and extended to depths of down to ~7.8 km.

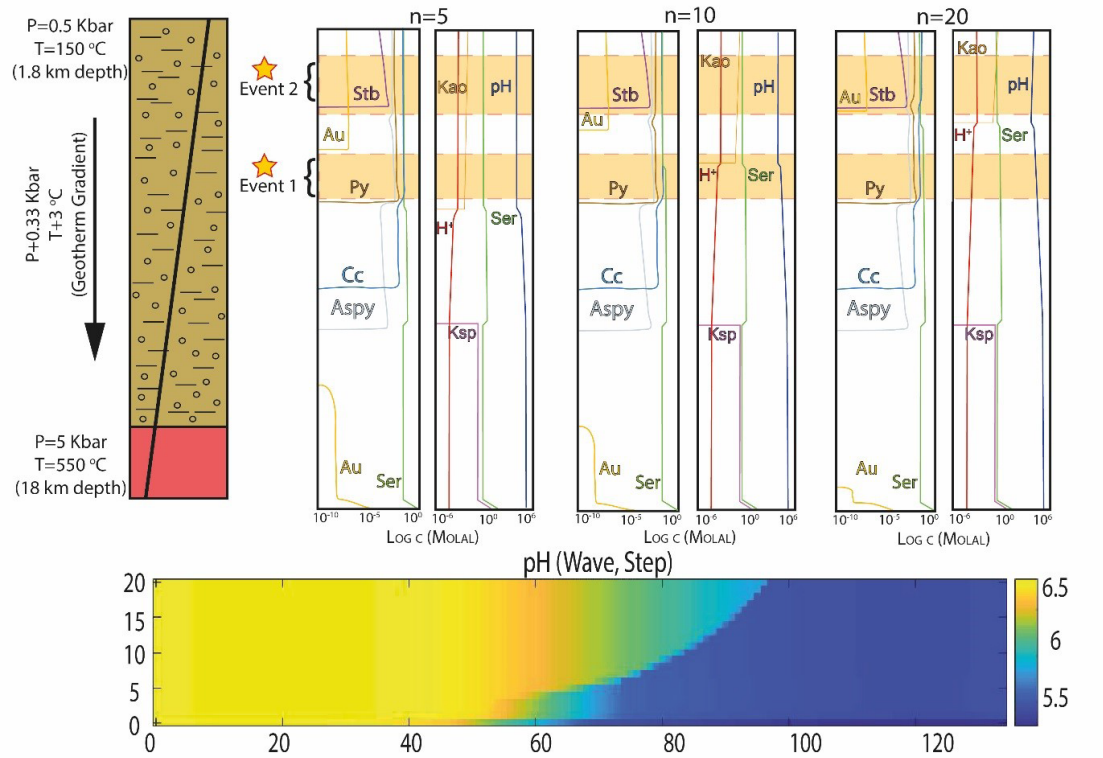

Figure 12:. HCh thermodynamic modelling of the Fosterville gold mine. Top: Schematic of the HCh thermodynamic model output showing theoretical rock column and parameters. Species shown on the left column of each n=x step are the dominant ore and alteration mineral species. Phases shown the right column are dominant species that control fluid pH and associated alteration. Lines represent relative mineral stability with concentration increasing to the right in each column. Bottom: A pH evolution map in reaction step (x-axis; depth decreasing to the right) vs. wave (y-axis) space. Fluid pH values of ≤ 5.5 (i.e., dark blue regions) are needed for Au-stibnite precipitation (see text). Steps correlate to crustal depth and associated P-T conditions with step 0 representing the bottom of the rock column (P=5 Kbar and T=550ºC) and step 130 representing the top (P=0.5 Kbar and T=150ºC). Waves correlate to fluid infiltration events (depicted by n values at the top of each column), 0 being un-reacted rock and 20 being the final fluid influx event with a cumulative fluid:rock ratio of 1000. Stars labelled Event 1 and Event 2, and their highlighted intervals, are the interpreted conditions for Fosterville mineralisation events (see text). Cc = calcite, Kao = kaolinite, Ksp = potassium feldspar

6. Discussion

6.1 Relative Timing and Styles of Mineralisation

Auriferous arsenopyrite and pyrite mineralisation at Fosterville is spatially associated with stockwork arrays of quartz-carbonate veins and is hosted within hangingwall and footwall rocks throughout the deposit. Given that the ubiquitous disseminated arsenopyrite and pyrite grains at Fosterville are in some samples aligned with S_2 cleavage (Figs. 6 & 7), and in others are unaffected (Fig. 5), this type of mineralisation is likely to have been introduced during and after the regional D_2 deformation, which developed during the Benambran Orogeny. This type of refractory mineralisation is not quite the same as that found in the other deposits of the Bendigo Zone, which tend to contain coarse, D_2-affected, gold-free arsenopyrite and pyrite disseminated in wall rocks and visible Au in quartz veins. However, the ore mineral assemblage, alteration geochemistry and D_2 relationship is the same as those associated with the Benambran Orogeny in that it comprises 'pyrite-arsenopyrite' assemblages. Comparisons of fluid inclusion data for the Western Lachlan Fold Belt indicate that inclusions in samples from the upper levels of Fosterville were trapped at lower temperatures and shallower crustal depths than those in the quartz reef style of Au deposits in the Bendigo Zone (Mernagh, 2001). The Fosterville fluid inclusions were enriched in N_2 and CH_4 compared to the relatively deeper deposits (e.g., Bendigo), which was attributed to extensive interaction with reduced fluids or carbonaceous matter in the sedimentary host rocks due to lower confining pressures around the veins. This difference in crustal level and fluid-rock interaction could explain why these different mineralisation styles formed during the same event, with equivalent host rock and geochemical signature manifesting themselves in mineralogically distinct ways.

At depth (~800 m from surface), the pyrite and arsenopyrite mineralisation is over-printed by stibnite ± Au mineralisation, as indicated by cross-cutting fractures, in-filled porosity, and pressure shadows filled with Sb minerals (Figs. 7 & 8). These micro-textures imply that Au-stibnite mineralisation event(s) post-date the deposition

of pyrite and arsenopyrite. Leader et al. (2010) suggested that stibnite mineralisation post-dates D2 deformation and Py-Asp mineralisation, and is genetically associated with later fault movement. Their interpretation was based on the observation that quartz-stibnite veins emplaced along the Fosterville and Phoenix faults truncate the S_2 cleavage, and wall rock fragments within the veins contain well-developed S_2 cleavage as well as arsenopyrite-pyrite mineralisation. These fault breccia fragments are also occasionally rimmed by stibnite, implying that Sb mineralisation is relatively late in the ore paragenesis. Cathodoluminescence imaging of Au-Sb veins from the Lower Phoenix and Lower Phoenix Footwall faults show that quartz has not been recrystallized or damaged after crystallization and crystal zoning is preserved (Fig. 9), implying no significant internal deformation or destruction after formation. Similarly, mineralized vughs and open cavities are present in Au-Sb veins and have not collapsed during subsequent deformation (Fig. 10 B). These observations not only support a shallow emplacement depth, required to develop open-space textures, but also that their formation was during the waning stages of deposit formation. These delicate structures would be lost to overprinting deformation associated with fault-valving/ seismic pumping.

Stibnite-quartz breccias at Fosterville are similar to stibnite-rich lodes found ~30 km away at the Costerfield deposit (Fig. 1). Costerfield is an example of the 'pyrite-arsenopyrite-stibnite' type of Au mineralisation that is found throughout the Melbourne Zone, which is associated with Tabberabberan deformation (Bierlein et al., 2001; Phillips et al., 2012). Wilson et al. (2017) described Sb-Au mineralisation at Costerfield as tabular sheets of 'dyke-like', fault-parallel, massive stibnite bodies that overgrew earlier quartz, similar to observations from the Lower Phoenix and Lower Phoenix Footwall faults at Fosterville (Fig. 9A). In their model, stibnite + Au ore bodies were rapidly emplaced into shallow crustal levels under supra-lithostatic fluid pressures, similar to the mobile hydrofracture model of Bons (2001). Many faults at Fosterville consist of laminated veins lacking vughs, and with intense localized hydrothermal alteration (i.e., pyrite and arsenopyrite), consistent with formation at interme-

diate crustal levels. However, the cross-cutting Sb ± Au splay faults form large dilated brecciated zones that are more indicative of shallow crustal formation (Faulkner et al., 2010; Wilson et al., 2017). The mineralogical and structural parallels between Au-Sb mineralisation at Fosterville and Costerfield is further supported by fluid inclusion data reported from both deposits. Fluid inclusions from Costerfield quartz veins have trapping conditions of < 280ºC and < 6 km depth, with enrichments in CH_4 and N_2; the same as Fosterville and similar to those reported from other high-level deposits in the Melbourne Zone (Changkakoti et al., 1996 ; Mernagh, 2001). For comparison, fluid inclusions from other Bendigo Zone deposits have formation depths of > 5 km and temperatures more than 300ºC, with little CH_4 or N_2 (Changkakoti et al., 1996). Based on these similarities, it is likely that the Au-Sb mineralisation event at Fosterville occurred during the Tabberabberan Orogeny and represents a part of the Bendigo Zone that was locally overprinted by a second generation of Au mineralisation (cf. Changkakoti et al., 1996; Bierlein et al., 2001; Phillips et al., 2003).

6.2 Mechanisms for Au-Sb Precipitation

Antimony is widely considered to be deposited at shallow crustal levels and is usually introduced late in hydrothermal mineral systems (Williams-Jones and Normand 1997; Groves et al. 1998), and these are consistent with the Au-Sb sample textures found at Fosterville (Figs. 9 & 10). Above 300 ºC, Sb is stable in hydrothermal fluids in concentrations up to thousands of ppm across a range of hydrothermal conditions (Krupp 1988), so in some systems the required drop in temperature to precipitate stibnite can be large, whereas at lower temperatures small changes make a large difference. For example, at a pH of 5.5, a drop in temperature from 250 ºC to 200 ºC would decrease Sb solubility by an order of magnitude causing significant stibnite mineralisation (Williams-Jones and Normand 1997; Hagemann & Lüders 2003). Our thermodynamic modelling of the Fosterville system shows that at pH of 5.5 stibnite precipitation occurs from 213 to 150ºC (Fig. 12). Cooling of ore fluids can occur by bringing deeply sourced fluids into relatively cool country rock, through fluid un-mix-

ing, or by adiabatic cooling associated with pressure decreases, such as during fluid ascent. The widely accepted fault-valve model for orogenic deposits predicts dramatic pressure fluctuations during seismic events through both localized fracture dilation and fluid ascent (Sibson et al., 1988). The pressure reduction of ascending ore fluids can lead to fluid unmixing at shallow levels in the crust, and when the fluids have equilibrated with carbonaceous sedimentary packages, CH_4, CO_2, and H_2S are partitioned into the vapour phase (Naden & Shepherd, 1989). This fluid unmixing can cause significant fluid temperature decreases, thus stibnite precipitation. The previous fluid inclusion studies of quartz veins from the upper level refractory ore shoots at Fosterville, which identified two populations at 270 ºC and 180ºC (Mernagh, 2001), could indicate fluid phase separation during Au-Sb mineralisation (cf. Hagemann & Lüders, 2003). Alternatively, these two populations could reflect two separate veining events at different P-T conditions. Phase separation could explain the Au-stibnite mineralisation found at Fosterville, however, in the Fe–Sb–S system, Au-Sb co-precipitation also requires a decrease in the fluid pH (Williams-Jones and Normand 1997). Therefore, the co-genetic precipitation of high-grade Au with stibnite at Fosterville will have required sulfidation and/or acidification to accompany a temperature decrease.

Sulfidation is a mechanism for the acidification of Au-Sb fluids that is driven by the precipitation of sulphide mineral assemblages such as pyrite and arsenopyrite. Given that some of the arsenopyrite and pyrite mineralisation overprints the S_2 foliation near the Au-stibnite ores at Fosterville (Fig. 5), it is plausible that a relatively late stage sulfidation event played a role in generating the Au-Sb ores. Figure 12 shows that both pyrite and arsenopyrite are stable across the entirety of the Au-stibnite and Au stability fields, so it is possible that sulfidation promoted acidification of Au-Sb mineralizing fluids at Fosterville. Additionally, ankerite spots in Fosterville wall rocks are variably sulfidized to pyrite. Such a reaction could consume excess H_2S by:

$$2FeCO_3 + 4H_2S + O_2 \rightarrow 2FeS_2 + 2CO_2 + 4H_2O \qquad 1.$$

This mechanism would also reduce fluid pH, and modelling shows the overlap of carbonate and Au-stibnite stability fields (Fig. 12). However, any relationship between these stability fields and fluid pH change in the results is subtle at best, and the occurrence of ankerite sulfidation at Fosterville is minor compared to sericite alteration. Thus, it is not likely that sulfidation reactions were significant enough to reduce ore-forming fluid pH on their own.

Many Phanerozoic orogenic Au (±Sb) deposits are hosted in turbidite packages that are rich in phyllosilicate minerals, which have the capacity to buffer large volumes of ore-forming fluids to relatively low pH (Williams-Jones and Normand 1997). Additionally, hydrolysis of carbonaceous material found in these shale packages can lower pH by producing CO_2 and CH_4 upon reaction with H_2O in infiltrating fluids (Williams-Jones and Normand 1997). Our modelling shows that Au-stibnite precipitation occurs not only at low temperatures, but also when fluid pH shifts from ~6.5 to 5.5 (Fig. 12). This same pH decrease is also coincident with a drop of Au solubility in HS and $(H_2S)^-$ bearing hydrothermal solutions by an order of magnitude, from 10 ppb to 1 ppb (cf. William-Jones et al. 2009), providing conditions favourable for both Au and Sb mineralisation. The pH change migrates up the rock column as a reaction front during successive fluid flux events and lengthens in vertical extent in the model (Fig. 12). This pH shift appears to be controlled by sericitization of the wall rocks, which provides a pH buffer for later fluid flux events. At depth in the model, sericitization is facilitated by the break-down of orthoclase by:

$$3KAlSi_3O_8 + 2H^+ + 12H_2O \rightarrow KAl_3Si_3O_{10}(OH)_2 + 4H_4SiO_4 + 2K^+ \qquad 2.$$

Then, at relatively shallow crustal levels sericite begins to break down to kaolin by:

$$KAl_3Si_3O_{10}(OH)_2 + 2H^+ + 3H_2O \rightarrow 3Al_2Si_2O_5(OH)_3 + 2K^+ \qquad 3.$$

Reactions 2 and 3 are consistent with the observed alteration mineralogy at Fosterville (cf. Bierlein et al., 1998), thus indicating that the pH of the infiltrating fluid was buffered by the potassic system to the conditions required for Au + stibnite mineralisation (Fig. 12). It is suggested that earlier fluid influx events altered the surrounding

wall rock to contain sufficient white mica to act as a pH buffer for later Au-Sb bearing fluids to deposit at discrete crustal levels, as observed on the mine scale at Fosterville. This agrees with the close spatial association of extensive wall rock sericitization with high-grade Au-stibnite ore, as well as sericite veinlets and porphyroblasts fringes that contain stibnite and aurostibite (Figs. 6 & 7).

Concurrent with, but slightly shallower than, the upward migration of the sericite to kaolinite transition with successive episodes of fluid infiltration, the Au-only stability interval also shifts upward (Fig. 12) and increases in magnitude. This deeper Au-only stability field, and overlying Au+Stb field, matches the observed metal distribution at Fosterville. The model further indicates that if the number of fluid infiltration events is low there would be low concentrations of Au dispersed across a broad depth interval (possibly Costerfield), whereas if the number of episodes is high, gold would be more concentrated at shallower levels (possibly Fosterville). The fluid pH buffer provided by sericite alteration of wall rocks allows for a fertile deposition interval for Au, as well as Sb, and is representative of the difference between a vertically extensive anomaly and a high-grade deposit.

6.3 Genesis of Ore Telescoping at Fosterville

It has been demonstrated that the Fosterville deposit is host to three distinct Au ore assemblages that formed either from one progressive mineralisation event or two separate events. Differences in the two styles of mineralisation include mineralogy, structural setting and P-T-X conditions, but interpretation of these deposit-scale characteristics must be considered in the context of the geological evolution of the Victorian gold province.

It is generally agreed that during crustal shortening and heating related to the Benambran Orogeny (440-420 Ma), hydrothermal fluids traveled along networks of fold-controlled second-order faults that developed during and after folding of turbidite successions, leading to the major Au mineralizing event throughout the Bendigo Zone (Fig. 2) (Phillips et al., 2012). At this point in time, we suggest that the Fosterville

locality sat below the P-T-X window of Au-Sb mineral stability, but within that of Py-Asp stability, so Au mineralisation formed as disseminated sulphide-hosted ore (Figs. 11 & 12). Thermodynamic modelling results place this arsenopyrite-pyrite stage at depths of 8.12 to 6.41 km and temperatures ranging between 297 and 255°C. At these temperatures, stibnite precipitation is prohibited unless Sb concentrations in crustal fluids exceed thousands of ppm (William-Jones & Normand, 1997). The refractory nature of this mineralisation stage may have been caused by phase separation upon interaction between the infiltrating fluid and the reduced fluids or carbonaceous matter in the sedimentary host rocks, which leads to CH_4, CO_2, and H_2S loss into the vapour phase (Naden & Shepherd, 1989; Mernagh, 2001). Phase separation is a pressure controlled process, and so may explain why the refractory mineralisation occurs at the shallow Fosterville system and not the deeper systems to the west. This interpretation is consistent with the disseminated sulphide ore at Fosterville being associated with fault-filled laminated bedding-parallel veins with broad zones of intense localized hydrothermal alteration (e.g., sulphides, carbonate and white mica), implying supra-lithostatic pressures and extensive fluid-rock interaction at intermediate crustal depths (Faulkner et al., 2010).

During waning stages of the Tabberabberan Orogeny, Au-mineralisation is largely restricted to the Melbourne Zone and eastern regions of the Bendigo Zone (Fig. 2) (Phillips et al., 2003; Willman et al., 2010; Phillips et al., 2012). With 60 to 40 m.y. between the Au mineralisation episodes, the erosion and uplift of the Fosterville deposit can be estimated to determine relative change in crustal level between these events. Using erosion rate values in relation to tectonics reported by Hecht and Oguchi (2017) and the tectonic reconstruction of the Victorian gold fields from Willman et al. (2010), it follows that the Fosterville deposit could have been exhumed by 3.2 to 5.9 km (avg = 4.55 km) between the Benambran and Tabberabberan Orogenies. Thermodynamic modelling results show Au-stibnite co-stability at depths between 4.81 km to 1.8 km and temperatures ranging between 255 °C and 150 °C. If the Fosterville deposit was exhumed roughly 4.55 km closer to the surface after the disseminated

refractory gold event, then it would exist within this Au-stibnite stability zone (Figs. 12 & 13). At these conditions, stibnite can precipitate from fluids that have Sb concentrations as low as 1 ppm (William-Jones & Normand, 1997). If fluid-flow was restricted to pre-existing networks of hydrothermally-altered (i.e., sericite-bearing) faults and fractures from the previous mineralizing event, then these pathways would act as the pH buffer needed the precipitation of Au along with stibnite (William-Jones & Normand, 1997). This is consistent with Au-stibnite mineralisation being restricted to the white mica altered splay faults that developed during late stages of D_2 when F_2 folds locked up (cf. Leader et al., 2010). These linkage faults would be ideal for re-activation during the Tabberabberan Orogeny (which also involved east-west compression; Willman et al., 2010), forming the large dilational breccias that host much of the Au-Sb mineralisation at Fosterville.

It is suggested that the Fosterville deposit formed via these two major Au mineralisation events, spaced 40 to 60 Ma apart: the 440-420 Ma 'pyrite-arsenopyrite' event and the 380 Ma 'pyrite-arsenopyrite-stibnite' event. Fosterville was situated in a structural corridor that was able to adopt both styles of mineralisation, due to its locality within the Bendigo Zone and proximal to the Melbourne Zone, and that alteration associated with the first pyrite-arsenopyrite event "primed" the wall rock for the second pyrite-arsenopyrite-stibnite event. Considering the temporal, spatial, and P-T-X relationships between ore mineral assemblages discussed here, it is more reasonable to consider Fosterville as two juxtaposed deposits, rather than one progressively evolving deposit. Therefore, we suggest that Fosterville is the first example to be recognized of a telescoped orogenic Au system, where relatively high-temperature mineralisation and alteration assemblages were overprinted vertically by later, lower temperature assemblages.

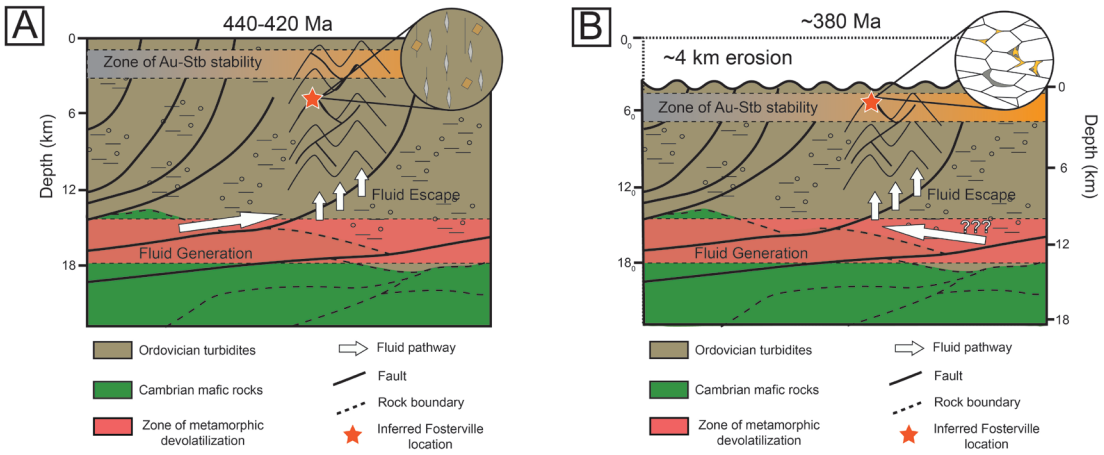

Figure 13: Simplified schematic showing stratigraphy, structural relationships and associated fluid flow for genesis of the Victorian Au deposits. The interpreted Fosterville goldfield location at both 440-420 Ma (A) and ~380 Ma (B) is shown by the red stars. Events 1 and 2 correspond to Figure 11. The zone of Au-Sb mineral co-stability, based on the HCh modelling results, is shown in grey/gold. Auriferous metamorphic fluid generation occurs in the zone highlighted in red. A) Hydrothermal fluids travel along networks of fold-controlled second-order faults that developed during and after folding of the turbidites successions during the 440-420 Ma Au mineralizing event. At this point in time, Fosterville lies below the window of Au-Sb mineral stability and Au mineralisation occurs as refractory sulphide ore only. B) Hydrothermal fluids travel along re-activated fault zone networks that were hydrothermally-altered (white mica + carbonate) in the previous mineralizing event(s) at 440-420 Ma. After ~40 Ma of erosion and uplift, Fosterville now lies ~4.55 km closer to the surface than in (A), and thus within the Au-Sb stability zone. Metamorphic fluids are interpreted to have been sourced from relatively unmetamorphosed distal turbidites in the Bendigo Zone, rather than already devolatilized source rocks, and/or possibly Melbourne Zone successions using Selwyn block underthrusting faults as a path way. Gold itself could be derived from these fluid sources and/or remobilised from earlier mineralisation in the reactivated fluid pathways; the latter is consistent with the Ag isotope results of Voisey et al. (2019).

7. Conclusion

The Fosterville deposit is an outstanding example of a telescoped orogenic Au system that changes mineralisation characteristics with depth. Refractory gold hosted in arsenopyrite and pyrite is pervasive throughout the deposit, a narrow window of vein-hosted Au-Sb mineralisation exists from ~800 to 1350 m depth, below which is vein-hosted Au-only mineralisation. Work here suggests that this system represents two separate deposits emplaced in the same locality during mineralisation events that were separated by as much as 60 m.y. This was made possible by a combination of Fosterville's location near the boundary of two tectonic blocks that underwent separate periods of gold deposit formation, and the formation of a well-connected fault-controlled plumbing system that had an orientation suitable for reactivation during the second event.

The auriferous sulphides at Fosterville were likely deposited during the Benambran Orogeny (ca 440-420 Ma), coincident with most other Bendigo Zone deposits, but owe their refractory and disseminated nature to their relatively shallow emplacement depth. The Au-Sb mineralisation is likely to have formed during the Tabberabberan Orogeny (ca 380-370 Ma), similar to deposits found in the nearby Melbourne Zone, and overprinted the earlier sulphide event. The relative timing of the Au-only mineralisation is less clear but, was likely coeval with stibnite-Au mineralisation due to similar spatial association (i.e., similar depth of emplacement and structural hosts), overprinting relationships, and geochemical modelling.

Our geochemical modelling and previous fluid inclusion studies are in fair agreement with a formation depth between ~1.8 km and 5.7 km, which is ideal for stibnite precipitation. However, co-genetic Au-Sb mineralisation requires fluid acidification to accompany cooling, and our modelling results indicate that fluid pH buffering in the second Au-introducing event was achieved by reaction with sericite alteration that was generated during the first mineralisation event. In this way, the juxtaposition of mineralisation was critical in concentrating high-grade Au-Sb at a discrete crustal

level during fault reactivation.

The reason for apparent rarity of telescoped orogenic gold deposits in nature may be due to the large distances separating distinct mineralisation styles/deposits across a given district, so they tend to be considered individually. Or, if vertical zonation was present in an individual deposit, it may have been lost to erosion, or simply not seen due to insufficient depth-extent of mining. However, considering that many of the giant and/or high-grade orogenic systems worldwide have experienced multistage mineralisation events of differing P-T-X assemblages (e.g., Kalgoorlie Western Australia; Val-d'Or, Quebec; Red Lake, Ontario; Obuasi, Ghana) it is likely that Fosterville is not the only example of a telescoped orogenic gold system. Thus, the scale and preservation of telescoping should be considered in ore genesis models for orogenic systems in general, and in exploration targeting. It also follows that the having successive periods of deformation that reactivate previously mineralised fault systems, which are able to tap separate fluid sources, may be a critical factor in the formation of some of the largest gold deposits.

Acknowledgments

We wish to thank Braden Verity, Simon Hitchman, Nathan Phillips, Caitlin Brown and the geological team at the Fosterville Gold Mine for their assistance, enthusiasm, and advice. We would also like to thank Rob Duncan and the Geological Survey of Victoria for their partnership in this endeavour. Matthew Kilburn and Jeremy Bougoure are thanked for their assistance, as well as persistence, with the NanoSIMS at the Centre for Microscopy, Characterisation and Analysis at UWA. This project was funded by the ARC Linkage grant (LP150100717) and supported by Australian Centre for Neutron Scattering project 5708.

References

Arne, D. C., Bierlin, F., Morgan, J. W., and Stein, H. J., 2001, Re-Os dating of sulphides associated with gold mineralisation in central Victoria, Australia: Economic Geology, v. 96, p. 1455-1459.

Bierlein, F., Fuller, T., Stüwe, K., Arne, D., and Keays, R., 1998, Wallrock alteration associated with turbidite-hosted gold deposits. Examples from the Palaeozoic Lachlan Fold Belt in central Victoria, Australia: Ore Geology Reviews, v. 13, p. 345-380.

Bierlein, F. P., Arne, D. C., Foster, D. A., and Reynolds, P. R., 2001, A Geochronological framework for slate belt-hosted gold mineralisation in central Victoria, Australia.: Mineral Deposita, v. 36, p. 741-767.

Bons, P. D., 2001, The formation of large quartz veins by rapid ascent of fluids in mobile hydrofractures: Tectonophysics, v. 336, p. 1-17.

Cayley, R., Taylor, D., VandenBerg, A., and Moore, D., 2002, Proterozoic–Early Palaeozoic rocks and the Tyennan Orogeny in central Victoria: the Selwyn Block and its tectonic implications: Australian Journal of Earth Sciences, v. 49, p. 225-254.

Cayley, R. A., Korsch, R. J., Moore, D. H., Costelloe, R. D., Nakamura, A., Willman, C. E., Rawling, T. J., Morand, V. J., Skladzien, P. B., and O'Shea, P. J., 2011, Crustal architecture of central Victoria: results from the 2006 deep crustal reflection seismic survey: Australian Journal of Earth Sciences, v. 58, p. 113-156.

Changkakoti, A., Gao, Z., Green, N., Kwak, T., Gray, J., and Krouse, H., 1996, Contrasting origins of Au-and Sb-bearing fluids, central Victoria, Australia: Neues Jahrbuch fur Mineralogie-Monatshefte, p. 271-285.

Dierick, M., Masschaele, B., and Van Hoorebeke, L., 2004, Octopus, a fast and user-friendly tomographic reconstruction package developed in LabView®: Measurement Science and Technology, v. 15, p. 1366.

Faulkner, D., Jackson, C., Lunn, R., Schlische, R., Shipton, Z., Wibberley, C., and Withjack, M., 2010, A review of recent developments concerning the structure, mechanics and fluid flow properties of fault zones: Journal of Structural Geology, v. 32, p. 1557-1575.

Garbe, U., Randall, T., Hughes, C., Davidson, G., Pangelis, S., and Kennedy, S., 2015, A new neutron radiography/tomography/imaging station DINGO at OPAL: Physics Procedia, v. 69, p. 27-32.

Gray, D., and Foster, D., 2004, Tectonic evolution of the Lachlan Orogen, southeast Australia: historical review, data synthesis and modern perspectives: Australian Journal of Earth Sciences, v. 51, p. 773-817.

Gray, D. R., and Foster, D. A., 1998, Character and kinematics of faults within the turbidite-dominated Lachlan Orogen: implications for tectonic evolution of eastern Australia: Journal of Structural Geology, v. 20, p. 1691-1720.

Groves, D. I., Goldfarb, R. J., Gebre-Mariam, M., Hagemann, S., and Robert, F., 1998, Orogenic gold deposits: a proposed classification in the context of their crustal distribution and relationship to other gold deposit types: Ore geology reviews, v. 13, p. 7-27.

Hagemann, S. G., and Lüders, V., 2003, PTX conditions of hydrothermal fluids and precipitation mechanism of stibnite-gold mineralisation at the Wiluna lode-gold deposits, Western Australia: conventional and infrared microthermometric constraints: Mineralium Deposita, v. 38, p. 936-952.

Hecht, H., and Oguchi, T., 2017, Global evaluation of erosion rates in relation to tectonics: Progress in Earth and Planetary Science, v. 4, p. 40.

Hitchman, S. P., Phillips, N. J., and Greenberger, O. J., 2018, Fosterville Gold Deposit: Australian Ore Deposits (Sixth Edition), v. Monograph Number 32.

Leader, L., Robinson, J., and Wilson, C., 2010, Role of faults and folding in controlling gold mineralisation at Fosterville, Victoria: Australian Journal of Earth Sciences, v. 57, p. 259-277.

Mason, B., and Moore, C. B., 1985, Principles of geochemistry.

Mernagh, T. P., 2001, A fluid inclusion study of the Fosterville mine: A turbidite-hosted gold field in the western Lachlan fold belt, Victoria, Australia: Chemical Geology, v. 173, p. 91-106.

Moresi, L., Betts, P. G., Miller, M. S., and Cayley, R. A., 2014, Dynamics of continental accretion: Nature, v. 508, p. 245.

Naden, J., and Shepherd, T. J., 1989, Role of methane and carbon dioxide in gold deposition: Nature, v. 342, p. 793.

Phillips, D., Fu, B., Wilson, C. J., Kendrick, M., Fairmaid, A., and Miller, J. M., 2012, Timing of gold mineralisation in the western Lachlan Orogen, SE Australia: A critical overview: Australian Journal of Earth Sciences, v. 59, p. 495-525.

Porter, T. M., 2016, The geology, structure and mineralisation of the Oyu Tolgoi porphyry copper-gold-molybdenum deposits, Mongolia: a review: Geoscience Frontiers, v. 7, p. 375-407.

Sillitoe, R. H., 1994, Erosion and collapse of volcanoes: Causes of telescoping in intrusion-centered ore deposits: Geology, v. 22, p. 945-948.

VandenBerg, A., 2000, The Tasman Fold Belt system in Victoria: geology and mineralisation of Proterozoic to Carboniferous rocks, Geological Survey of Victoria.

Voisey, C. R., Willis, D., Tomkins, A. G., Wilson, C. J. L., Micklethwaite, S., Salvemini, F., Bougoure, J., Rickard, W. D. A., 2020, Aseismic Refinement of Orogemic Gold Systems. Economic Geology.

Williams-Jones, A. E., and Norman, C., 1997, Controls of mineral parageneses in the system Fe-Sb-SO: Economic Geology, v. 92, p. 308-324.

Willman, C., Korsch, R., Moore, D., Cayley, R., Lisitsin, V., Rawling, T., Morand,

V., and O'Shea, P., 2010, Crustal-scale fluid pathways and source rocks in the Victorian gold province, Australia: Insights from deep seismic reflection profiles: Economic Geology, v. 105, p. 895-915.

Wilson, C. J., Moore, D. H., Luzin, V., and Salvemini, F., 2017, Costerfield antimony-gold deposit, southeast Australia: Coupling between brittle deformation and dissolution-precipitation reactions in the Melbourne Zone: Ore Geology Reviews, v. 91, p. 741-764.

Chapter 5

Gold Accumulations in Quartz Driven by Earthquake-Induced Piezoelectricity

Christopher R. Voisey[1], Andrew G. Tomkins[1], Nicholas J. R. Hunter[1]

[1]*School of Earth, Atmosphere & Environment, Monash University, Clayton, VIC 3800, Australia*

"If it works, or even if it doesn't, this is awesome."
-Words of a hopeful man

Chapter 5

Abstract

For thousands of years people have observed that coarse gold nuggets occur almost exclusively in quartz veins (except when eroded from the primary rock), commonly as highly interconnected fracture-hosted networks, and wondered how they formed. The current paradigm posits that gold is precipitated together with quartz from hot H_2O-rich fluids (hydrothermal fluids) in rock fractures in response to changes in temperature, pressure and fluid chemistry. However, the extremely rich concentrations of gold seen in some samples presents a paradox because quartz is one of the least chemically reactive minerals, and there is no previously described chemical reason why they should be so closely associated. If, as widely believed, chemistry plays an important role in gold precipitation, why is gold not preferentially accumulated at the much more reactive minerals in the host rock? Here, we investigate whether piezoelectric discharge from quartz during earthquakes can explain this globally ubiquitous gold-quartz association. Quartz is the only abundant piezoelectric mineral on Earth, and the cyclical nature of the earthquake activity that drives orogenic gold deposit formation means that quartz crystals in veins will experience thousands of episodes of deviatoric stress, and thus piezoelectric discharge. In this earthquake-proximal setting auriferous fluid repeatedly infiltrates existing quartz veins because these are the focus of fracturing in heterogeneous rocks. The elastic rattling of quartz crystals within each vein during seismic activity leads to oscillating piezoelectric discharge and thus alternating oxidation-reduction reaction fronts on crystal surfaces. If stress on crystals is sufficient to generate enough voltage to shift the energy of the quartz valence band above that of the redox potential of Au-bearing ligands – $Au(HS)_2^-$ and/or $Au(HS)^-$ – gold will be electrochemically deposited. Because gold is an outstanding conductor, existing gold grains will be the focus of ongoing piezoeletroplating as fluid infiltration is repeated many times, allowing creation of the observed highly interconnected gold networks. We thus suggest that the piezoelectric effect is the solution to the long standing ‘gold nugget problem’.

1. Introduction

In orogenic Au systems, Au-bearing fluids from the mid to lower crust are transported along fracture networks by seismic ruptures associated with regional compressional tectonics (Sibson, 1975; Cox, 1995). These systems are hosted in rocks of variable metamorphic grade involving mid- to upper-crustal temperatures and pressures between 200-650 °C and 1-5 kbar (Groves, 1993; Tomkins and Grundy, 2009). Under these conditions, the abundant episodic quartz-carbonate veining found in these deposits indicates formation from fluids that attained supralithostic pressures numerous times during deposit formation (Sibson, 1975; Cox, 1995). The cyclic nature of these seismic events means that fractures up-structure are continually opened and filled with fluids via a 'crack-seal' mechanism, resulting in spatially focused quartz-Au vein systems (Cox and Etheridge, 1983; Ramsay, 1980; Renard et al., 2000). In the Central Victorian Au province, turbidite-hosted quartz-Au lodes are associated with the Bindian and Tabberabberan orogenic events, which in part resulted in the extensive Lachlan Orogen (Cox et al., 1991; Gray et al., 1988). The most remarkable feature of this province is the presence of coarse-grained 'nuggety Au' found within quartz veins, making Victoria one of the most Au-rich regions on Earth, producing approximately 2,500 tonnes of Au since the mid 1800's. Nuggety Au occurs at numerous deposits around the world, but is particularly well developed in Victoria, which is home to the largest Au nuggets ever found.

Orogenic Au systems are of exceptional commercial importance, responsible for ~75% of the Au recovered globally through history, if their derived placer deposits are considered (Groves et al., 1998; Goldfarb and Groves, 2001; Phillips and Powell, 2015). Yet the mechanism(s) by which Au is concentrated into quartz veins from hydrothermal fluids, and in particular how nuggety Au forms, is poorly understood. Geochemical studies tend to focus on phenomena related to local changes in fluid chemistry to explain the deposition of Au, whereas structural geologists focus on physical mechanisms such as drops in pressure and temperature. However, it's not uncommon that field evidence does not support either discipline's proposed mechanisms, and Au

can be found “floating” in quartz veins with no obvious signs of chemical or physical processes to explain its precipitation.

One potential precipitation trigger, not previously investigated, which we consider here for the first time, is piezoelectric discharge from quartz. Quartz is one of few natural crystals that lacks a center of symmetry (‘non-centrosymmetric’), and exhibits both left- and right-handed crystal forms (Fig. 1). When a mechanical force is applied, an anisotropy arises in the internal electrical configuration of the crystal, causing electrical polarisation on crystal surfaces, resulting one of the strongest examples of electrical polarisation in nature (Bishop, 1981b). Quartz is by far the most abundant piezoelectric mineral in nature.

The piezoelectric effects of quartz have undergone extensive research in the engineering and materials science space, fuelled largely by industrial and commercial manufacturing uses. A wealth of commercial products has been manufactured, such as watches, resonators, oscillation circuits, and sonar detection devices (Cady, 1947; Cady, 1964; Saigusa, 2017). Conversely, the role of quartz piezoelectric phenomena in nature, particularly in Earth processes, remains poorly understood. This is surprising, given the abundance of quartz in the crust, its distribution across various tectonic settings, and the critical role that silica-rich fluids play in ore deposit settings.

Several workers have found that vein quartz emits a measurable piezoelectric charge when a mechanical stress is applied (Ghomshei and Templeton, 1989; Parkhomenko, 1971; Sreedhar Murthy and Bhimasankaram, 1985), which in many cases is enhanced where there is preferred orientation of the polycrystals, or ‘texture’ (Bishop, 1981b). Evidence from historical literature demonstrates that quartz veins typically exhibit such non-random textures necessary for this enhanced charge, in particular in crack-seal type veins associated with orogenic Au deposits (Ramsay, 1980; Cox and Etheridge, 1983). It is thus reasonable to suggest that textured quartz, when subjected to the seismic stresses that occur during earthquake-associated fluid transfer events, could generate surficial electric potentials capable of concentrating Au from hydro-

thermal solutions by electrochemical reduction (e.g., Möller & Kerstein, 1994; Maddox et al., 1998).

This review synthesises current literature on the piezoelectric properties of quartz, with emphasis on the role of texture, piezocatalysis in material surface-fluid chemical reactions, electrochemical processes in metal deposition. These phenomena are considered in context of orogenic Au systems. The review concludes with implications for exploration techniques.

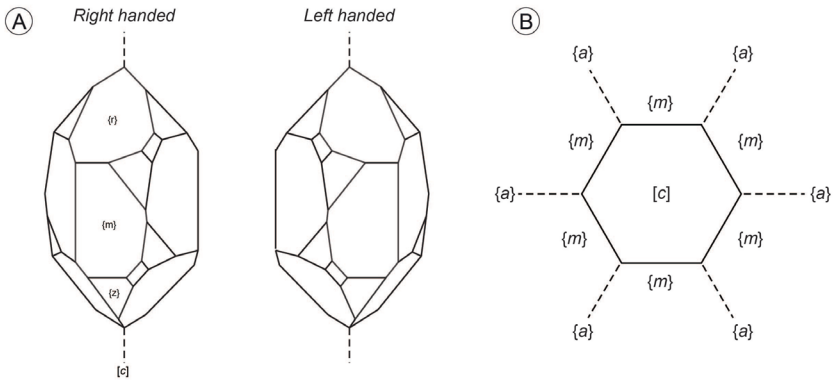

Figure 1:A) Crystallography of left- and right-handed quartz. The prismatic and rhombohedral planes are indicated. Minor planes, such as bipyramidal and acute rhombohedral, are not shown. B) Quartz crystal viewed parallel to the [c] basal axis. Here, the first- {m} and second- order {a} prismatic planes can be easily distinguished.

2. Piezoelectricity and Quartz

Piezoelectricity is a characteristic property observed in a small group of naturally occurring minerals, in which an applied mechanical force generates electrical polarisation on crystal surfaces (Curie & Curie, 1880). The source of this phenomenon is the specific distribution of electric charge in the unit cell of the crystal, and thus depends on the geometric arrangement of its atomic framework. In a crystal where the atoms are symmetrically arranged (i.e. possessing a 'centre of symmetry'), the electrical charges between atoms are equally balanced. Such crystals cannot be piezoelectric, as no net polarisation is achieved when an applied force distorts the crystal. Thus, piezoelectricity is almost entirely observed in 'non-centrosymmetric' crystals, those that lack a centre of symmetry. Non-centrosymmetric crystals distorted under stress

have an imbalance in their internal electric configuration, resulting in an electrical potential – or voltage – across the crystal that is directly proportional to the applied mechanical force (Neishtadt et al., 2006).

In low temperature geological settings (below ~575 ºC), quartz is stable in the trigonal crystal system (α-quartz; Laue group: -3m; point group: D_{3d}; space groups: $P3_121$−$P3_221$) (Le Page and Donnay, 1976). The trigonal quartz crystal system is described by several important crystal planes variably oriented about a main basal axis [*c*]: (i) three first order {*m*} and three second order {*a*} prismatic planes; and (ii) three positive {*r*} and three negative {*z*} rhombohedral planes. These crystal features are summarized in Figure 1. The effect of applying a mechanical force to a quartz crystal framework is shown in Figure 2. Here, a mechanical pressing stress is applied toward the *X*-axis, which displaces the electrical centre defined by the three Si^+ and O^- atoms and polarization toward *X* occurs. In quartz, piezoelectric polarisation occurs along the {*a*} planes (Fig. 2B). It should be mentioned that β quartz, although more symmetric than α-quartz (belonging to the 622-point group), is still piezoelectric when deformed off-axis (Uno & Noge, 1998). However, considering its occurrence is only prevalent at temperatures higher than those relevant to this study, only α- quartz will be discussed further.

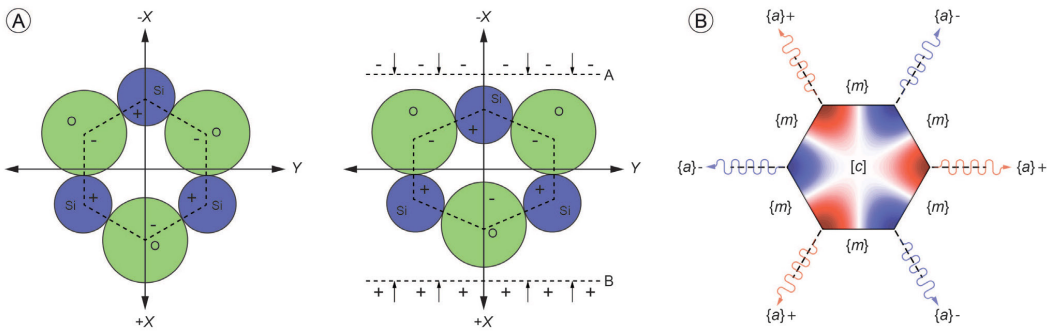

Figure 2:A) Effects of an applied mechanical stress (parallel to X) on a quartz crystal framework. When the framework is distorted the electric field becomes imbalanced, resulting in polarisation. Modified from (Saigusa, 2017). B) Distribution of piezoelectric polarisation (red - positive; blue - negative) in a quartz crystal. Note that only the {a} axes are piezoelectrically active

2.1 Previous Studies of Piezoelectricity in Geological Materials

Following the discovery of piezoelectric properties in single crystals by Curie and Curie (1880), geology-based research was championed heavily by Soviet workers to aid mineral exploration (Neishdadt and Osipov, 1958; Parkhomenko, 1971; Volarovich and Parkhomenko, 1954; Volarovich and Sobolev, 1969), with additional work in the engineering and materials science communities to calibrate the piezoelectric coefficients of quartz materials (Bechmann, 1958; Ogi et al., 2006). Subsequent studies focused on characterising the magnitude of piezoelectric potentials in quartz rocks, typically by applying a stress to the sample and measuring the resulting electric signal with charge amplifiers (Bishop, 1981a, b; Murthy et al., 1981; Tuck et al., 1977). The results of these experiments ranged from no detectable non-stochastic effect (Tuck et al., 1977); minor effects in select samples (Bishop, 1981b); to large effects in specific rock types (Murthy et al., 1981; Parkhomenko, 1971; Sreedhar Murthy and Bhimasankaram, 1985). Most comparative studies have found that vein quartz is significantly more piezoactive than other quartzose rocks, likely due to having preferred mineral orientation (Ghomshei and Templeton, 1989; Parkhomenko, 1971; Sreedhar Murthy and Bhimasankaram, 1985). Overall, the modest amount of historical literature on piezoelectric phenomena in geology predominantly comprises laboratorial calibration, with the application typically to inform industrial manufacture and geophysical exploration. Research investigating the role of piezoelectric phenomena in geological processes is severely limited.

3. Textures in Quartz Veins

Piezoelectric polarisation in polycrystalline materials is intimately linked to their degree of crystallographic preferred orientation (CPO), or ‘texture’. In geology, the alignment of crystal planes into preferred orientations has been known for over a century (Becke, 1892; Bouchez, 1977; Fellows, 1943; Holmquist, 1926; Malavieille and Etchecopar, 1981), and is observed in many quartz-bearing rocks as the result of igneous, sedimentary and metamorphic/tectonic processes (Skrotzki, 1994). Materials with well-defined textures (i.e., strong CPOs) result in strong directional variation

in their piezoelectric polarisation, due to favourable alignment of the electric poles (Mainprice et al., 2015). In Figure 3, the quartz *a*-axes in two model specimens are shown in three-dimensional space: the axes on the left specimen are strongly oriented, whereas the axes on the right are random. The corresponding piezoelectric tensors (Fig. 3B) reveal that the left specimen exhibits strongly anisotropic electrical polarization, whereas the right specimen does not. Plastically deformed rocks (e.g. quartz mylonites) typically develop strong textures during various tectonic processes, and thus often exhibit highly polarised piezoelectric fields, or 'piezoelectric fabrics' (Bishop, 1981b). In order to investigate the presence of such piezoelectric fabrics in quartz veins, and their potential to influence Au mineralization, there is an increased need to understand the textures of Au-bearing quartz veins in ore deposit settings.

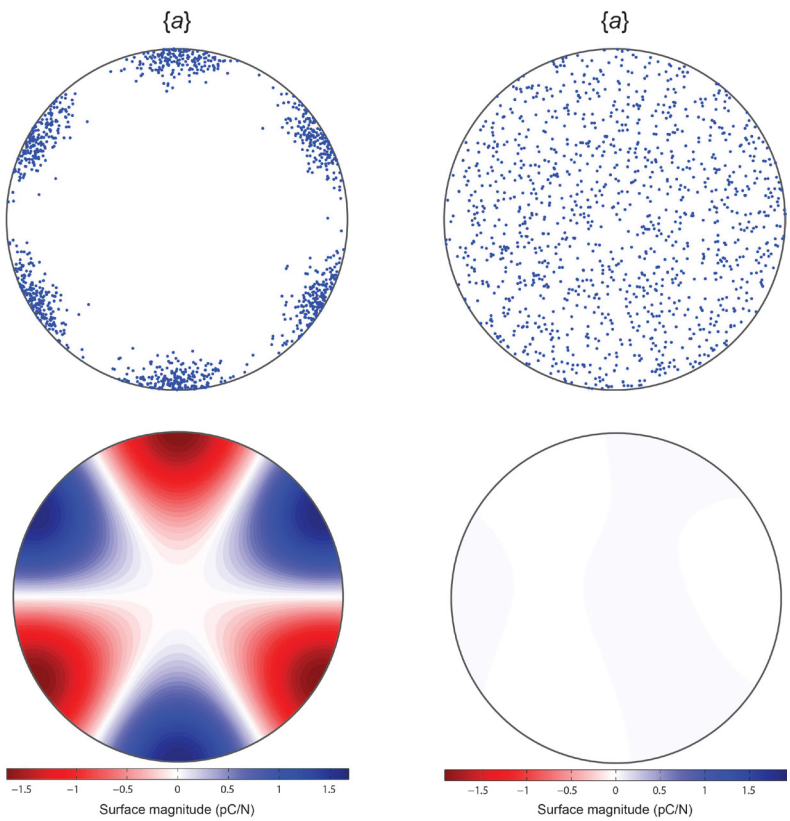

Figure 3: Quartz crystal models depicting the relationship between a crystallographic preferred orientation ('texture') and piezoelectric polarisation. Where a strong preferred orientation is present in the quartz {a} axes (top left), the piezoelectric tensor (bottom left) is highly polarised. Conversely, when {a} axis orientations are uniformly distributed (top right), the tensor exhibits very poor polarisation (bottom right).

Although quartz texture development is well understood in most geological settings, knowledge in the context of Au-bearing vein systems is comparatively poorer. However, evidence from the broader literature on tectonic quartz veins may be applied. In vein settings, preferred orientations form due to the oriented nucleation of quartz precipitates. Grains are always in competition with respect to crystal growth. In crack-seal settings, where crystal growth is pervasive, certain crystal orientations are more favourable for growth than others. Specifically, grains favourably oriented with respect to the extension directions will outgrow those that are unfavourably oriented (Bons, 2001; Fisher and Brantley, 1992). For example, crystal growth along in quartz *c*-axis is the most energetically favourable in many vein settings (Fisher and Brantley, 1992; Laubach et al., 2004).

The process of competitive growth leads to a preferred orientation in quartz veins and, where multiple crack-seal events occur, subsequent crystal overgrowths may lead to an increasingly refined texture (Nollet et al., 2005). It has also been proposed that quartz textures may form due to dissolution-precipitation creep or pressure solution (Bons and Den Brok, 2000; Egglseder et al., 2016). In almost all cases, quartz *c*-axes are commonly oriented parallel to the vein wall (Bons, 2001; Cox and Etheridge, 1983; Egglseder et al., 2016; Fisher and Brantley, 1992; Nollet et al., 2005; Nüchter and Stöckhert, 2007).

3.1 Piezoelectric Tensors in Au-Quartz Veins

In this section, we bring together the concepts of quartz vein textures and piezoelectric properties by plotting the piezoelectric tensor in a representative Au-bearing quartz vein specimen. This sample was collected from a fault exposure at the Costerfield deposit (Central Victoria) and is oriented parallel to the vein wall (Fig. 4). The texture of the bulk sample (i.e. the orientation of its crystals) was measured using neutron diffraction at the Australian Nuclear Science and Technology Organisation (ANSTO, Lucas Heights) in August 2016.

Neutron diffraction reveals that crystals inside the sample have a preferred orienta-

tion. The c-axes of crystals inside the sample are oriented parallel to the vein wall, as observed in quartz veins from other tectonic settings (Bons, 2001; Cox and Etheridge, 1983; Egglseder et al., 2016; Fisher and Brantley, 1992; Nollet et al., 2005; Nüchter and Stöckhert, 2007). The a-axes are correspondingly oriented in a great circle at a low angle to the extension direction (N-S; Fig. 4). The piezoelectric tensor shows the orientation of net polarisation based on the orientation of these piezoelectric a-axes. Positive and negative polarisation are both defined by two strong maxima in the sample, oriented perpendicular to the vein wall and parallel to the a-axis topology (dashed line; Fig. 4). These data are evidence that quartz-Au veins in orogenic Au settings are appreciably piezoelectric.

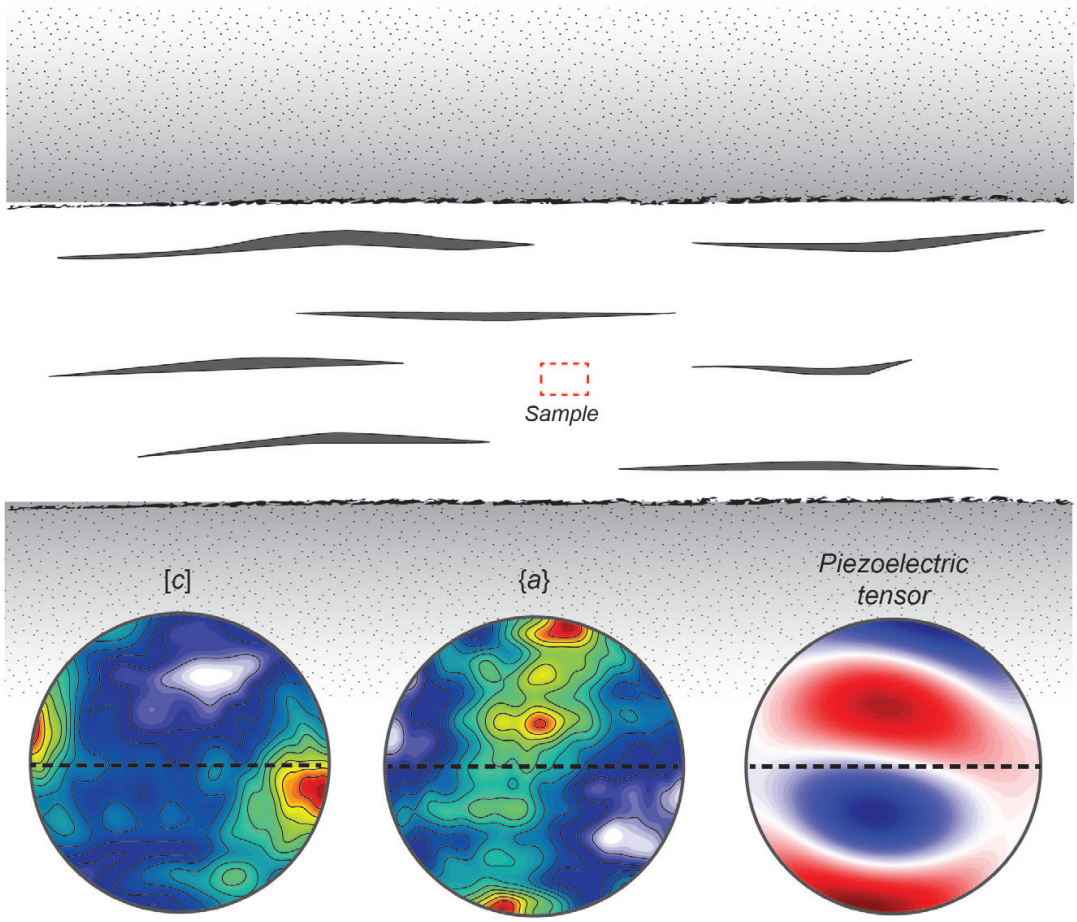

Figure 4: Texture and corresponding piezoelectric tensor of a quartz-vein sample from the Costerfield deposit, Central Victoria. This sample (MH178a) was oriented parallel to the fault exposure (red dashed lines) prior to collection. The orientation of the c and a crystal axes are shown as lower hemispheric pole figures. The piezoelectric tensor shows the distribution of positive (red) and negative (blue) polarisation.

4. Piezoelectricity & Electrochemical Processes

Piezoelectric polarization, when coupled with electrochemistry, makes it possible to investigate potential redox reactions between the surface of a strained piezoelectric material and a surrounding chemical solution. The electric field established by a strained piezoelectric material has a significant effect on the electronic properties both inside and outside of the material itself. In an insulator, such as quartz, no charge is able to freely move to counteract the piezoelectric field and the electric field that is generated linearly augments the energy of occupied (valence band) and unoccupied (conduction band) states across the material (Fig. 5) (Starr & Wang, 2015). The resulting electronic rearrangement within the piezoelectric material disturbs the distribution of free charges between the material and any adjacent medium, such as an ionic solution. The interactions of any particle(s) that carry a charge and are free to move (e.g., electrons and ions), depends on the occupiable electronic states between the material and solution, and the amount of charge free to move between the two (Wang, 2010, 2012; Zang et al., 2011). In this way, mechanically deforming a piezoelectric material causes a shift in energy, leading to the flow of electrons from the material's surface to species in solution, or vice-versa (Fig. 5). If the energy shift causes the electric potential of the piezoelectric material to exceed that of unoccupied (conduction band) states in solution, there will be a net electron flow from occupied (valence band) states in the material into the solution. If energy shifts cause the electric potential of the piezoelectric material to drop below that of occupied (valence band) states in solution, then there will be a flow of electrons from the solution species into the material. This electron exchange is capable of driving electrochemical reactions at the material-solution interface (Hong et al., 2010; Hong et al., 2012; Starr et al, 2012).

4.1 Band Energy & Redox Potential

Solid-liquid electrochemical reactions rely critically on the energy levels of the solid (i.e., valence and conduction band) as well as the energy levels of oxidizing or reducing agents in the solution (i.e., their redox potential). An energy model that

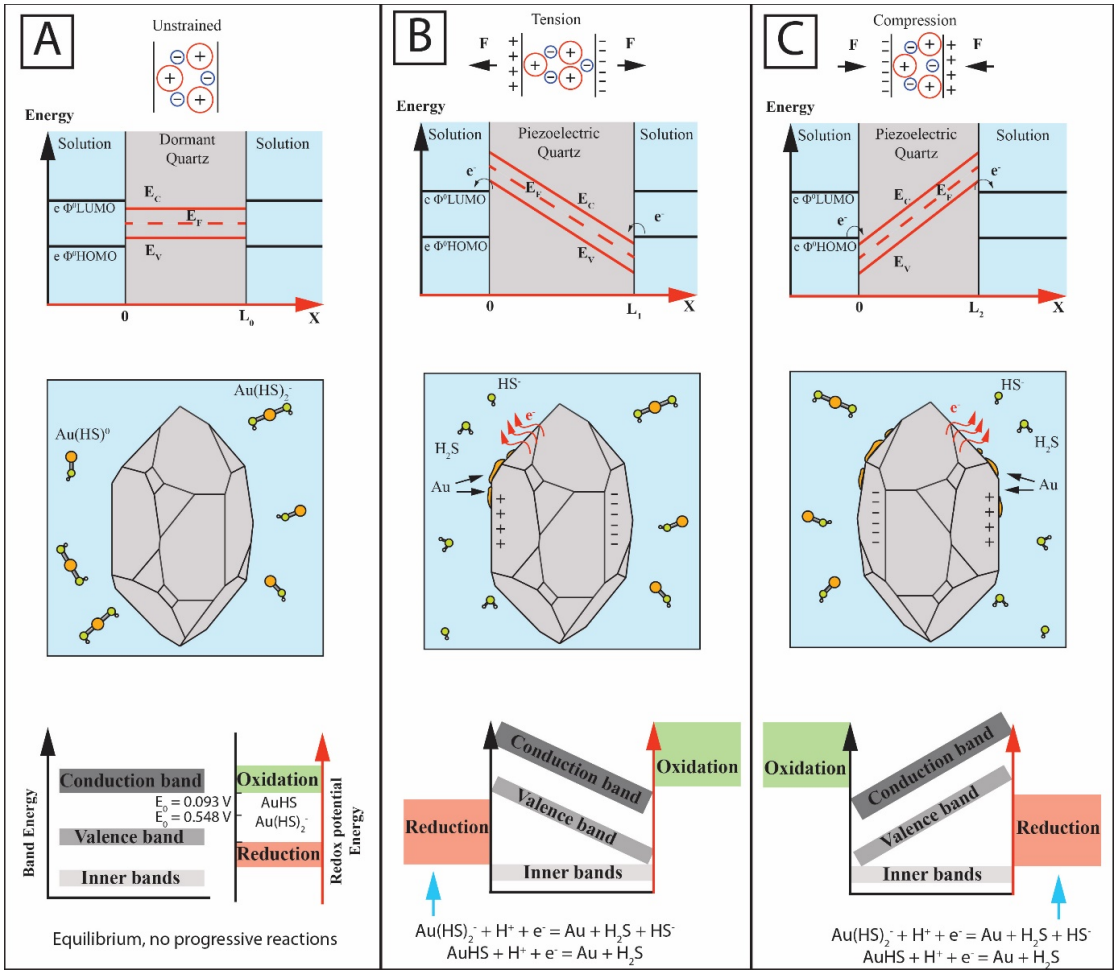

Figure 5: A) Quartz crystal unstrained and in equilibrium with its chemical surroundings. LUMO= lowest occupied molecular orbit HOMO = highest occupied molecular orbit. Top image is modified from Starr et al., (2015). Valence and Conduction bands are not shifted, the redox potential of $Au(HS)_2^-$ and $Au(HS)^0$ lie within the "forbidden energy gap" whereby electron exchange does not occur. B) Tensile strain has changed the energy state of occupied and unoccupied states across the quartz crystal, making electron transfer possible out of the valence band and into the conduction band with the surrounding fluid. Electron transfer occurs on the left side in this schematic, energy shifts exceed the redox potential of Au-ligands and leads to electrochemical reduction of Au by: $Au(HS)_2^- + H^+ + e^- = Au^0 + H_2S + HS^-$ and/or $AuHS + H^+ + e^- = Au^0 + H_2S$. C) Compressional strain has changed the energy state of occupied and unoccupied states across the quartz crystal in an equal and opposite way to (B). Electrochemical reduction of Au in solution now occurs on the right side in this schematic.

allows the prediction of electron exchange between a semiconductor and an electrolyte has been developed (Gerischer & Ekardt, 1983). This model compares the energy levels of the conduction and valence bands in the semiconductor to the redox couple in the solution on the same scale. The difference between the energy levels of the solution redox couple and the conduction/valence bands of the solid can be considered a potential barrier that electrons must overcome to react with solid material (Fig. 5) (LeBlanc & Fogler, 1986). The smaller this potential barrier is for electron transfer, the higher reaction rates will be. This concept provides a means of predicting reductive or oxidative dissolution/precipitation processes in fields such as electroplating, mineral processing, and electromechanics. Here, we will use this concept to explain piezoelectrically driven chemical reactions on the surface of quartz within an aqueous solution.

4.2 The Piezocatalyst

Piezoelectric enhancement or suppression of electrochemical reactions that occur at the interface between the material and solution is referred to as piezocatalysis (Starr et al, 2012). There have been investigations into the effects of dynamic piezocatalytic reactions, where the material is continuously alternated between tensile and compressive strains (Starr et al, 2012). The result is a large, varying piezoelectric field within the material that prevents the achievement of thermodynamic/electrochemical equilibrium with its environment, allowing an enduring exchange of charge between the piezoelectric material and surrounding solution. This phenomenon was experimentally shown by comparing the surface charge generated on a strained piezoelectric material to the amount of H_2 produced by the reduction of H_2O into H_2 and O_2. The results show that the amount of H_2 produced is dependent on both the frequency and amplitude of strain within the piezoelectric material, as well as electrolyte concentrations in solution. The time between intervals of strain needs to be sufficiently long to allow the energized surface charges to react with the solution. The majority (90%) of voltage generated by the piezoelectric material diminished within the first 0.06 s,

whereas almost all (99%) was gone by 1.46 s. The difference between time intervals of 0.05 s to 1.2 s increased piezocatalytic efficiency from 0.2% to 2.4%. In these experiments H_2 production was drastically impaired by the increase in electrolyte concentration (Starr et al, 2012). Charged ions in an electrolyte solution can effectively 'screen' the effects of surface charge on the piezoelectric material and subdue the free-energy difference between surface and solution. This results in a reduction of electrochemical reaction rates. Therefore, in more solute-rich fluids higher voltages – derived from high magnitudes of strain within the material – are required to increase the amount of energized surface electrons available for reaction with the surrounding solution to counteract the effects of screening ions. As long as the evolution of a chemical species depends on electrical charge transfer (i.e., redox), the electric field generated within a local piezoelectric material will affect the directionality and locality of these chemical reactions.

4.3 Electrochemistry for Metal Deposition

It has been shown that adsorption-reduction reactions on material surfaces are important for the deposition of Au by the reduction of Au^+ in solution to Au^0 (Möller & Kerstein, 1994; Maddox et al., 1998). This is facilitated by the dissolution of semiconducting sulfide electrodes (e.g., pyrite and arsenopyrite) by redox and solid-state electrochemical processes. The main driver for these processes is the mixed open-circuit potential of these materials (Maddox et al., 1998). The open-circuit potential of a semiconductor reflects the thermodynamic tendency of that material to participate in electrochemical corrosion, or likewise precipitation, within a surrounding electrolyte, even if no external voltage is applied. Similar to the band gap energy concept above, the open-circuit potential of a material relative to the redox potential of surrounding aqueous species governs the rate of chemical reactions between the two. If the open-circuit potential of a material is lower than the redox potential of a neighbouring aqueous species, electrons will not be transferred from the material into solution, and reduction of the species will not occur. Likewise, if the open-circuit potential of a

solid is higher than the redox potential of the aqueous species, then electron transfer from the material into the solution can drive chemical reduction of dissolved aqueous species.

This mechanism has been shown to be significant for the accumulation of Au on pyrite and arsenopyrite by coupled reduction-oxidation reactions that take place on the mineral surfaces, driving sulphide corrosion (Möller and Kersten, 1994; Maddox et al., 1998; Laird et al., 2015, 2018). The semiconducting properties of both arsenopyrite and pyrite are governed by As content (i.e., change from n-type to p-type conductance with an increase in As concentration), where n-type conductors are considered to act as anodes (e^- donors) and p-type conductors are considered to act as cathodes (e^- acceptors) in a linked system (Möller and Kersten, 1994). The adsorption of Au has been shown to preferentially occur on As-rich cathodic (p-type conductivity) domains of these sulphide minerals in H_2S-saturated solutions (Möller and Kersten, 1994; Maddox et al., 1998; Laird et al., 2015, 2018). This is facilitated by the donation of electrons from the cathodic surface along the sulphide-solution interface, leading to reduction of Au-bearing ligands in the fluid phase and dissolution of the anodic sulphide species. Gold may deposit from solution on cathodic surfaces by $Au^+ + e^- \leftarrow\rightarrow Au^0$ or, to a lesser extent, on anodic surfaces by $Au(HS)_2^- \leftarrow\rightarrow Au^0 + 2S + 2H^+ + 3e^-$ (Möller and Kersten, 1994).

Colloidal Au particles can also be adsorbed onto minerals with positive surface charge (p-type conductors) by electrostatic attraction (William-Jones et al., 2009; Buttard et al., 2011). If any Au nanoparticles are present along arsenopyrite-fluid or pyrite-fluid interfaces, they would also be preferentially adsorbed onto the cathodic surfaces of these sulfides (Fig. 6).

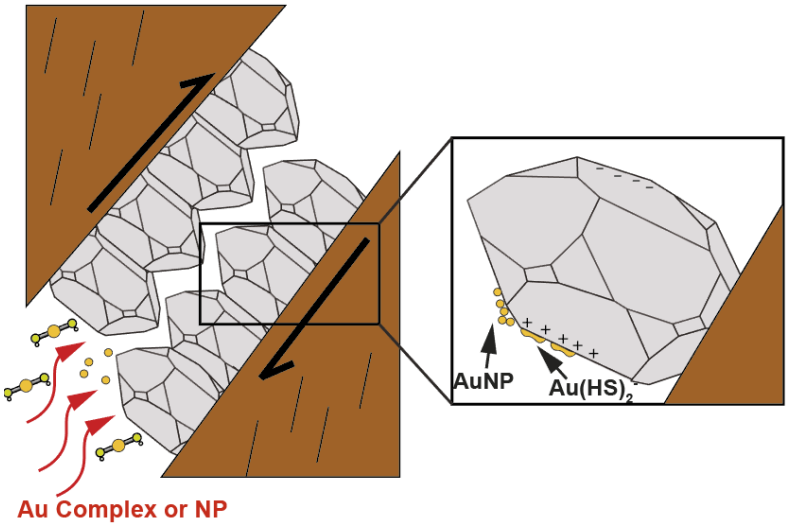

Figure 6: Schematic of Au deposition from Au-ligands by electrochemical reduction and adsorption of Au nanoparticles by electrostatic attraction during hydrothermal fluid infiltration associated with seismic activity. Schematic shows only one snap shot of strain, and therefore piezoelectric polarisation, on the quartz crystals in the vein.

5. Piezopotential of Orogenic Gold Systems

These electrochemical concepts beg the question as to how the band energy shifts in a piezoelectric material, such as quartz, may push or pull electrons from the material's surface into a Au-bearing solution to drive electrochemical precipitation of Au. Given that electron transfer between sulphide minerals and auriferous solutions has been demonstrated to be significant for Au deposition, and that piezocatalytic chemical reduction of H_2O driven by electron transfer from piezoelectric material surfaces into solution is well known, we suggest that it is likely that strain-induced voltage generated by quartz promotes Au mineralisation. Here, we will discuss the fundamental concepts explained above in the context of an evolving orogenic Au system.

In orogenic mineral systems, abundant crack-seal textures in quartz veins indicate their formation from fluids that attained supralithostic pressures numerous times over the period of deposit formation (Sibson et al., 1988; Cox et al, 1995). We have shown that these crack-seal veins contain a preferred orientation of quartz crystals, which would produce larger piezoelectric tensors and associated piezoelectric potential if strained. Therefore, during any given strain event, the highest charge

within a veined volume of rock will be developed within the quartz veins. The cyclical nature of the fault-valving underpinning orogenic Au deposit formation means that these quartz veins form and repeatedly fracture incrementally, and will experience multiple episodes of deviatoric stress during their formation (Robert, 1995). Since orogenic deposits are hosted by secondary and tertiary fault structures (Goldfarb & Groves, 2001), they are the focus of tens of thousands of earthquake aftershocks during their formation (Micklethwaite et al., 2010). Aftershocks form clusters, and can maintain permeability on aftershock-hosting faults for extended periods of time, with reactivation of the same structures (Micklethwaite et al., 2010). This setting is ideal for maintaining infiltration of auriferous fluid through and past preferentially oriented quartz veins that are experiencing syn-shock strain. The elastic rattling of quartz crystals within the vein during seismic activity will lead to oscillation of the oxidation-reduction reaction fronts on either side of the crystal surfaces (Figs. 5 & 6). If strain on crystals within the vein is sufficient to shift the energy of the quartz valence band above that of the redox potential of Au-bearing ligands - $Au(HS)_2$ and/or Au(HS) – then Au will be electrochemically deposited within the vein (Fig. 5). If the fluid contains any Au nanoparticles, they will be preferentially adsorbed onto quartz surfaces acting as cathodes (Fig. 6). Each primary earthquake event has hundreds to thousands of associated aftershocks (Omori, 1894), and multiple primary earthquakes will occur during the tens of thousands to millions of years of deposit formation. Gold is an outstanding electrical conductor, so once formed, existing Au grains will transfer charge from quartz, allowing them to be the focus of ongoing piezoeletroplating as fluid infiltration is repeated many times. This mechanism would allow creation of the observed highly interconnected networks of Au within quartz. In this way, we suggest that piezoelectric Au accumulation is the solution to the long standing ‘gold nugget problem’.

6. Implications for Gold Exploration

The utility of the piezoelectric properties of quartz for geophysical prospecting was first investigated by Soviet workers (Neishdadt and Osipov, 1958; Parkhomenko, 1971; Sobolev et al., 1984; Volarovich and Sobolev, 1969), informed in part by a method patented by Volarovich, Parkhomenko and Sobolev in 1965 (Neishtadt et al., 2006). The rationale of these early piezoelectric exploration methods was that mechanical energy (seismic waves) is converted to electromagnetic energy (piezoelectric waves). In practice, a seismic pulse is triggered from the surface that excites the elastic fields in the underlying rocks. A piezoelectric effect will occur in electrically polarised materials, the signals of which are recorded with grounded electrodes and subsequently amplified for analysis. Figure 7 presents typical piezoelectric anomalies recorded during such operations (Eppelbaum, 2017; Neishtadt et al., 1986; Neishtadt et al., 2006). The detection of piezoelectric anomalies through such methods has been used for several decades to target quartz-hosted Au ore deposits (Maxwell et al., 1992; Neishtadt et al., 1986; Neishtadt et al., 2006; Russell et al., 1992), and other deposit types (Bishop and Emerson, 1999).

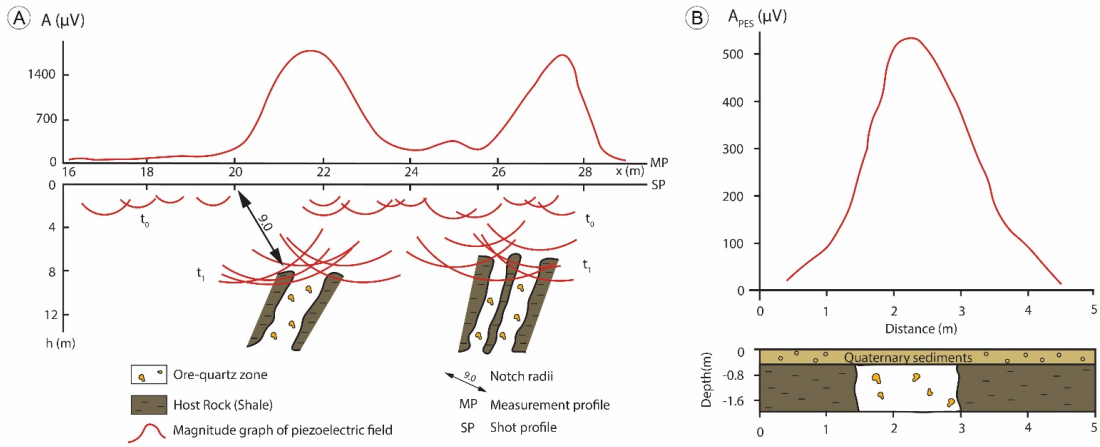

Figure 7: Examples of geophysical exploration using piezoelectric phenomena. Piezoelectric anomalies (measured in microvolts; μV) are taken from (A) a Au-bearing quartz deposit in Yakutia, Russia (Neishdaht et al. 1986); and (B) a Au-bearing quartz vein in southern Israel (Neishdaht et al. 2006).

Research into quartz piezoelectric phenomena has the potential for further developing such exploration techniques. Perhaps one of the most exciting aspects of this is the presence of preferred orientation textures in quartz-Au veins, and the resulting non-random piezoelectric tensor properties (Figs. 3 and 4). Surprisingly, much of the piezoelectric exploration theory has been modelled on assumptions that the textures (and thus piezoelectric *a*-axes) are random in quartz-Au veins (Neishtadt et al., 2006; Tatarinov and Karyakin, 1975), whereas we have demonstrated that this is not the case for some Au-bearing samples (Fig. 4). This observation implies that there are possibilities for further refining the exploration method. However, a number of uncertainties remain regarding the textures in quartz-Au veins: (i) the prevalence of such textures; (ii) differences in texture between barren, disseminated and nuggety Au quartz veins; (iii) the diversity of texture topologies. If it can be shown that a relationship exists between texture characteristics and Au distribution, the corresponding piezoelectric tensor properties may be targeted accordingly. For example, if the highest-grade Au is known to be associated with a particular quartz vein texture, this may be targeted with a specific orientation of the exploration exercise. Moreover, textured quartz rocks have coincident differences in their wave propagation properties compared to non-textured rocks (Mainprice et al., 2015). It is thus possible that there may be differing seismic and magnetic anomalies for quartz rocks, coinciding with their textures (Neishtadt et al., 2006). Today, there exist state-of-the-art techniques in texture acquisition and calculation of piezoelectric and other tensor properties of quartz-bearing rocks. This means we are now in a position to refine and advance exploration methods to target and possibly differentiate certain types of quartz veins in ore deposit settings, based on their material properties.

7. Conclusions

We have reviewed the historical literature on piezoelectricity in quartz-rich materials and how piezoelectricity can promote electrochemical reactions with a surrounding fluid. Literature on piezoelectric minerals, in particular quartz, predominantly focusses on material and physical properties, industrial manufacture, and exploration strategies. Conversely, there is a paucity of studies investigating the role of quartz piezoelectric phenomena in geological processes. Despite this, several observations suggest that vein quartz with an appreciable texture may be suitably piezoelectric to facilitate Au accumulation in orogenic Au system settings. This deposit setting is ideal for research regarding piezoelectric mineralization mechanisms in that their formation requires flow of auriferous fluid past quartz veins that are experience multiple strain events. The elastic rattling of quartz crystals within orogenic veins during seismic activity is hypothesised to shift oxidation-reduction reaction fronts on quartz crystals that may electrochemically reduce Au from ligands in infiltrating fluids. Repetition of this mechanism over the formation history of the deposit could possibly be the solution to the long standing 'gold nugget problem'. Preliminary data from a Au-rich quartz vein shows that at least some of these have crystallographic preferred orientation and thus must exhibit appreciable piezoelectric behaviour during earthquakes.

Acknowledgments

The authors wish to thank Braden Verity, Simon Hitchman, Nathan Phillips and the geological team at the Fosterville Gold Mine for their assistance and advice. We would also like to thank Rob Duncan and the Geological Survey of Victoria for their partnership in this endeavour. This project was funded by the ARC Linkage grant (LP150100717).

References

Bechmann, R., 1958, Elastic and Piezoelectric Constants of Alpha-Quartz: Physical Review, v. 110, p. 1060-1061.

Becke, F., 1892, Petrographische Studien am Tonalit der Rieserfer, *in* Tschermak, G., ed., Mineralogische und petrographische mitteilungen, XIII: Vienna, Springer-Verlag, p. 379-464.

Bishop, J. R., 1981a, Estimating quartz fabrics from piezoelectric measurements: Journal of the International Association for Mathematical Geology, v. 13, p. 261-289.

Bishop, J. R., 1981b, Piezoelectric effects in quartz-rich rocks: Tectonophysics, v. 77, p. 297-321.

Bishop, J. R., and Emerson, D. W., 1999, Geophysical properties of zinc-bearing deposits: Australian Journal of Earth Sciences, v. 46, p. 311-328.

Bons, P. D., 2001, Development of crystal morphology during unitaxial growth in a progressively widening vein: I. The numerical model: Journal of Structural Geology, v. 23, p. 865-872.

Bons, P. D., and Den Brok, B., 2000, Crystallographic preferred orientation development by dissolution-precipitation creep: Journal of Structural Geology, v. 22, p. 1713-1722.

Bouchez, J. L., 1977, Plastic deformation of quartzites at low temperature in an area of natural strain gradient: Tectonophysics, v. 39, p. 25-50.

Cady, W. G., 1947, Nature and use of piezoelectricity: Electrical Engineering, v. 66, p. 758-762.

Cady, W. G. b., 1964, Piezoelectricity : an introduction to the theory and applications of electro-mechanical phenomena in crystals: N.Y., N.Y. : Dover Pubs.

Cox, S., Wall, V., Etheridge, M., and Potter, T., 1991, Deformational and metamorphic processes in the formation of mesothermal vein-hosted gold deposits—examples from the Lachlan Fold Belt in central Victoria, Australia: Ore geology reviews, v. 6, p. 391-423.

Cox, S. F., and Etheridge, M. A., 1983, Crack-seal fibre growth mechanisms and their significance in the development of oriented layer silicate microstructures: Tectonophysics, v. 92, p. 147-170.

Curie, J., and Curie, P., 1880, Développement par compression de l'électricité polaire dans les cristaux hémièdres à faces inclinées: Bulletin de minéralogie, v. 3, p. 90-93.

Egglseder, M. S., Cruden, A. R., Tomkins, A. G., and Wilson, C. J. L., 2016, Deformation-induced silica redistribution in banded iron formation, Hamersley Province, Australia: Lithos, v. 266–267, p. 87-97.

Eppelbaum, L., 2017, Quantitative Analysis of Piezoelectric and Seismoelectric Anomalies in Subsurface Geophysics: Proceedings of the Transactions of the

13th EUG Meeting Geophysical Research Abstracts, Vienna, Austria, 2017, p. 23-28.

Fellows, R. E., 1943, Recrystallization and flowage in Appalachian quartzite: Geological Society of America Bulletin, v. 54, p. 1399-1432.

Fisher, D. M., and Brantley, S. L., 1992, Models of quartz overgrowth and vein formation: Deformation and episodic fluid flow in an ancient subduction zone: Journal of Geophysical Research: Solid Earth, v. 97, p. 20043-20061.

Ghomshei, M. M., and Templeton, T. L., 1989, Piezoelectric and a-axes fabric along a quartz vein: Physics of the Earth and Planetary Interiors, v. 55, p. 374-386.

Gray, D., Allen, R., Etheridge, M., Fergusson, C., Gibson, G., Morand, V., Vanden-Berg, A., Watchorn, R., and Wilson, C., 1988, Structure and tectonics, Geology of Victoria, 5, Geological Society of Australia, Victorian Division Melbourne, p. 1-36.

Holmquist, P. J., 1926, Zur Morphologie der Gesteinsquarze: Geologiska Föreningen i Stockholm Förhandlingar, v. 48, p. 410-428.

Laubach, S. E., Reed, R. M., Olson, J. E., Lander, R. H., and Bonnell, L. M., 2004, Coevolution of crack-seal texture and fracture porosity in sedimentary rocks: cathodoluminescence observations of regional fractures: Journal of Structural Geology, v. 26, p. 967-982.

Le Page, Y., and Donnay, G., 1976, Refinement of the crystal structure of low-quartz: Acta Crystallographica Section B, v. 32, p. 2456-2459.

Mainprice, D., Bachmann, F., Hielscher, R., Schaeben, H., and Lloyd, G. E., 2015, Calculating anisotropic piezoelectric properties from texture data using the MTEX open source package: Geological Society, London, Special Publications, v. 409, p. 223-249.

Malavieille, J., and Etchecopar, A., 1981, The Effect of Deformation on Rocks Ductile shear deformation of quartzite in an alpine crustal thrust (Ambin Massif): Tectonophysics, v. 78, p. 65-71.

Maxwell, M., Russell, R. D., Butler, K. E., and Kepic, A. W., 1992, Field tests of piezoelectric exploration for quartz: 1992 SEG Annual Meeting, 1992, p. 443-445.

Murthy, Y. S., Murali, S., and Bhimasankaram, V. L. S., 1981, A simple dynamic method for the evaluation of the piezoelectric activity of rock samples: Proceedings of the Indian Academy of Sciences - Earth and Planetary Sciences, v. 90, p. 85-89.

Neishdadt, N., and Osipov, L., 1958, On using of seismoelectric effects of the second type observed by pegmatites searching: Trans. VITR (All-Union Inst. Tech. Prospect. Methods), v. 11, p. 63-71.

Neishtadt, N., Mazanova, Z., and Suvorov, N., 1986, The application of the piezoelectric method for searching ore-quartz deposits in Yakutia: Seismic methods of studying complicated media in ore regions: NPO Rudgeofizika, p. 109-116.

Neishtadt, N. M., Eppelbaum, L. V., and Levitski, A. G., 2006, Application of piezoelectric and seismoelectrokinetic phenomena in exploration geophysics: Review of Russian and Israeli experiences: Geophysics, v. 71, p. B41-B53.

Noge, S., & Uno, T., 1998, Piezoelectric Resonance Properties of a β Phase Quartz Plate. Japanese journal of applied physics, 37(5S), 2874.

Nollet, S., Urai, J. L., Bons, P. D., and Hilgers, C., 2005, Numerical simulations of polycrystal growth in veins: Journal of Structural Geology, v. 27, p. 217-230.

Nüchter, J.-A., and Stöckhert, B., 2007, Vein quartz microfabrics indicating progressive evolution of fractures into cavities during postseismic creep in the middle crust: Journal of Structural Geology, v. 29, p. 1445-1462.

Ogi, H., Ohmori, T., Nakamura, N., and Hirao, M., 2006, Elastic, anelastic, and piezoelectric coefficients of α-quartz determined by resonance ultrasound spectroscopy: Journal of Applied Physics, v. 100, p. 053511.

Parkhomenko, E. I., 1971, Electrification phenomena in rocks, Springer Science & Business Media.

Peterson, E. C., and Mavrogenes, J. A., 2014, Linking high-grade gold mineralization to earthquake-induced fault-valve processes in the Porgera gold deposit, Papua New Guinea: Geology, v. 42, p. 383-386.

Phillips, D., Fu, B., Wilson, C. J., Kendrick, M., Fairmaid, A., and Miller, J. M., 2012, Timing of gold mineralisation in the western Lachlan Orogen, SE Australia: A critical overview: Australian Journal of Earth Sciences, v. 59, p. 495-525.

Ramsay, J. G., 1980, The crack–seal mechanism of rock deformation: Nature, v. 284, p. 135-139.

Renard, F., Gratier, J.-P., and Jamtveit, B., 2000, Kinetics of crack-sealing, intergranular pressure solution, and compaction around active faults: Journal of Structural Geology, v. 22, p. 1395-1407.

Russell, R. D., Maxwell, M., Butler, K. E., and Kepic, A. W., 1992, Electromagnetic Responses from Seismically Excited Targets A: Piezoelectric Phenomena at Humboldt, Australia: Exploration Geophysics, v. 23, p. 281-285.

Saigusa, Y., 2017, Chapter 5 - Quartz-Based Piezoelectric Materials, *in* Uchino, K., ed., Advanced Piezoelectric Materials (Second Edition), Woodhead Publishing, p. 197-233.

Skrotzki, W., 1994, Mechanisms of texture development in rocks, *in* Bunge, H. J., Siegesmund, S., Skrotzki, W., and Weber, K., eds., Textures of Geological Materials: Verlag, Germany, Deutsche Gesellschaft für Metallkunde, Informationsgesellschaft, p. 167-186.

Sobolev, G., Demin, V., Narod, B., and Whaite, P., 1984, Tests of piezoelectric and pulsed-radio methods for quartz vein and base-metal sulfides prospecting at Giant Yellowknife Mine, NWT, and Sullivan Mine, Kimberley, Canada: Geophysics, v. 49, p. 2178-2185.

Sreedhar Murthy, Y., and Bhimasankaram, V. L. S., 1985, Experimental results of the piezoelectric activity of quartzose rocks: 1985 SEG Annual Meeting, SEG 1985, 1985, p. 102-105.

Tatarinov, P., and Karyakin, A., 1975, Course of hard deposits of useful minerals, Nedra Publications (in Russian).

Tuck, G. J., Stacey, F. D., and Starkey, J., 1977, A search for the piezoelectric effect in quartz-bearing rocks: Tectonophysics, v. 39, p. T7.

VandenBerg, A., 2000, The Tasman Fold Belt system in Victoria: geology and mineralisation of Proterozoic to Carboniferous rocks, Geological Survey of Victoria.

Volarovich, M., and Parkhomenko, E., 1954, Piezo-electric phenomenon of rocks: Doklady Academy of Science USSR (Reports of the Soviet Academy of Sciences).

Volarovich, M., and Sobolev, G., 1969, Piezoelectric method of exploration for quartz and pegmatite veins, Nauka Publishers (in Russian).

Wang, Z. L., 2010, Piezopotential gated nanowire devices: Piezotronics and piezo-phototronics: Nano Today, v. 5, p. 540-552.

Wang, Z. L., 2012, Progress in piezotronics and piezo-phototronics: Advanced Materials, v. 24, p. 4632-4646.

Willman, C., Korsch, R., Moore, D., Cayley, R., Lisitsin, V., Rawling, T., Morand, V., and O'Shea, P., 2010, Crustal-scale fluid pathways and source rocks in the Victorian gold province, Australia: Insights from deep seismic reflection profiles: Economic Geology, v. 105, p. 895-915.

Zhang, Y., Liu, Y., & Wang, Z. L., 2011, Fundamental theory of piezotronics. *Advanced Materials*, *23*(27), 3004-3013.

Chapter 6

Conclusions

"That wasn't so bad."
-Words of a bewildered man

1.1 Key Outcomes

This thesis provides insights regarding the formation of orogenic Au deposits using diverse techniques from various disciplines on multiple scales. Principles from stable isotope geochemistry, petrography, microstructural geology, thermodynamics, electrochemistry, and material science were employed in ways not previously considered by the economic geology community. Considering the formation conditions of orogenic-type Au deposits, there is no way to directly monitor their formation and therefore all research chapters aim to advance the understanding of the processes responsible for their formation. A number of the deposits in the central Victorian Au fields are considered on a regional scale using stable Ag isotopes (Chapter 2), the genesis of the Fosterville deposit is addressed in the context of an evolving tectonic system over 40-60 m.y. using deposit- to micro-scale observations and thermodynamic modelling (Chapter 4), the generation of ultra high-grade Au veins are interpreted on the nano- to macro- scale using principles from micromeritics and micro-tectonics (Chapter 3), and finally, a novel Au precipitation mechanism is proposed on the atomic- to nano-scale using principles from electrochemistry and material science (Chapter 5). By integrating different disciplines over a range of scales, I have aimed to have provide original insights into orogenic deposit formation.

1.2 Summary of Findings

1.2.1 Extreme Ag Isotope Variation in Orogenic Gold Systems Implies Multi-Staged Metal Remobilization During Ore Genesis

This chapter, published in Voisey et al., 2019, reports the first Ag isotope data for the Paleozoic orogenic Au deposits in the Victorian Au fields. Ag isotope fractionation mechanisms in ore deposit settings are discussed and new perspectives into large-scale orogenic ore genesis are suggested. The main findings of this study are:

- Despite their relatively uniform geology, deposits in Victoria show a wide range in $^{107}Ag/^{109}Ag$ ratios in native Au ($\varepsilon^{107}Ag$ -6.6 to +8.3, relative to the NIST SRM 978a Ag standard), comparable to the entire previously known terrestrial range (-9.4 to +5.3).
- The data show no correlation with mineralization age or host rock composition, and no obvious isotopic link to established 'mantle' or 'crustal' Ag isotope values, implying that source rock signatures are unlikely to be the main control on Ag isotope variations.
- The Ag isotopic variation is primarily related to physico-chemical processes, particularly Ag isotope fractionation during redox reactions such as conversion of Ag^0 in native Au to Ag^+ in dissolved $Ag(HS)_2^-$ or sulfide-borne Ag.
- Repeated $Ag^0 \leftrightarrow Ag^+$ reactions along transport pathways and at sites of ore accumulation are thought to have generated the wide range in $\varepsilon^{107}Ag$.
- Ag isotope fractionation via numerous deposition-dissolution cycles provides perspective into large-scale ore genesis that has not previously been recognised for orogenic Au systems; multi-staged metal remobilization along fluid transport pathways is standard during their formation.

1.2.2 Aseismic Refinement of Orogenic Gold Systems

This chapter, published as Voisey et al. *In Press*, investigates the processes responsible for development of anomalously high-grade ore (upwards of 3% Au) found in quartz veins at the Fosterville Au mine using optical, scanning and transmission electron microscopy, nanoscale secondary ion mass spectrometry, as well as 3-D neutron tomography. An ore upgrading model, referred to as "aseismic refinement", is suggested and the generation, transport and growth of Au nanoparticles in orogenic systems are discussed. The main findings of this study are:

- Au is concentrated along pressure-solution seams (PSS) associated with wall-rock selvages; (ii) as nano- to micro-scale "dusty Au seams" parallel to PSS; and (iii) in micro-scale tension fractures perpendicular to stylolitic seams.
- The distribution of Au in arsenopyrite and pyrite hosted within PSS changes as a function of the extent of deformation.
- It is proposed that Au supersaturation in fluids introduced during seismic periods led to the deposition of abundant Au nanoparticles in quartz-carbonate veins.
- Pressure-dissolution of vein minerals during inter-seismic intervals allowed for episodic increase in the gold/quartz ratio, and permitted liberation and migration of Au nanoparticles, promoting Au grain growth in favourable textural settings.
- Galvanic corrosion and brittle fracturing of auriferous sulfides during the inter-seismic period allowed additional remobilization and/or enrichment of sulphide-hosted Au.
- This Au ore upgrading model, referred to as "aseismic refinement", provides a new insight for the genesis of ultra-rich Au mineralization and, based on textures reported from many Au deposits, may be a globally significant component in the formation of orogenic Au deposits.

1.2.3 The First Analysis of a Telescoped Orogenic Gold System: Insights from the Fosterville Deposit.

This chapter, submitted to *Economic Geology*, discusses the various styles of Au mineralisation at the Fosterville deposit as a telescoped orogenic system. Microscopy, neutron tomography, nanoscale secondary ion mass spectrometry and field observations were conducted to investigate mineralogical and structural controls on the various styles of Au mineralisation. These observations were used as the foundation for equilibrium geochemical modelling using HCh software. Results are considered in the context of an evolving mineral system over the formation history of the deposit. The main findings of this study are:

- Refractory Au mineralisation is found throughout the deposit, whereas visible Au ± stibnite occurs deeper in the system (>800 m depth from surface).
- It is suggested that Fosterville formed via two major Au mineralisation events, 40 to 60 Ma apart: the 440-420 Ma 'pyrite-arsenopyrite' event and the 380 Ma 'pyrite-arsenopyrite-stibnite' event.
- Fosterville was situated in a structural corridor that was able to adopt both these styles of mineralization, due to its locality within the Bendigo Zone and proximal to the Melbourne Zone.
- HCh modelling indicates that fluid pH buffering in the second Au event was achieved by sericite alteration that had been introduced during the first mineralisation event, and this was critical in concentrating high-grade Au-Sb.
- Fosterville is an example of a telescoped orogenic Au system, where relatively high-temperature mineral assemblages were overprinted vertically by later, lower temperature assemblages.

1.2.3 Piezoelectricity in Earth's Crust and the Potential to Form Gold Deposits

This chapter synthesises current literature on piezoelectric effects in quartz, with emphasis on the role of texture, piezocatalysis in material surface-fluid chemical reactions, electrochemical processes for metal deposition, and finally, considers the role these play accumulation of Au in quartz. A new Au precipitation mechanism is proposed for orogenic gold systems. The main findings of this study are:

- Piezoelectricity is a property observed in a small group of minerals, including quartz, in which an applied mechanical force generates electrical polarisation on crystal surfaces.
- Deforming a piezoelectric material can cause a sufficient shift in energy to induce the flow of electrons from the material's surface to species in adjacent solutions.
- Quartz in veins in orogenic gold deposits is demonstrated to have a preferred orientation, leading to a larger piezoelectric tensor and associated piezoelectric potential when strained.
- The cyclical nature of the fault-valving that drives orogenic Au deposit formation means that quartz veins will experience multiple episodes of deviatoric stress during their formation.
- Orogenic deposit settings are ideal for allowing numerous stages of fluid flow past preferentially orientated quartz veins that are experiencing stress.
- The elastic rattling of vein quartz during seismic activity will lead to oscillation of oxidation-reduction reaction fronts on either side of individual quartz crystals.
- If strain on crystals is sufficient enough to shift the energy of the quartz valence band above that of the redox potential of Au-bearing ligands – $Au(HS)_2$ and/or Au(HS) – Au will be electrochemically deposited within the vein.

2.0 Holistic Implications of the Research Results

The fault systems that host orogenic deposits behave episodically, cycling between increased and decreased fluid pressures and permeability, which is attributed to the periodicity of earthquakes (Chapter 1 and references therein). Differential stress changes combined with metamorphic fluid release act together to trigger periodic brittle failure in the Au source region. Gold leached by metamorphic fluids is then transported upwards during earthquakes via crustal-scale fault networks for many kilometers from amphibolite facies rocks in the mid to deep crustal source to the upper to lower greenschist facies rocks that host deposits in the mid to upper crust.

The economic geology community is challenged to understand of the processes occurring along this very long fluid transfer pathway, or even range in vertical extent possible in individual orogenic gold deposits. Although the latter remains unanswered, this study has provided new insights into gold behaviour during large scale fluid transfer. The cyclic nature of the fault-valving mechanism in conjunction with observational evidence for multiple remobilization events within Au deposits themselves imply that remobilization should be expected along deeper parts of the fault-hosted fluid pathways. Chapter 2 provided isotopic evidence, in the form of extensively fractionated Ag isotopes, to confirm that remobilisation is a widespread occurrence in orogenic systems. Multi-staged remobilization can upgrade the Au concentration in individual fluid migration events, assuming that later infiltrating fluids are under-saturated in Au. Alteration on the fluid pathways during early influx events can aid in this endeavour by extending the range in which Au is soluble in solution (Chapter 4). Thus, both Chapters 2 & 4 provide evidence that Au remobilisation along fluid pathways, results in higher grade Au mineralisation.

During periods of active seismicity, when auriferous fluids are flushed into the ore system, Au saturation may lead to precipitation directly from solution, or if extreme super-saturation occurs, Au may nucleate as colloidal particles forming Au nanoparticles (Chapter 3). The elastic rattling of quartz crystals within veins during

seismic activity generates piezoelectric fields across the crystals, leading to oscillation of oxidation-reduction reaction fronts on either side of the crystal(s) surface (Chapter 5). If present in the fluid, Au nanoparticles would then be preferentially adsorbed onto those quartz surfaces acting as cathodes. Furthermore, when strain on crystals is sufficient to shift the energy of the quartz valence band above the redox potential of Au-bearing ligands, Au will be electrochemically deposited onto quartz a-axes. Furthermore, considering that experiments using piezoelectrics have been shown to promote hydrolysis of H_2O, it is possible that the generation of H_2 and O_2 generation could shift fluid pH sufficiently destabilise Au complexes in orogenic systems. It is also possible that this mechanism would increase the proportions of CO_2 and CH_4 sufficiently to promote fluid unmixing (Chapters 1 & 5).

During inter-seismic periods, mechanisms such as mineral precipitation, compaction, and pressure-solution promote sealing of fault surfaces leading to a new period of increasing fluid-pressure that builds until the next failure event. During this period at lower fluid pressure, pressure-dissolution causes localised removal of quartz and carbonate vein material, focused at impurities such as Au grains and wall-rock selvages (Chapter 3). This will naturally concentrate Au that is already in the quartz veins, and at the same time enhance in interconnection of Au particles into the permeable microfracture network within individual quartz veins. In this way, when a new seismic event occurs existing Au will be in position to be accessed by newly infiltrating fluids percolating along fractures in the quartz. Some Au particles may conduct the charge generated by piezoelectric quartz and become the focus for additional Au precipitation. This process would increase Au grade and Au particle size, eventually pseudomorphing the fracture network.

It is also likely that the aseismic period promotes liberation of Au nanoparticles trapped in quartz into grain boundary fluids (Chapter 3). Once liberated, these Au nanoparticles would behave as colloids and migrate to allow growth by diffusion-limited aggregation along wall-rock selvages, adsorption onto p-type sulfides hosted within wall-rock selvages, or accumulation on defect areas of high surface rough-

ness such as tension fractures and brecciated sulfides. Fluid overpressure in the vein system during late aseismic periods allows for fluid-rock interaction by percolation into adjacent wall-rocks, allowing for development or replacement of lattice-bound Au mineralization in sulfides depending on fluid chemistry. At this stage, it is possible that Au may be liberated from replaced sulfides during the build-up to the next major mineralization event, when the fluids can be drawn into the vein. Therefore, redistribution of Au is also possible on a relatively small scale during the "quiet" periods of deposit formation.

The interpretation preferred here is that several processes combine to form the extreme concentrations of Au seen in quartz in orogenic systems globally. Remobilisation of the transport pathway likely plays a role. Gold occurs preferentially in quartz in these systems and less so in others because its piezoelectric properties are more effective in the low salinity fluids that are almost exclusively seen in metamorphic fluids. Enrichment processes occur in both the seismic and aseismic periods and enhance the probability of each other; (1) co-seismic addition of Auinto quartz creates impurities that become the focus of later pressure-dissolution, and (2) aseismic permeability enhancement focused on Au particles ensures that they are accessible to later fluid infiltration events.

3.0 Recommendations for Future Work

Further studies of the effects of temperature, redox, ligand and mineral speciation on the fractionation of Ag isotopes are needed, as is a better understanding of the diversity in crustal Ag isotope reservoirs. Laboratory leach experiments could aid in constraining Ag isotope fractionation factors under varying conditions reflective of ore deposit settings. The remobilisation model proposed in Chapter 2 is consistent with the inferred episodic nature of fluid transport within orogenic Au systems during their formation. If, as the model implies, Ag isotopic heterogeneity exists on the large scale, it may also be recorded at the grain scale. Spatially-resolved Ag isotope work in Au grains (e.g., nanoSIMS) would be useful to further explore this aspect of the mod-

el suggested for the ore genesis of orogenic Au deposits in the Victorian Goldfields. A follow up Ag stable isotope study of vein-hosted Au from different depths of the Fosterville deposit would be insightful regarding the extent of the step-wise remobilisation model suggested in Chapter 2. Step-wise remobilisation events involving native metal should extract progressively more isotopically heavy fluid (i.e., lower ε^{107}Ag), leaving any silver remaining in the source isotopically lighter, while depositing ^{109}Ag enriched Au further up the fluid pathway. If this process repeats, perhaps as a series of steps along the larger scale transport pathway, a progressive zonation of ^{107}Ag/^{109}Ag ratios in Au would develop with decreasing depth whereby shallow-level Au is ^{109}Ag enriched and Au left at depth is ^{107}Ag enriched. Therefore, investigation of intra- and inter-deposit variations in ^{107}Ag/^{109}Ag ratios in Au grains from Fosterville and across Victoria would provide further insights into whether remobilisation is significant on the deposit and/or regional scale.

Research into metal nanoparticles in ore deposit settings is already beginning to take off with increased documentation of their occurrence, partly due to the improved resolution of imaging techniques (e.g., TEM). Further study into the significance that these particles play in building ore deposits is ushering in a new era of economic geology that will surely lead to exciting results and hypotheses. The largest hurdle regarding nanoparticle research appears to be confirmation of their presence during transport for particular deposit types where analogous systems are not able to be monitored (e.g., orogenic-type deposits). Laboratory experiments attempts are made to generate nanoparticles given the appropriate source material, fluid compositions, and P-T conditions may prove to be critical moving forward to address this issue. With regards to the refinement model suggested in Chapter 3, experimental studies involving pressure-dissolution of Au-doped quartz could confirm this proposed mechanism. In-situ monitoring of a stressed quartz aggregate containing nanoparticulate Au would provide insights into the transport and growth of Au during conditions reflective of aseismic intervals and could be possible using an instrument such as DINGO at Australia's Nuclear Science and Technology Organisation.

Future research regarding orogenic Au systems with contrasting mineral assemblages may want to consider the telescoping model suggested in Chapter 4, perhaps as well as other mechanisms present in other deposit "families". Considering that many of the giant and/or high-grade orogenic systems worldwide have experienced multistage mineralization events of differing P-T-X assemblages (e.g., Kalgoorlie Western Australia; Val-d'Or, Quebec; Red Lake, Ontario; Obuasi, Ghana) it is likely that Fosterville is not the only example of a telescoped orogenic Au system. It is suggested that the scale and preservation of telescoping should be considered in ore genesis models for orogenic systems in general, and in exploration targeting. This may eventually provide insights into the limitations of vertical extent of individual orogenic deposits. With regards to the formation model suggested for Fosterville in Chapter 4, it is still open for debate whether metal deposition was controlled by ongoing physiochemical changes at a shallow level in the crust in one evolving mineralization stage, or instead that the deposit formed during two or more periods of fluid infiltration, each potentially tens of millions of years apart. Based on the results presented here, it was suggested that the latter is more likely. However, considering that the two deformation, and associated Au mineralisation, events are in the same orientation, it is suggested that careful Re-Os dating of sulfide assemblages associated with each mineralisation style be carried out to resolve this ambiguity.

Several observations discussed in Chapter 5 suggest that vein quartz may be sufficiently piezoelectric to facilitate Au accumulation by electrochemical redox reactions in orogenic Au system settings. This theoretical chapter is by far the most stimulating facet for future research regarding ore genesis, at least in the author's opinion. Our team at Monash University plan to pursue this research by investigating the textural and piezoelectric properties of quartz veins from selected Victorian gold mines and linking these to Au mineralisation. We have obtained a sample set of Au-bearing veins ranging from high grade to barren. Funds have been secured to perform neutron diffraction and neutron tomography on these samples to link the piezoelectric properties of quartz with the distribution, morphology and preferred orientation of the Au grains.

Computational modelling work in conjunction with material scientist colleagues at the University of Wisconsin-Madison will establish the potential energy required to transfer electrons between piezoelectric quartz and Au particles. This modelling work will provide the information needed to confirm if instantaneous stress experienced by quartz crystals during seismic activity is sufficient to electrochemically destabilize Au from hydrothermal solutions during ore genesis. Further recommended research following these experiments will be to set up an experimental apparatus capable of performing these reactions in-situ, confirming the observational and model-supported evidence above. Such an apparatus would involve having a single crystal of quartz attached with electrodes connected to a computer-controlled actuator for applying strain. By submerging the quartz crystal in an Au-saturated solution, the induced strain is anticipated to cause oscillating Au precipitating redox reactions on either side of the deforming crystal. This future work will hopefully confirm the validity of the novel Au precipitation mechanism proposed here, and further provide new insights into the genesis of – what the author believes to be – one of the most exciting systems in the field of geology.